



## Melt electrospinning today: An opportune time for an emerging polymer process



Toby D. Brown <sup>a</sup>, Paul D. Dalton <sup>a,b,\*</sup>, Dietmar W. Hutmacher <sup>a,c,d,\*</sup>

<sup>a</sup> Institute for Health and Biomedical Innovation, Queensland University of Technology, 60 Musk Avenue, Kelvin Grove 4059, Australia

<sup>b</sup> Department for Functional Materials in Medicine and Dentistry, University of Würzburg, Pleicherwall 2, 97070 Würzburg, Germany

<sup>c</sup> Institute for Advanced Study, Technical University Munich, Lichtenbergstraße 2a, 85748 Garching, Germany

<sup>d</sup> George W Woodruff School of Mechanical Engineering, Georgia Institute of Technology, 801 Ferst Drive Northwest, Atlanta, GA 30332, USA

### ARTICLE INFO

#### Article history:

Received 29 March 2015

Accepted 14 January 2016

Available online 22 January 2016

#### Keywords:

Additive manufacturing

Additive biomanufacturing

Polycaprolactone

Tissue engineering & regenerative medicine

Direct writing

*In vitro* disease models

### ABSTRACT

Over the last decade, melt electrospinning has emerged as an alternative polymer processing technology to alleviate concerns associated with solvents in traditional electrospinning. This has resulted in the fabrication of ultrafine fibers from an increasing range of synthetic polymers and composite systems, to materials including ceramics, driving new applications in technical areas such as textiles, filtration, environment and energy as well as biomedicine. In this article, we review the significant advancements in theoretical modeling of the underlying physical principles, coupled with experimental validation using a variety of technical devices and designs that allows well-controlled fiber formation using optimized material and operating parameters. Innovative device designs are indicating avenues towards higher throughput of randomly collected melt electrospun fibers for the production of commodity nonwoven substrates, similar to solution electrospinning and many other industrial fiber-forming processes. However, we identify a recent shift in perception towards melt electrospinning in the literature, where the adaptation of additive manufacturing approaches to device designs enables precise fiber placement with filament resolutions not yet demonstrated by more established melt-extrusion based direct writing technologies. New, highly ordered arrangements of ultrafine fibers with distinctive surface topology, encapsulating and sensing properties are opening new fields of application in areas such as drug delivery, biosensors and regenerative medicine as high performance materials. The development of these materials is reviewed with an emphasis on an area of current research, where melt electrospun scaffolds are contributing to promising treatment strategies to regenerate or replace human tissue and for the new field of *in vitro* disease models as well as humanized mice models.

© 2016 Elsevier Ltd. All rights reserved.

\* Corresponding authors at: Institute for Health and Biomedical Innovation, Queensland University of Technology, 60 Musk Avenue, Kelvin Grove 4059, Australia.

E-mail addresses: [daltonlab@gmail.com](mailto:daltonlab@gmail.com) (P.D. Dalton), [dietmar.hutmacher@qut.edu.au](mailto:dietmar.hutmacher@qut.edu.au) (D.W. Hutmacher).

## Contents

1.	Introduction .....	118
2.	Historical perspective .....	120
3.	Existing fiber fabrication technologies.....	122
3.1.	Solution spinning .....	122
3.2.	Emulsion spinning.....	123
3.3.	Application of pressurized gas .....	123
3.4.	Melt spinning .....	123
4.	Principles of melt electrospinning .....	124
4.1.	Jet thinning .....	126
4.2.	Quenching of the melt electrospinning jet .....	126
4.3.	Crystallization of melt electrospun fibers .....	127
4.4.	Charge interactions.....	127
4.4.1.	Creation of charge carriers.....	127
4.4.2.	Charge transport .....	127
4.4.3.	Residual charge .....	128
4.5.	Fiber deposition .....	128
4.5.1.	Pore size and porosity .....	130
4.5.2.	Mechanical properties .....	130
5.	Polymer parameters for melt electrospinning.....	130
5.1.	Electrical conductivity .....	140
5.2.	Molecular weight .....	141
5.3.	Tacticity .....	141
5.4.	Thermal properties/extensional viscosity .....	142
6.	Melt electrospinning configurations and instrument parameters .....	143
6.1.	Polymer melt supply zone .....	143
6.1.1.	Spinneret design .....	143
6.1.2.	Application of high voltage .....	144
6.2.	Melt electrospinning jet zone .....	145
6.3.	Fiber collection zone .....	145
6.3.1.	Collector material .....	146
6.3.2.	Moving collectors .....	146
6.4.	Instrument parameters .....	146
7.	Melt electrospinning and direct writing .....	148
8.	Research translation and industrial potential .....	150
8.1.	Energy .....	151
8.2.	Environment, filtration and separation .....	152
8.3.	Textiles .....	153
8.4.	Biomedical engineering .....	153
8.4.1.	Growth factor/drug delivery .....	153
8.4.2.	Biosensors .....	154
8.4.3.	Tissue engineering & regenerative medicine .....	154
9.	Conclusions & future perspectives .....	158
	Acknowledgements .....	159
	References .....	159

## Nomenclature

*PCL	three-arm star poly( $\epsilon$ -caprolactone)
1D	one-dimensional
2D	two-dimensional
3D	three-dimensional
$\gamma$	surface tension
$\epsilon$	relative permittivity
$\eta_{melt}$	melt viscosity
$\mu$	viscosity
$\rho$	density of fluid
$\sigma_q$	surface charge density
$\omega$	buckling frequency
AFD	average fiber diameter
Al	aluminum

AM	additive manufacturing
a-PP	atactic poly(propylene)
CAD	computer-aided design
CaP	calcium phosphate
CBT	crystal violet lactone bisphenol A, 1-tetradecanol
Cu	copper
CNT	carbon nanotube
CVL	crystal violet lactone
$d$	melt electrospinning jet diameter
Da	Dalton unit (1 Da = 1 g/mol, 1 kDa = 1000 g/mol)
$d_i$	inner diameter of spinneret
$e$	electric charge
$E$	electric field strength

$E_a$	activation energy for viscous flow	TCD	spinneret to collector distance
ECM	extracellular matrix	TE	tissue engineering
EHD	electrohydrodynamic	TEC	tissue-engineered construct
$E_o$	breakdown electric field strength in air	$T_g$	glass transition temperature
EVAL	poly(ethylene-co-vinyl alcohol)	TIC	thermally-induced crystallization
EVOH	ethylene vinyl alcohol	$TiO_2$	titanium dioxide
FDM	fused deposition modeling	$T_m$	polymer melt temperature
$f_e$	electrostatic force	UV	ultraviolet
FIC	flow-induced crystallization	$v$	melt electrospinning jet velocity
$g$	gravity (driving force per unit mass)	V	applied voltage
GAME	gas-assisted melt electrospinning		
HA	hydroxyapatite		
hOB	human osteoblast cell		
HV	high voltage		
i-PP	isotactic poly(propylene)		
IR	infrared		
KCl	potassium chloride		
LDPE	low-density polyethylene		
MFI	melt flow index		
MFR	melt flow rate		
$M_n$	number average molecular weight		
MSC	mesenchymal stem cell		
$M_w$	average molecular weight		
N6	Nylon-6		
N12	Nylon-12		
NaCl	sodium chloride		
$p_c$	capillary pressure		
PCL	poly( $\epsilon$ -caprolactone)		
PCM	phase change material		
PCTM	phase change thermochromic material		
PDMS	poly(dimethyl siloxane)		
$p_e$	electrostatic pressure		
PE	Polyethylene		
PEG	Polyethylene glycol		
PEG- <i>b</i> -PCL	Poly(ethylene glycol)-block-poly( $\epsilon$ -caprolactone)		
PEN	Poly(ethylene naphthalate)		
PET	Poly(ethylene terephthalate)		
PLA	polylactide		
PLGA	Poly(lactic-co-glycolic acid)		
PLLA	Poly(L-lactide)		
PMMA	Poly(methyl methacrylate)		
PP	Polypropylene		
PPE	personal protective equipment		
PS	polystyrene		
PU	Polyurethane		
$Q$	volumetric flow rate		
$r$	mean curvature of surface		
$R$	melt electrospinning jet radius		
$R_c$	radius of curvature of Taylor cone apex		
RM	regenerative medicine		
RT	room temperature		
$R_u$	universal gas constant		
SD	standard deviation		
SEM	scanning electron microscopy		
SFFF	solid freeform fabrication		
SLA	stereolithography		
SLS	selective laser sintering		
SO	sodium oleate		

## 1. Introduction

The electrostatic drawing (electrospinning) of polymer fibers is a unique technology for the fabrication of one-dimensional (1D), two-dimensional (2D) and three-dimensional (3D) materials [1,2]. While nanorods and nanotubes offer fiber lengths from 100 nm to tens of microns, in principle, electrospun fibers can be kilometers in length [3,4]. Over the last two decades electrospinning has attracted rising scientific output in the form of an almost exponential rise in publications. The maturation of the field is acknowledged with corporate interest in diverse industry sectors such as: air and water filtration [5]; device routed pharmacology [6–9], tissue engineering and regenerative medicine (TE & RM) [10–12]; as well as industrial areas relying on nano- and sub-micron fibers with specific non biological material and/or physicochemical properties [13–15]. The fields of energy storage, generation and electronics could also gain from technological advances from the so called 1D-characteristics of an ultrafine fiber; where the highly orientated structural elements along the length of the fiber strongly restrict material and electronic diffusion distances perpendicular to the fiber axis [15]. Presently a range of fabrication and synthesis methods for such materials exist [16–19]. Although these technologies enable laboratory scale production of 1D organic nanostructures and polymer fibers, electrospinning combines unrivalled operational simplicity in the laboratory with the potential for industrial production [20].

Electrospinning is a spinning fiber forming process based on an electrohydrodynamic (EHD) phenomenon that uses electrostatic force to draw continuous fibers, in the form of a liquid jet, from a polymer solution or melt. Fig. 1 shows a graphical illustration of a simple melt electrospinning device. Since the fiber deposits continuously onto a collector, this allows the formation of thin, two-dimensional (2D) nonwoven films with the unique properties provided by a nanofibrous architecture. Such nonwoven meshes offer high surface-area to volume ratios and tuneable porosity of up to 90% [21,22] and their use in the manufacture of highly efficient filters is established within industry [23].

Though it has long been appreciated that electrospinning can be performed on polymer melts as well as polymer solutions [24,25], there has been significantly less research into melt electrospinning as the yielded fibers generally have larger diameters compared to solution electrospinning. This lack of published research is being

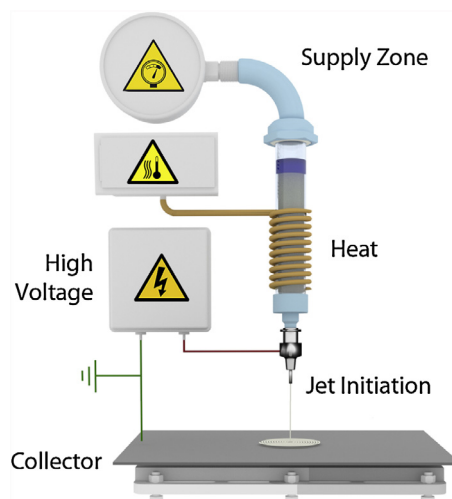


**Fig. 1.** Schematic of melt electrospinning onto a static collector. A supply zone (here shown using air pressure) forces a molten polymer through a spinneret to a jet initiation point. A high voltage potential difference between the spinneret and collector induces an electrical force on the polymer emerging from the spinneret at the jet initiation point. The emerging polymer is then electrostatically drawn as a molten polymer jet to the collector where it solidifies as an ultrafine filament. There are many different melt electrospinning system design iterations, including where the voltage is instead applied to the collector to prevent interference with the electrical heating components that surround the polymer and spinneret. Unpublished figure components provided by Felix Wunner, Queensland University of Technology, Australia.

rectified, with over half of the melt electrospinning literature published between 2012 and 2015. Even with this recent increase in publications, melt electrospinning contributed today to less than 1% of the overall electrospinning literature. The inherent challenge of achieving sufficient economies of scale has been a key factor in the establishment of other processes such as melt spinning and melt blowing in the commodity fiber industry [20]. However during the last decade, developing applications such as biomaterials and TE provide opportunities for melt electrospinning to be applied, where the required throughput and hence economics of scale of TE scaffold manufacture are at this stage more suitable. A number of publications also demonstrated that obtaining melt electrospun fibers with single-micron and sub-micron diameters is possible. Furthermore, there is compelling rationale for electrospinning of fibers from the melt in certain specialized applications where the absence of solvent is a condition *sine qua non* compared to solution electrospinning.

The design and development of high performance optoelectronic devices and circuits requires the capability to fabricate in an exceptionally reproducible and high throughput manufacturing modality. One of the drawbacks of solution electrospinning is that the electrically charged jet is often unstable during flight (when the lowered viscosity ( $\mu$ ) of the polymer in solution cannot suppress repulsive Coulombic charge interactions), and causes fiber deposition to be inherently randomized [4]. This leads to technical challenges where architectures and larger structures with controlled fiber arrangements, rather than a nonwoven, are required. Today, a significant proportion of solution electrospinning research is focused on creating ordered fiber deposition, with limited success [26,27]. In contrast, an important phenomenological aspect of melt electrospinning is that the flight path of the melt jet is stable (where the viscosity of the polymer melt ( $\eta_{melt}$ ) is sufficient to suppress repulsive Coulombic charge interactions), and

therefore fiber deposition is reasonably predictable and not as chaotic as in solution electrospinning. This allows improved control over fiber placement compared to solution electrospinning and other nonwoven fiber forming processes such as melt blowing [28,29].

In biomedical applications, many residual solvents in solution electrospun materials are toxic to cells and tissues [30]. Hence from a regulatory and translational research point of view the inherent complexity and cost required to extract solvents during solution electrospinning, and accompanying post-processing, is undesirable and can be challenging [30,31]. Melt electrospinning provides an alternative polymer processing technology where medical grade polymers can be processed “as received” from the supplier. For the development of biomedical devices and implants such as scaffolds, meshes etc. this means that the regulatory approval timeline can potentially be reduced. Next to the scientifically driven research motivation to analyze and study the melt electrospinning process, this key factor has been largely responsible for the resurgence of research interest in melt electrospinning in the commercially oriented biomaterials and TE fields [32].

Recently, the biomedical community has largely embraced the rapidly emerging additive manufacturing (AM) phenomenon [33–35]. In solution electrospinning, residual repulsive charge on the collected fibers compromises the ability to fabricate substrates with consistent density and thickness. In addition, the amount of fibrous layers that can be fused together is limited, and therefore the effective thickness of such substrates is often less than 1 mm. In contrast, the predictable location of the melt electrospinning jet makes this form of electrospinning amenable to being reconfigured with the adaptation of AM principles into a direct writing process, similar to AM processes based on melt extrusion processes. The result is well defined architectures with size, shape and volume so far not achieved with solution electrospinning (Fig. 2).

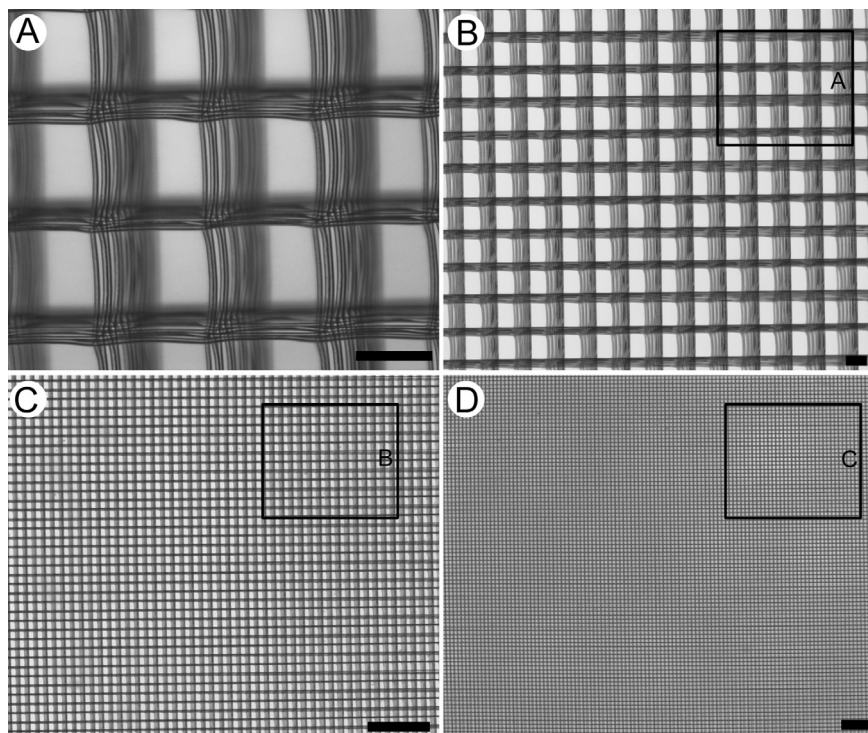


**Fig. 2.** Stereomicroscope images of a melt electrospun PCL scaffold fabricated using a direct writing approach ( $AFD = 8 \mu\text{m}$ ). Fibers are accurately placed  $150 \mu\text{m}$  apart both vertically and horizontally to create repeating “boxes”. Such “high-performance” materials are key to the adaptation of melt electrospun fibers for industrial products—scaffolds for RM and TE is one such area currently under intensive research. Scale bar for ((A) and (B)) and ((C) and (D)) is  $100 \mu\text{m}$  and 1 mm, respectively. Unpublished Figure provided by Paul D. Dalton from the University of Würzburg, Germany.

Based on the above, as well as ever multiplying needs for more environmentally friendly and safer manufacturing alternatives, the demand to understand the feasibility of electrospinning from a polymer melt is warranted. However, very little research has been performed in this area so far. Currently, with less than 100 published articles, the field of melt electrospinning research is truly in its infancy. There are indications though that melt electrospinning can be applied effectively to a large number of both basic and translational research fields: in which highly ordered sub-micron structures are required in combination with the absence of solvents. This review provides an overview of melt electrospinning in the historical context of traditional solution electrospinning methods, including established research that describes the process through experimental observation as well as mathematical models. A comprehensive and up-to-date list of the polymers that have been melt electrospun is presented, as well as a discussion on their suitability to be processed using this technique. The flexibility of the melt electrospinning process is demonstrated, where various device configurations developed by different research groups are described, including a critical discussion on system operating parameters and processing conditions.

## 2. Historical perspective

A recent and extensive review by Tucker et al. outlines the inventions and discoveries that have led to the

development of the electrostatic fabrication and drawing of fibers commonly referred to as “electrospinning” [36]. In 1600 the English physician W. Gilbert first recorded the EHD phenomenon, observing that a water droplet placed on a wooden table became electrically charged “when a piece of rubbed amber is held in its proximity”, causing it to deform at the liquid–air interface into a conical shape now known as a Taylor cone [37,38]. Following further observations of how a charged water jet rapidly generates separated drops [39–41], it was not until the beginning of the 20th century that Zeleny performed the first systematic studies on EHD, where he described the discharge (electrospraying) from electrified predominantly Newtonian liquid surfaces [42,43].

It was also around this time that the opportunity for commercialization of EHD processes was recognized, where the original versions of electrospinning devices were patented by Cooley and Morton (1902) and Morton (1903) [44–46]. For these devices, a negatively charged metallic chain was used as a collector. Almost three decades later, Hagiwara et al. reported the electrospinning of silk [47]. A scientific breakthrough was the electrospinning of polymer solutions by Formhals in 1934 (and can be traced back to a German patent filing in 1929) [48]. Interestingly, none of these early patents could be commercially exploited, possibly due to challenges with scale-up and the lack of characterization equipment capable of probing the sub-micron physical features of the electrospun material [23].

The industrial production of electrospun materials advanced much faster in the former USSR, where by the late 1930s the first industrial facility for Petryanov filters used in gas masks was established [49]. The factory output capacity is believed to have reached an equivalent of 6.5 kg/h during the 1950–1960s [50,51]. Only recently has information related to the manufacture of these products been circulated outside of the USSR, where such filters remained a military secret to protect soldiers and civilians against potential radioactive aerosols [49]. Unexpectedly, in the 1970s, Simm et al. were able to file a patent for the production of fibers with diameters of sub-micron diameter fibers [2], however these innovations were not consolidated in the West until the 1980s when Donaldson Co., Inc. were the first to commercialize electrospun fiber technology in the US [52,53], followed by DuPont in 1989 (micro-denier fibers) [54]. In 1991 companies from the nonwovens sector within the fiber technology industry were the first to commercialize this technology in the form of filtration products [2].

Electrospinning from a solution had been largely overtaken by other fiber fabrication technologies until the mid-1990s where the activities of the Reneker group, who recorded and reported on the high added-value of the resulting organic nanomaterials [4,55,56] led to substantial academic attention to the method in the materials research and more specifically nanotechnology fields. Mathematical models formulated to examine Taylor cone formation [57] and polymer jet emergence [58] have been further developed to describe the asymptotic decay [59], stability [60,61] and bending of the jet [62]. The interdependence of fiber surface properties on polymer and instrument parameters was also studied in detail [63].

Currently solution electrospinning is a vibrant research area, demonstrated by the ever increasing rate of scientific publications per year. Agarwal et al. report that more than 2000 journal articles are published on electrospinning of polymers annually [15]. The leading nations by publication output are the USA, China, and South Korea, comprising approximately 70% of Web of Science listed publications. A growing proportion of solution electrospinning research is focused in the area of TE & RM on scaffold design parameters such as fiber diameter, pore size, porosity and pore architecture. From a processing point of view, key research questions include consistency of the electric-field and full control over 3D inter-fiber placement and intra-fiber molecular alignment [64–67]. Interestingly, the bulk of research papers focus on the varying applications of spinnable materials and solvent combinations [3,68]. A key concern is the accumulation of the evaporated solvent in solution electrospinning that not only can influence fiber quality and limit the control of experiments due to the necessity for configurations in well-ventilated areas [31], but pose environmental and health issues from exposure to solvents as well as recycling challenges for both research and industrial applications [69]. In fact, one of the great challenges for the large solution electrospinning community is the transition to real world products and industrial scale production. Although from a research point of view this field is largely driven with a nanotechnology perspective, the observation should be made that most

publications show fiber diameters in the sub-micron rather than nanoscale range, where the National Nanotechnology Initiative defines nanotechnology as “the manipulation of matter with at least one dimension sized from 0.1 to 100 nm” [70].

The physical nature of charged jets, with a large and complex degree of material/solvent, process and environmental parameters to account for and control makes process optimization challenging; often due to sub-optimal viscoelastic properties, limited numbers of molecular interactions and inadequate solubility [20]. For that reason, the high throughput and reproducible fabrication of products built by nanofibers is a key question to be answered before any successful commercialization can take place. A large number of patents related to membranes and devices built via electrospinning are focused on filtration systems [71]. A recent patent survey by Persano et al. shows that the number of issued patents has significantly increased in the 21st century, with more than 160 patents issued in 2011 and close to one thousand patents published in the last decade [23]. DuPont (6%) and Donaldson (4%) as well as the University of Akron lead the patent listings. In addition to air and water filtration [56], reported potential applications of electrospinning include protective clothing and armor [72] and composite reinforcement [73]. Though to date, limitations in the scale-up capacity of electrospinning and the ability to produce sufficient quantities within reasonable time frames have been acknowledged [70]. However it has been reported that these manufacturing issues are being addressed [74]. The application of electrospun fibers to photovoltaic, energy storage devices and management devices is also gathering significant interest, where less volume of material may be required [75–78]. Furthermore, it has been highlighted that biomedical and healthcare applications require relatively small quantities of electrospun fibers and are an increasingly popular area of investigation for wound dressings, implant interfaces, drug delivery devices, scaffolds for TE applications and/or *in vitro* disease platforms [63]. Electrospinning from the melt has been investigated to a lesser extent, since it typically results in larger diameter fibers than from solution. Recent publications demonstrate that melt electrospinning fibers with single-micron and sub-micron diameters is possible [31,79–83]. Thus, there remains room for improvement when looking towards process scale-up and optimization of most current solution electrospinning technologies.

To our knowledge, melt electrospinning was first described in a patent in 1936 [84] and it was not until 45 years later that a series of three papers described the same process [58,85,86]. In fact, only the first of these papers demonstrated electrospinning of polymer melts, producing polyethylene (PE) and polypropylene (PP) fibers [58]. The second paper investigated melt electrospinning using silicone oil as a model fluid [85] while the final paper described the droplet deformation of PE or Nylon-12 (N12) dissolved in hexane [86]. The resulting electrospun fibers had diameters ranging from 75  $\mu\text{m}$  to 400  $\mu\text{m}$ . Studying variables that influence the electrospinning process, Larrendo and St. John Manley first reported that the diameter of the fibers decreases with increasing applied voltage ( $V$ ) (where an increased electric field strength ( $E$ ) induces

greater acceleration and electrostatic drawing on the jet) and higher melt temperature ( $T_m$ ) (that decreases  $\eta_{melt}$  and resistance to being electrostatically drawn) [86].

Another extended period followed without publications on the melt electrospinning process. In 2000, Kim and colleagues compared the thermal properties of polyesters poly(ethylene terephthalate) (PET) and poly(ethylene naphthalate) (PEN) before and after electrospinning, to assess the suitability of such fibers for various applications. Electrospinning was reported to increase the crystallinity and decrease the glass transition temperature ( $T_g$ ) as well as the crystalline peak temperature, potentially due to reduced average molecular weights ( $M_w$ ) following thermal degradation [87]. In 2001, a series of conference abstracts followed by a journal article by Reneker & Rangkupan described the melt electrospinning of PE, PP, PET, and PEN in a vacuum [88–91].

The next important publication that presented further understanding of the melt electrospinning process and significantly contributed to the design of prototypes and devices was presented by Lyons et al. [79,92]. Fibers from PP and PET were produced with a diameter range from hundreds of nanometers to hundreds of micrometers. It was described that the  $M_w$  of the polymer is a key parameter in the electrospinning process: with a relatively weak E it might become impossible to develop a Taylor cone and spin a continuous fiber using a high  $M_w$  polymer, where the higher degree of polymer chain entanglements provide too much resistance to the electrostatic drawing force. Alternatively, using a too low  $M_w$  polymer with relatively high E would result in breakup of the jet stream. The increase in nozzle temperature resulted in a decrease in the average fiber diameter (AFD) [79].

Since these early publications, melt electrospinning research slowly gained traction. Five research groups in particular have contributed to the current main body of research and its future directions. Joo and colleagues have focused on theoretical modeling of the process with experimental validation using Nylon-6 (N6) [93], PP [94], and poly(lactic acid) (PLA) [80–83,95]. Ogata and colleagues have similarly focused on the effects of processing parameters during a laser melt electrospinning process [96–101]. Dalton and colleagues have initially sought to optimize the processing conditions for biodegradable polyesters [29–31,102–104], while beginning to explore applications for melt electrospun fibers in biomedical areas such as the production of TE scaffolds [105,106]. Collaboration between the Dalton and Hutmacher laboratories resulted in melt electrospinning used in a direct writing approach for a range of scaffold designs used originally in different TE applications and more recently as an important component in the development of *in vitro* and *in vivo* disease models [27,28,32,103,105,107,108]. Finally, a significant amount of research has been recently published on needleless melt electrospinning systems by Yang and colleagues including the scale-up production for applications such as filtration [109–114].

More than 70 melt electrospinning journal articles have been published since 2010, as opposed to 22 publications between 2006 and 2009, and only three prior to 2006. Assuming such progression in the scientific literature, we

hypothesize that by 2020, over 100 papers focused on melt electrospinning will be published annually. In many regards, melt electrospinning research is a processing technology in its infancy and this review aims to invite and motivate the polymer research community in large to increase our knowledge on this topic and expand both the academic and industrial applications in which melt electrospinning is used.

### 3. Existing fiber fabrication technologies

To appreciate the full technical dimension, and how melt electrospinning move forward from a basic and translational research point of view and ultimately towards being a viable process choice for specific industry sectors, it must deliver added value or provide unique applications not achievable by currently established polymer fiber forming processes. Therefore, a discussion of other fiber technologies is warranted in this review. Currently applied spinning technologies are all based on extrusion of a polymer through a spinneret, allowing the continuous production of single or multi-filament materials. The polymer is either mechanically drawn as it is wound onto a spool (spinning), blown by pressurized gas or subject to centrifugal forces. The properties of the end product of each spinning technology depend on the specific process, material chosen and processing parameters adopted. Typically, spinning methods are classified into three groups according to the mechanism of solidification of the extruded material: solution spinning (evaporation or coagulation); emulsion spinning (phase separation); or melt blowing/spinning (cooling) [115]. The number of different polymers that can be processed by using solution electrospinning is almost endless; however from a manufacturing point of view, the production of polymeric fibers based on melt processing is often still preferred [23]. Table 1 lists selected fiber processing technologies with their advantages and disadvantages.

#### 3.1. Solution spinning

Similar to solution electrospinning, other solution spinning techniques rely on solvent vaporization. This work is extensively reviewed by Persano et al. [23] and Luo et al. [50] and includes: wet spinning [116–118]; dry spinning [119,120]; flash spinning [121,122]; liquid crystal spinning [123,124]; and gel spinning [125,126]. Advantages with using solution spinning include processing those polymers that are thermally unstable [23].

The solvent removal process varies between wet and dry spinning. For wet spinning, the dissolved polymer thread passes through a coagulation bath that contains a solvent that is miscible with the spinning solvent. However this coagulation bath solvent is a non-solvent for the polymer and assists in fiber solidification. This process is slower than dry spinning, where fiber solidification requires evaporation or gas-assisted drying around the extruded filament. Another variation on solution spinning is flash spinning. This approach relies on a difference in pressure that drastically affects fiber formation.

**Table 1**

Selection of fiber manufacturing processes and their advantages and disadvantages.

	Fibre diameter	Advantages	Disadvantages
Melt electrospinning	<100 nm to 500 $\mu\text{m}$	Direct writing capability; solvent free; low cost; diameter is proportional to mass flow rate	Low output; device is time consuming to build. Limited number of polymers tested. Polymers require some thermal stability
Solution electrospinning	<50 nm to 10 $\mu\text{m}$	Simple to establish; low cost; suitable for many polymers; sub-micron diameters readily attained	Low output; direct writing is difficult; significant solvent is generated
Melt spinning	1 $\mu\text{m}$ to 500 $\mu\text{m}$	High output; very consistent production; can be used in weaving technologies; industrially successful	Requires drawing onto a spool. Variable diameters at high stretching; difficult to attain sub-micron diameter fibers; significant cost to establish
Solution spinning	1 $\mu\text{m}$ to 200 $\mu\text{m}$	Can process thermally unstable polymers; diversity in the number of configurations (e.g. flash, liquid crystal, gel spinning); industrially successful	Solvent requires removal. Complex coagulation baths needed for wet spinning. Dry spinning requires significant solvent removal systems
Melt blowing	<500 nm to 10 $\mu\text{m}$	High output; industrially successful	High cost to establish, therefore to perform research; difficult to control fibre architecture

### 3.2. Emulsion spinning

Emulsion spinning is typically employed to produce fibers from insoluble and non-melting compounds. The method is particularly well suited for processing high melting point fluorocarbons [127], inorganic materials [128] and flame retardant formulations [129]. Finely ground materials are mixed into different polymer solutions: with the emulsion extruded into a coagulation bath (wet emulsion spinning); or into air, where it solidifies through evaporation (dry emulsion spinning) [129]. Key topics of interest for emulsion electrospinning include pharmaceutical encapsulation [130] or functional dopants and light emitting dye, as well as to induce high alignment of both polymer and composite fibers [23].

### 3.3. Application of pressurized gas

Melt and jet blowing are capable of generating micro- and nanofibers from polymer melts, rather than polymers in solution. Low  $\eta_{\text{melt}}$  polymer melts extruded through a spinneret (die) are disrupted with a high velocity gas/air stream that is often heated [131–133]. These processes take place over relatively short spinneret to collector distances (TCDs). The deformation forces due to the pressurized gas jet rapidly reduce the filament diameter: where fibers can be elongated from macro- to sub-micron diameters in  $5 \times 10^{-11}$  s, and the depositing fibers are instantly spun bonded as a nonwoven [134].

Currently, the highest industrial yield of ultrafine fibers is produced from melt blowing. Though nanofibers have been achieved, melt-blown nonwovens often have a broad diameter distribution that ranges to above 20  $\mu\text{m}$  [135]. The smallest, most uniform commercialized melt-blown fibers have diameters of 2  $\mu\text{m}$  [136]. Challenges include inconsistent fiber properties, limited number of suitable polymers, spherical particles also contained in the fiber mat, breakup between the die and collector and achieving fibers with diameters smaller than 500–800 nm

[18,137,138]. Much of the complexity of the process lies in the die design that must be optimized for each material to be processed and the required diameter distribution profile [131].

Recently, Hills Inc. and Irema Filters developed an innovative melt blowing technique that can generate PP nanofibers down to 250 nm AFD [139]. However, only PP types with high melt flow index (MFI) are suitable. Furthermore, high investment costs are required for melt blowing machinery with very fine orifices, and the equipment requires a high material throughput. Thus the application of this technology is linked strongly to economics of scale of the target product [139].

### 3.4. Melt spinning

In contrast to pressurized gas processes, melt spinning takes place over relatively long TCDs, allowing sufficient cooling of the filament so that there is no spin bonding that would create a nonwoven fibrous mat. Instead a single filament is continuously wound onto a spool, where mechanical drawing of the solidified filament reduces the AFD [140]. For melt spinning, the take-up speed, drawing temperature and draw ratio largely govern the eventual mechanical properties, particularly if flow induced crystallization (FIC) is induced. Annealing can further enhance the properties of the fiber, including an earlier onset of strain hardening [141]. Melt spinning allows the highly reproducible production of kilometer length fibers that are often used in knitting, weaving, or braiding [142,143].

Avoiding solvent use as part of melt spinning means no residue or solvent recovery challenges: there is no requirement for recycling/removal of toxic solvents, improving the safety and throughput of the process [23]. Therefore, melt spinning has much higher productivity and lower manufacturing costs than solution spinning [144]. Additionally, there are solvent evaporation issues from a health and safety point of view for the work force,

where the toxicity of residual solvent is an issue for biomedical applications. Furthermore, polymers having no appropriate solvent at room temperature (RT) (such as PE, PP and PET) can be processed. Many of these advantages of melt processing over the use of solvents can be extrapolated to the comparison between melt and solution electrospinning.

Melt spinning also provides the advantage of producing multi-component systems and products: where many combinations of components have few common solvents, that would otherwise highly complicate the manufacturing process [83]. While the large spinning speeds allow high throughput, drawing instabilities may cause non-uniformity in the fiber diameters. A further limitation is that the high  $\eta_{melt}$  needed for melt spinning makes it very difficult to create sufficiently high forces to mechanically reduce fiber diameters to less than 1  $\mu\text{m}$  [23].

Recently, scalable techniques such as film splitting [144] and centrifugal spinning [145–148] have been developed that produce nonwoven mats with fiber diameters as small as 100 nm. Template melt extrusion is another complex process that allows isolated fibers with diameter ranges from 150 to 400 nm. However, fiber lengths correspond to the length of the template pores and are relatively short (i.e. 60 mm) [149]. Although currently melt electrospinning does not offer the same volumes of production, sub-micron diameter filaments are achievable without the inherent mechanical complexity of these processes and over relatively short distances by using electrostatic rather than mechanical drawing [29,83].

Flash spinning, melt and jet blowing and centrifugal methods are known as random-type production methods producing nonwoven fibrous mats [150,151]. However aligned fibers are generally difficult to obtain using these methods due to the speed of fiber collection and bonding after leaving the spinneret [151]. Melt electrospinning is similar to these processes in the sense that fibers will collect as a nonwoven on a static collector. However, since the elongation of the melt electrospinning jet is relatively slow, by mounting a collector surface onto a translating stage, fibers can be accurately placed and stacked upon each other with considerable precision (Fig. 2). Therefore, melt electrospinning offers the potential for improved control over fibrous substrate characteristics including complex porous features. Moreover, through modified spinneret designs, melt electrospinning permits the fabrication of composite fibers as in melt spinning. Future industrial niches for melt electrospinning most likely reside in the production of new high-performance materials that augment existing fiber technologies.

#### 4. Principles of melt electrospinning

Fundamentally, the electrospinning process involves applying an electrical potential between a polymer solution or melt and an electrically conducting collection surface. Typically the polymer is supplied from a storage chamber to a capillary, known as a spinneret. Some force (i.e. plunger, air pressure) within the chamber forces the polymer solution/melt to the spinneret [58]. When the polymer emerges from the spinneret, an electrical charge is introduced onto

the surface of the polymer meniscus in the presence of an electric field. These electrical charges generate forces that draw the polymer fluid towards the collector.

As charge in the fluid builds up, resulting repulsive interactions cause the droplet to deform according to EHD principles, where the deformation is influenced by two competing forces: the surface tension ( $\gamma$ ) of the fluid that favors spherical shapes with small surface areas; whereas repulsive Coulombic forces promote large surface areas. When forces due to charge repulsion exceed the  $\gamma$  of the droplet, the drop deforms into a conical profile termed the “Taylor cone” (Fig. 3A–C) [152]. Once a critical  $V$  is exceeded, and provided the liquid resists breakup, a charged jet ejects from the Taylor cone and is electrostatically drawn across a spinning zone towards the collection surface that maintains a different electrical potential [1].

The principle behind the formation of a Taylor cone on the surface of a liquid is believed to be universal: if the electrostatic pressure ( $p_e$ ) overcomes the capillary pressure ( $p_c$ ) then a Taylor cone forms [40].  $p_e$  on the liquid surface is defined as [153]:

$$p_e = \frac{1}{2} \varepsilon E^2 \quad (1)$$

where  $\varepsilon$  is the relative permittivity of the surrounding gas, and  $E$  is the intensity of the electric field.  $p_c$  is defined from the Laplace–Young equation in the form [153]:

$$p_c = \frac{2\gamma}{r} \quad (2)$$

where  $r$  is the mean curvature of the surface. In the most common experimental setup for electrospinning, high voltage (HV) is applied to the capillary that acts as an electrode. In this case the mean curvature of the surface is represented by the inner radius of the capillary. Thus, the condition for formation of the Taylor cone can be written as [153]:

$$p_e \geq p_c \quad (3)$$

Solution electrospinning relies on solvent evaporation from the electrified jet before it reaches the collector, where it deposits as solidified polymer fibers. Initially the electrified jet travels directly towards the collector in an initial thinning zone. As the jet begins solidification, the current flow switches from Ohmic to convective as the electric charge ( $e$ ) moves to the fiber surface resulting in a second zone of fiber formation. In this secondary zone, as the surface charge density ( $\sigma_q$ ) increases, small perturbations in the jet caused by non-axisymmetric bending instabilities are exaggerated by the electrostatic repulsion of like charges. As a result, the jet is subject to a “whipping” phenomenon where it accelerates laterally to the flight path, causing it to rapidly bend and turn [154,155].

Fiber morphology is influenced by the competing forces that the solution electrospinning jet is subjected to. Newtonian liquid jets not subject to electric forces but subject to axisymmetric Rayleigh instabilities (where  $\gamma$  becomes non-uniform along the jet) tend to break up into droplets (as do electrosprayed polymers) to reduce free surface energy [40]. These axisymmetric Rayleigh instabilities are suppressed by the additional elongational stresses due to the electric field in electrospinning, so the electrified jet is

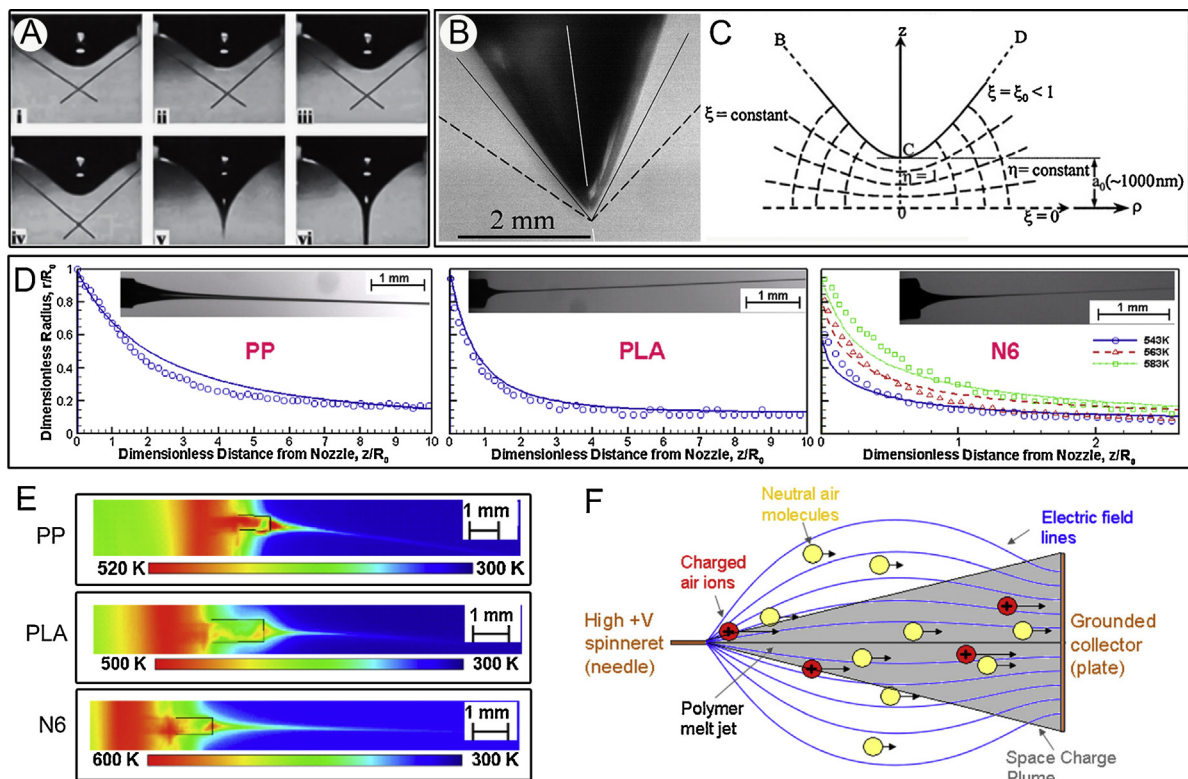


**Fig. 3.** ((A)–(C)) The evolution of the profile of a charged fluid droplet leaving a spinneret. The rounded conical profile becomes increasingly pointed until  $p_e$  in the droplet overcomes  $p_c$ , where a jet emanates downwards from the apex of the cone to form a “Taylor cone”. The electrically charged jet rapidly elongates away from the droplet, causing it to thin towards a collector. A stable shape is maintained along the Taylor cone provided that the volume of polymer departing via the jet is balanced by the volume of polymer delivered to the spinneret. The Taylor cone profiles shown in ((A)–(C)) are taken from solution electrospinning experiments [154,374], since this fundamental work is not yet comprehensively characterized for melt electrospinning. (D) The electrified melt jet, however, has been modeled and finite element analysis used to predict the diameter of the jet (travelling horizontally in these examples) as a function of spinneret diameter. (E) Temperature profiles showing rapid cooling of melt electrospun PP, PLA and N6 jets. The degree of EHD-driven cooling can be modified by strategies including varying the electric potential between the spinneret and collector or increasing convection though the airborne zone (F). Schematic of EHD-driven air flow in melt electrospinning. Copyright Permission Sources: (A) [374], Copyright 2001, AIP Publishing; ((B) and (C)) [154], Copyright 2001, AIP Publishing; ((D)–(F)) [95], Copyright 2011, AIP Publishing.

continuously maintained. The viscoelastic polymer jet generates “beads-on-strings” as a result of slower jet breakup or uniform fibers when there is no jet breakup at all. Two additional conducting instability modes [156] have been reported: an axisymmetric conducting instability (where charge is not equally distributed along the jet); and the non-axisymmetric bending instability that causes whipping [60]. Both the processing parameters and the fluid properties greatly influence which one of these modes dominate.

The whipping instability dominates (as reported in most electrospinning literature) when using sufficiently high electric potentials [157]. Due to whipping, the electrified jet travels a longer distance prior to deposition, allowing more time to be stretched [158]. This subsequent elongation and thinning leads to the formation of fibers with reduced sub-micron scale diameters by the time the jet arrives at the collector. However deposition is characteristically chaotic, where the jet deposits randomly to create a nonwoven mesh of solidified fibers [70]. Residual charges not transferred to the collector can remain on the solidified fibers and affect how subsequent fibers are deposited.

Electrospinning research has been focused towards the fabrication of nanofibers. The majority of this research involves the use of solution electrospinning and there has been less investigation into melt electrospinning since this method most commonly produces fibers larger than 1  $\mu\text{m}$ . In solution electrospinning, the jet can thin by an order of magnitude solely due to the evaporation of solvent. Solvent also contributes largely to  $\sigma_q$ , that is responsible for the bending instabilities causing the jet to whip [154,155]. On the other hand, by using high  $\eta_{\text{melt}}$  and non-conductive polymer melts (typically with electrical conductivity less than  $10^{-10} \text{ S/m}$ ) [82], the absence of a solvent greatly reduces  $\sigma_q$  and therefore dampens the bending instabilities. When the temperature of the electrified jet is below the  $T_g$  of the polymer, rapid solidification of the molten jet further suppresses whipping; since greater disturbance forces are required to overcome the  $\gamma$  [28]. The initial region of the electrified molten jet has often a considerable volume and movement from the midline is reduced [31]. The suppression of bending instabilities considerably reduces the degree of stretching the melt electrospinning jet encounters before it solidifies [63]. With the

additional lack of thinning from solvent evaporation, melt electrospinning has typically been characterized by larger diameter fibers than from solution [82].

Through careful process design, optimization and control, sub-micron fibers can be obtained in melt electrospinning [81]. Similar to in melt extrusion systems, this can be accomplished by control of the extensional viscosity and solidification of the filament via the thermal environment [159,160]. However since melt electrospinning is a further convoluted problem, electric field and charge transfer effects must be considered in addition to the heat transfer effects on momentum and mass conservation, viscoelastic properties, and, in some cases, in-flight crystallization [95]. Recently, researchers have demonstrated that by making additional material modifications prior to processing, fiber diameters approaching true nanoscale magnitudes can be produced using polymer melts [161]: rather than delivering the polymer in a solution, including additives to increase the electrical conductivity of the polymer melt is another strategy to increase the charge density on the melt jet, thereby inducing a greater degree of stretching on the jet during flight [161,162].

#### 4.1. Jet thinning

Extensional viscosity is one of the main factors that affects thinning of the jet. For a polymer melt, both the temperature and molecular architecture are two key parameters that have a great impact on the final fiber quality and especially the dimensions. While the temperature of each zone can be controlled during melt electrospinning experiments, it is usually non-uniform throughout the spinning zone. HV is typically applied through an isolated spinneret that is in contact with air, rather than a parallel plate (that would create a uniform field). Joo and colleagues have developed a non-isothermal model for melt electrospinning based on the non-uniform electric field from the spinneret to collector typically established in such needle-plate geometry experiments [82].

By approximating negligible interactions between the surface charges with the applied external electric field and negligible axial conduction, the initial  $\sigma_q$  can be calculated at the Taylor cone, assuming the fluid at the spinneret to be nearly Newtonian. Here, a momentum term balance requires that Newtonian stresses,  $\gamma$ , and the electric driving force are balanced. For most Newtonian fluids and shear-thinning fluids with low  $\mu$  and viscoelasticity, they exhibit:

$$R_{(z)} \propto z^{1/4} \quad (4)$$

scaling of the jet radius far away from the spinneret (in the stable zone), where  $R$  is the jet radius and  $z$  is the axis of jet travel. This scaling arises from the balance between the tangential electric stress and the fluid inertia occurring far down the stream where other contributions to the momentum balance decrease to zero. However the underlying assumption of the balance of inertial and electrical forces in the asymptotic region does not apply to highly viscous and viscoelastic fluids (e.g. polymer melts). Highly viscous and viscoelastic fluids exhibit high tensile forces throughout the spinning zone, particularly in non-isothermal conditions. Here, the inertia is often minimal, and the tensile

forces due to the polymer melt can balance the electric field driving force towards the collector [82].

#### 4.2. Quenching of the melt electrospinning jet

In their development of a melt electrospinning heat transfer model, Joo and colleagues performed a steady state shell balance on a fluid element in the Lagrangian frame to satisfy the conservation of energy requirement. They reported that ultimately, the change in internal energy of the polymer melt is especially balanced by radial convection to the surrounding cooling air [95]. This radial convection derives from the jet surface heat flux boundary condition and enters the conservation equation when a thin filament approximation (one-dimensionalization of the problem) is used. The heat transfer coefficient is typically obtained from empirical correlations, that relate system geometry and fluid flow characteristics to the thermal boundary layer formation.

Although correlations widely used in conventional melt spinning literature produce good agreement with experimentally observed thermal profiles, infrared (IR) measurements of the electrified molten jet show rapid thermal quenching that is an order of magnitude greater than would be expected. A number of alternative heat transfer mechanisms and enhancements were considered, including: natural convection (that is typically neglected in favor of forced convection due to relatively high jet velocities); radiation (typically negligible below  $\sim 600\text{ K}$  compared to convection); and humidity (where literature suggests that air humidity can result in as much as 20% heat transfer enhancement) [163,164]. However, such conventional heat transfer mechanisms were not expected to produce the experimentally evident 10-fold heat transfer enhancement. Turning to the heat exchange and electronic circuit literature [165–173], Joo and colleagues found that the largest heat transfer enhancement mechanism that separates melt electrospinning from melt spinning is due to EHD effects: strong electric fields can result in significant corona currents, that disturb the thermal boundary layer and can enhance the heat transfer rate as much as 60-fold in some applications.

In contrast with electrically conducting polymer solutions in electrospinning, polymer melts can be highly insulating. When HV is applied to a needle-plate geometry separated by dielectrics (air and the polymer melt), a corona field is often produced. This condition is obtained when the applied potential exceeds the corona onset, but is below the air gap breakdown  $V$ . During the corona discharge, the local electric field near the needle tip exceeds the breakdown  $E$  in air:

$$E_0 = 3.2 \times 10^6 \text{ V/m}; \quad (5)$$

and as a result, air molecules become ionized. This region is referred to as the ionization zone, and it contains ions of both polarities. Further away from the needle, where the local electric field decreases below  $E_0$ , no further ionization occurs. However, in the drifting zone, also known as the space charge plume, ions of the same polarity as the needle are transported from the needle to the plate due to action of the electrostatic forces. Along their flight path, the

ions can exchange momentum with and accelerate neutral air molecules. When a positive HV is applied to the needle, a positive corona is formed, and thus, positive air ions are observed in the drifting zone [82]. When air is used as the quenching fluid, heat transfer is typically enhanced by an order of magnitude [165–167,172,173]. Fig. 3D and E show experimental jet radius and temperature profiles presented by Joo and colleagues for (a) N6, (b) PP and (c) PLA compared to model predictions, where the charge effects on thinning of the melt jet are considered.

#### 4.3. Crystallization of melt electrospun fibers

Electrospinning of polymer melts results in amorphous or semi-crystalline structures. The alignment of molecular chains due to the jet being electrostatically drawn can induce further crystallinity. Joo and colleagues found that fast-crystallising polymers such as Nylon can produce semi-crystalline fibers when processed at high temperatures [80]. In this case, the electrified molten jet undergoes rapid elongation and therefore thinning, resulting in a build-up of internal stresses. Initially only limited thermally-induced crystallization (TIC) occurs in this region of the jet due to the higher temperatures and limited polymer chain orientation. However, as the temperature of the electrified jet drops below the melting point the resulting high  $\eta_{\text{melt}}$  reduces the thinning rates. At this point, the jet is reaching a cylindrical profile. The build-up of significant internal stresses causes chains to align rapidly, reversing the trend of crystallization from that in the initial thinning region. At this stage because the jet is so thin, the temperature profile and radial stresses are approximately uniform. Due to the brief in-flight residence time of the molten jet, the TIC is not significant. However, the large internal stresses which develop result in significant polymer chain alignment that can facilitate the onset of flow-induced crystallization (FIC) (that occurs much more rapidly than TIC) due to enhanced chain reptation and chain segment nucleation [80].

Joo and colleagues attributed the onset of rapid FIC from TIC due to the competition of thermal and stress effects of crystallization on the elongational viscosity of the jet. At lower  $T_m$ , the viscosity dominates, while at higher  $T_m$ , there is a rapid increase in viscosity caused by rapid flow induced phase transition, where rapid FIC can have a significant impact on the final fiber diameter. Increased  $T_m$  results in greater initial jet thinning and higher internal stresses, causing the faster onset of FIC. In their modeling of the melt electrospinning jet, Joo et al. identified that the “more complex issues of crystalline phase morphology formation and evolution in FIC remain to be addressed” [80].

#### 4.4. Charge interactions

The unique feature of electrospraying and electrospinning is that oppositely charged electrodes are separated by a space that is not filled with a liquid through which charge convection can take place. Instead, the EHD driving forces cause the fluid containing the charge carriers to span the air space between the electrodes. The observed phenomenon is that the fluid physically traverses

the distance from one electrode to the other. As such, there are three process domains of charge interaction in electrospinning which have been identified as important: formation of charge carriers; charge transport; and residual charge.

##### 4.4.1. Creation of charge carriers

For the majority of electrospinning equipment configurations, the needle-like spinneret has a relatively small radius of curvature compared to the collector surface. As such, the mode of charge carrier generation is due to high electric field induced emission: the process of ejection of electrons into the surrounding medium from the surface of an electrode under the influence of a locally high electric field. In typical laboratory electrospinning experiments, the high fields necessary for emission can only be achieved at the tips of needles or at blade-edges [174]. Under these conditions, electrons can associate with polymer melt molecules and become ionic current carriers. Similarly, ion emission is the process of ejecting ions into the surrounding fluid as a consequence of the withdrawal of electrons into the electrode. Field emission requires electric fields on the order of  $10^9$ – $10^{10}$  V/m in order that electrons can cross the boundary between the metal electrode into the fluid by a quantum tunneling mechanism [174].

The outcome of using a high electric field is to increase the possibility of electrons appearing on the liquid side of the metal-liquid boundary. Electrons emitted in this manner will be trapped to form a negative ion or a charge-shielding polarized complex. Unlike the immobile traps in solids, the liquid traps are mobile and will move down the electric field gradient away from the emitter. The momentum interchange that results as a consequence of collisions between the mobile, charged traps and the neutral molecules of the liquid imparts a kinetic energy to the liquid that causes it to flow along the path of charge flow [175,176].

##### 4.4.2. Charge transport

The electrical conductivity of the electrified polymer melt jet is often low and accurate measurement of the current has proven difficult. Joo et al. assume instantaneous radial charge, where the component of the electric field at the spinneret normal to the jet surface can be approximated as zero. The “leaky dielectric” model, better suited to slightly conducting liquids [177,178] proposes that  $e$  segregates rapidly to the jet surface. As the jet cools, the decreasing conductivity dampens the significance of axial conduction. Here, the decreasing surface charges are assumed to not affect the applied external electric field [82].

HV applied to a spinneret can result not only in charge injection into the molten polymer, but also the less dense ambient atmosphere. Joo and colleagues have shown this leads to corona discharge in the vicinity of the spinneret that causes charged air surrounding the jet to be rapidly accelerated towards the collector. Shown in Fig. 3F, this air charge transport mechanism takes on a near conical shape and the space charge density decreases with distance from the spinneret due to Coulombic repulsion. Calculated air velocity profiles for N6 were compared to the jet velocities

and shown to be three orders of magnitude higher than the jet velocities in the initial thinning zone. Subsequently, the driving electric field rapidly decreases and the air velocity approaches its asymptotic value.

While there is vast literature on the mechanisms for initiating and generating electrospun fibers, there appears no consensus on the physical mechanism for the “discharging” or transfer of charge from electrospun fibers to the collector as they are deposited. Collins et al. have comprehensively reviewed the literature addressing charge characteristics of solution electrospun fibers, however there is currently no literature addressing this issue specific to melt electrospun fibers [174].

A simple model of discharging assumes that most of the charges on solution electrospun fibers eventually discharge to the conducting substrate. However, this assumption is questionable: although the injected polymer solution does allow charge transport in the liquid phase, the fiber solidifies before it reaches the collector. It is widely reported that even after some portion of charge on electrospun fiber mats is dissipated, a measurable amount of residual charge remains [174]. After solidification, any residual charges are trapped either within the fiber or on the surface of the fiber. Since the polymer fibers are essentially electrically insulating, it is highly unlikely that the trapped charges could flow as a constant current through the insulating fiber mat to the conducting substrate at a sufficiently high rate to maintain the electrospinning process. Therefore, it has been proposed that charges are carried not only by the polymer jet, but by other charge transport mechanisms including: the corona discharges surrounding the Taylor cone; corona discharges of the deposited fiber mat to the conducting substrate; parasitic electrospraying; and charge evaporation [174].

#### 4.4.3. Residual charge

According to Collins et al., a mat of electrospun fibers is essentially an electret: a dielectric material exhibiting the ability to retain or store electric charge over long periods of time [174,179]. Electrets are understood to dissipate excess charge by different mechanisms, depending on the polymer dielectric properties, solvent properties, ambient humidity/temperature and, specially, the locus of where the charges are trapped in the material. Prior to addressing mechanisms of charge dissipation, the mechanisms and location of charge storage in polymers warrants discussion.

Research on the physics of electrets highlights multiple ways for charge to be stored in polymers, including: electrostatic polarization due to the presence of dipole orientation (heterocharges), that can be attained either by orienting permanent dipole moments in the polymer or by inducing the polarization of mobile charges within the polymer; or by real charge injection (homocharges) where free charges can be injected into the polymer by a multitude of mechanisms including corona charging (previously discussed) [174]. In polymer electrets charge storage is dependent on an array of parameters including crystallinity [180], polymer structure and the presence of additives [181].

Current models describe localized states of chemical groups present in the polymer structure, called traps, that are distributed on the surface and in the volume of the

material. In a semi-crystalline polymer, traps are believed to exist at the interface of crystals and amorphous regions, as well as in the inner regions of spherulites [182]. In a purely amorphous polymer, charges are trapped in specific domains of the structure, such as heteroatoms and aromatic rings [183]. According to Sessler, surface traps may be due to surface defects, impurities, adsorbed molecules and broken chains, while volume traps are located at three distinct levels: atomic sites, molecular chains and crystalline region or crystalline-amorphous interfaces [184]. Since these charge carrier traps are dynamic systems dependent on environmental and structural characteristics, the typical valence-conduction band model does not fully apply.

The counterpart to charge storage or trapping is charge dissipation, that is also related to detrapping of the charges, and is dependent on charge movement through the bulk or surface of the dielectric. Since molecular relaxation due to chain movement is a major cause for detrapping, temperature plays a significant role in these events [185]. Moreover, holes and electrons may present large differences in mobility [185]. Three basic models attempt to describe molecular motions in viscoelastic polymers: (i) the barrier model where different conformations are separated by an energy barrier (activation energy), (ii) the Rouse model where chains are described as series of springs connected by nodes, and (iii) the reptation model where molecular motion is compared to a snake-like motion [174].

Although literature correlating viscoelastic models with charge decay processes is scarce, Lowell proposed a model where conduction currents in polymers submitted to electric fields may be generated based on a charge hopping mechanism: that involves the elastic displacement of a polymer chain that transports a charge from a trapped site to an empty site [186]. According to this model, even considering the limited mobility involved, rotation of side chains or pendant groups results in charge movement generating a decaying transient current.

It is widely recognized that the build-up of residual charge on solution electrospun fibers creates an insulating layer that eventually repulses the like charged electrospinning jet and therefore limits the achievable substrate thickness. Similarly, Reneker and colleagues have reported a disruption to straight electrified jets, observed as a pendulum-like motion caused by repulsive Coulombic forces between residual charges on the already collected fibers and the similarly charged molten jet that is deposited on the collector. The pendulum-like motion of the jet is sustained by the elastic stresses within the jet, and causes arching of the initially straight jet [187].

#### 4.5. Fiber deposition

In the absence of whipping instabilities, the melt electrospinning jet travels in a straight line from the spinneret to the collector. As the jet deposits onto a stationary collector, it buckles under compression (similar to that of falling viscous fluids) and the fibers coil around the midline. The patterns that result from coiling closely resemble those made by highly viscous fluids falling from a height and impinging a hard flat surface. The theoretical buckling frequency ( $\omega$ ) may be fitted by the following formula [188]:

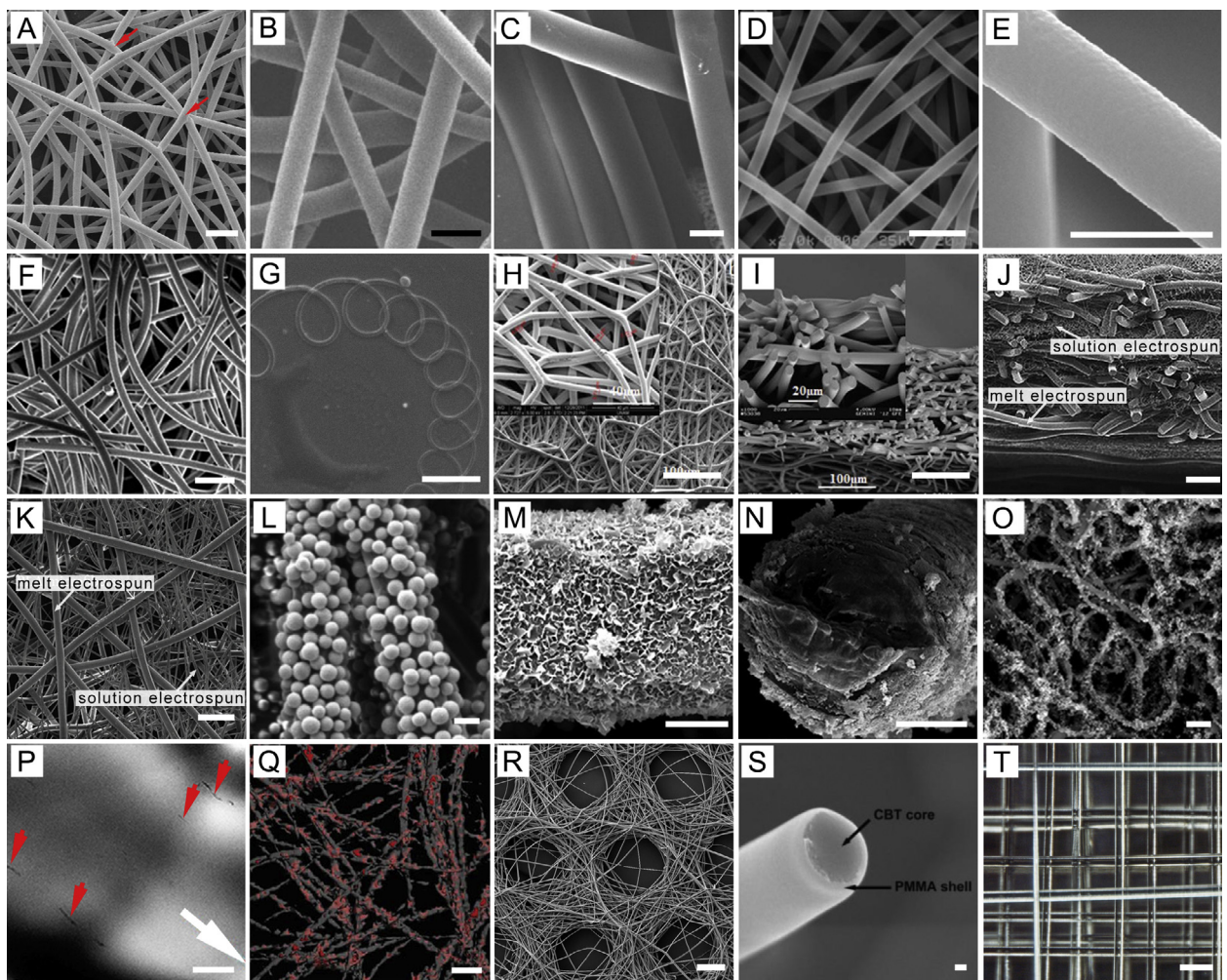


**Fig. 4.** Various melt electrospun materials. (A) Melt electrospun fibers often fuse at their crossover points (red arrows), shown here with a PEG-b-PCL/PCL blend [31]. Similar nonwoven melt electrospun fibers obtained using (B) PLLA [254], (C) low-density polyethylene (LDPE) [199], (D) poly(ethylene-co-vinyl alcohol) (EVAL) [97], (E) gas-sensing pitch fibers [242]. (F) a low molecular weight compound 1,3,5-triaminobenzene [201], and (G) nanoscale with a typical fiber diameter of ~100 nm [202]. (H) Top and (I) side views of a PU material show the typical morphology of a nonwoven [205], where uniform fibers deposit randomly onto a flat stationary collector. Multiphasic scaffolds that contain both sub-micron and micron scale fibers have been developed from (J) PLA [207] and (K) PLGA [206]. (L) Scaffolds have also been used as a base substrate to collect solution electrosprayed microspheres, containing encapsulated protein, which adhere to the melt electrospun PCL fibers to form a controlled release system which can be implanted *in vivo* [212]. (M) and (N) CaP coatings are important for bone TE scaffolds and can be deposited upon PCL fibers prior to cell culture [214]. (O) Particulates have been included, such as TiO<sub>2</sub> melt electrospun with PP [217]. (P) multi-walled CNTs (red arrows) [218] and (Q) strontium-substituted bioactive glass (red particles) within PCL fibers in order to provide key nutrients to seeded hOBs [219]. (R) When using electroconductive collectors with patterned voids, the gross melt electrospun fibre morphology replicates the pattern of the conductive material, shown here with PCL [221]. (S) Coaxial melt electrospinning has also been performed using thermochromic core-shell PMMA nanofibers loaded with CBT [222]. (T) While translating a collector under certain melt electrospinning conditions allows the controlled arrangement of fibers from materials such as poly(2-oxazoline) [223]. Scale bars are ((A)/(B)) 10 µm, (C) 20 µm, (D, E, F) 10 µm, (G) 1 µm, ((H), (I) and (J)) 100 µm, (K) 50 µm, (L) 10 µm, ((M) and (N)) 5 µm, (O) 10 µm, (P) 500 nm, (Q) 200 µm, (R) 200 µm, (S) 100 nm and (T) 100 µm. Copyright Permission Sources: (A) [31], Copyright 2007, Elsevier Ltd; (B) [254], Copyright 2012, John Wiley & Sons Inc; (C) [199], Copyright 2009, John Wiley & Sons Inc; (D) [97], Copyright 2007, John Wiley & Sons Inc; (E) [242], Copyright 2014, Springer Science + Business Media; (F) [201], Copyright 2012, the Royal Society of Chemistry; (G) [202], Copyright 2012, AIP Publishing; (H) and (I) [205], Copyright 2014, John Wiley & Sons Inc; (J) [207], Copyright 2013, Creative Commons Contribution Licence, Hindawi Publishing Corp; (K) [206], Copyright 2010, Elsevier Ltd; (L) [212], Copyright 2013, John Wiley & Sons Inc; (M) and (N) [214], Copyright 2012, Elsevier Ltd; (O) [217], Copyright 2014, Springer Science + Business Media; (P) [218], Copyright 2014, the American Chemical Society; (Q) [219], Copyright 2013, John Wiley & Sons Inc; (R) [221], Copyright 2014, Elsevier Ltd; (S) [222], Copyright 2009, John Wiley & Sons Inc; (T) [223], Copyright 2014, Elsevier Ltd. (For interpretation of the references to color in this figure legend, the reader is referred to the web version of this article.)

$$\log \left( \frac{\omega}{v} \frac{d}{\rho} \right) = -0.0194 \log \left( \frac{\mu Q}{\rho g d^4} \right) + 0.2582 \quad (6)$$

where  $d$  is the jet diameter,  $v$  is the jet velocity normal to the collector (where  $d$  and  $v$  are measured near the collector),

$Q$  is the volumetric flow rate in the jet, and  $\rho$  is the density of the liquid. For an uncharged viscous fluid jet, the driving force per unit mass  $g$  is gravity. However, in melt electrospinning the effects of  $g$  are negligible compared to the electric force per unit mass on the charged jet [188].

The low-speed and low-strain-rate phenomenon of buckling in these circumstances results in Newtonian behavior with  $\mu$  being equivalent to the zero shear viscosity [188].

#### 4.5.1. Pore size and porosity

The wavelength of electrospun fiber coiling has been shown to be inversely proportional to  $\omega$ ; where increasing the fiber diameter will increase the wavelength of the coiling and therefore the inter-fiber distance in a resulting nonwoven mesh [63,189,190]. Eichhorn and Sampson present a theoretical model that demonstrates the prevailing role that AFD has in defining the scaffold porosity of random fiber networks. They provide an extensive review of the structural features that such networks exhibit, including mass distribution, surface area, fiber intersections and contact distributions, overall porosity and pore distribution [191].

#### 4.5.2. Mechanical properties

Electrospun fibers should possess enhanced mechanical properties compared to the bulk material from which they were processed due to higher chain orientation; resulting from being stretched in the electrified jet as discussed earlier [4,192]. Tan et al. conducted a study to determine the mechanical properties of single-strand electrospun poly( $\epsilon$ -caprolactone) (PCL) ultrafine fibers with AFDs of approximately 1  $\mu\text{m}$  and below [192]. They found that increases in the AFD decreased both the tensile strength and yield stress, and increased the strain at break. The yield strain was also inversely proportional to the fiber diameter [192]. Interestingly, no correlation was found between elastic modulus and electrospun fiber diameter. In comparison, gravity spun PCL fibers with AFDs around 100  $\mu\text{m}$  were reported to have tensile strength, yield stress and elastic moduli an order of magnitude lower than the fibers obtained by Williamson et al. [193]. The strain at failure for gravity spun fibers was approximately twice that obtained by Tan et al. [192].

Collecting electrospun fibers onto a rotating drum or wheel at speeds above the jet speed aligns the fibers in the direction of rotation. The electrospun jet is stretched further, with smaller diameter fibers and higher molecular orientation than nonwoven electrospun fibers [106]. Therefore, electrospun fibers produced with additional mechanical forces have higher elastic moduli and tensile strength. However, ductility is reduced and a lower strain at break is observed with fibers that have a reduction in diameter due to the higher 'draw ratio' applied [192].

The mechanical properties of electrospun nonwovens can also be influenced by how they are deposited. Influential factors include porosity; friction between fibers; thickness of the fibrous substrate and geometry; as well as the polymer  $M_w$  and its distribution [194–196]. Ko et al. reported that as AFD decreases in a melt electrospun PCL nonwoven substrate, the porosity of the substrate increases, leading to a decrease in elastic modulus and an increase in yield strength [190]. Croisier et al. performed macrotensile measurements on PCL fiber substrates fabricated using a higher  $M_w$  PCL compared to Ko et al. and showed a higher elastic modulus [196].

On a stationary collector surface, coiling of melt electrospun fibers is relatively focused and extended periods of fiber collection are required for the deposited fibers to expand over a large surface area as seen in solution electrospinning. Eventually the fibers collected directly under the spinneret will begin to affect the electric field exerted on the molten jet. At the same time, as described earlier, these fibers retain a small amount of residual Coulombic charge. Over time this stored charge accumulates so that the next fibers to be deposited are repelled away from the midline [187]. With increasing collection time, this results in a non-woven mesh with distinct circular patterns radiating from the centre of the collector [197]. As the melt electrospun mesh continues to thicken, newly depositing fibers will be increasingly insulated from the collector, causing the effect of the driving electrostatic force to be reduced. The fibers become less compacted, and eventually stack vertically to form a conical structure under the spinneret [198].

Improved theoretical understanding of the heat transfer, stress response, in-flight crystallization, charge transfer and dissipation mechanisms for viscoelastic melt electrospun polymer materials, coupled with knowledge of their behavioral response over varied operating parameters, spinning zone conditions and deposition effects will assist in improved process optimization, performance and applications of melt electrospun fibers.

## 5. Polymer parameters for melt electrospinning

Today, only a fraction of polymers commercially available have been melt electrospun (Fig. 4; Tables 2–4). Some are polymers that are difficult to dissolve and process into fine fibers using conventional fiber processing methods. For example, polymers such as polyolefins, and polyamides are only soluble in specific solvents and require high processing temperatures [28]. An appealing property of melt electrospinning is that with a homogenous polymer under suitable conditions, highly uniform fibers are readily achievable, that can be collected over a long period of time and exhibit very little inhomogeneity and/or changes in the fiber diameter [28,31]. The capacity to reach a consistent level of high fiber quality is definitely an advantage for batch-to-batch reproduction. Dalton et al. reported diameters of  $\pm 2\%$  for poly(ethylene glycol)-block-PCL/PCL) (PEG-*b*-PCL/PCL) blends (Fig. 4A) [29], while high uniformity was also achieved with PLA (Fig. 4B) [83,96,112], low-density polyethylene (LDPE) (Fig. 4C) [199] poly(ethylene-co-vinyl alcohol) (EVAL) (Fig. 4D) [97], electron-beam irradiated pitch (Fig. 4E) [200], self-assembling small compounds (Fig. 4F) [201] and even glass (Fig. 4G) [202].

PP, which cannot be readily dissolved in a solvent, was one of the first thermoplastics to be melt electrospun [58]. It has received significant interest due to its toughness, flexibility and unusual resistance to many chemical solvents, bases and acids, making it a widespread engineering plastic, particularly attractive in textile technologies. PP is currently used in many applications, and additives are widely available that can assist with specific processing purposes [28].

**Table 2**

Summary of melt electrospun PP with processing parameters and resultant fiber diameters.

Description	Viscosity related property	Melt heating	Feed rate	Spinneret diameter [mm]	Voltage <sup>a</sup> [kV]	Collector distance [mm]	Spin zone <sup>b</sup>	Collector <sup>c</sup>	Fiber diameter [ $\mu\text{m}$ ]	Ref
Isotactic, Sigma Aldrich	$M_w$ 190,000	Extruder; 200 °C	–	1.5	10–15/cm (Collector +ve)	20	–	Cu plate	10	[79]
Isotactic, Sigma Aldrich	$M_w$ 106,000	Extruder; 200 °C	–	1.5	10–15/cm (Collector +ve)	20	–	Cu plate	6.9	[79]
Isotactic, Sigma Aldrich	$M_w$ 12,000	Extruder; 200 °C	–	1.5	10–15/cm (Collector +ve)	20	–	Cu plate	3.5	[79]
Isotactic, Poly-Mirae	Melt index 900	Ceramic heater around syringe; 330–410 °C	–	–	35	100–180	Part of spin line 25, 100, 150 °C	Stainless steel plate	25–40	[244]
Isotactic, Poly-Mirae	Melt index 1500	Ceramic heater around syringe; 330–410 °C	–	–	35	100–180	Part of spin line 25, 100, 150 °C	Stainless steel plate	15–25	[244]
Isotactic, Sigma Aldrich	$M_n$ 5000	Cartridge heater; 230 °C	Heated piston Reservoir; gravity feed	Needle-less, with "rod" and "cleft" electrodes	20–30	100	–	Metallic plate	–	[153]
Isotactic, Shell 5520	Melt index 0.5	Electrically heated Al jacket; 220–240 °C	Air cylinder operated plunger; order of 1 m/min (spin rate)	2.2	10–23	10–30	Air, ambient temperature	Metallic plate	20–180	[58]
Isotactic, Moplen HP 561	MFI 44 cm <sup>3</sup> /10 min at 230 °C, zero-shear viscosity 23 Pa s	Glass syringe/heat gun; 320 °C	Syringe pump; 0.05 mL/h	0.58	20 (Spinneret –ve)	40	–	SEM stub	8.6	[31]
Isotactic, Novolen	$M_w$ 210,000 g/mol, MFI 15 cm <sup>3</sup> /10 min at 230 °C, zero-shear viscosity 75 Pa s	Glass syringe/heat gun; 270 °C	Syringe pump; 0.05 mL/h	0.58	20 (Spinneret –ve)	40	–	SEM stub	36	[31]
Isotactic, Novolen, Irgatec additive (1.5 wt%)	Zero-shear viscosity 33 Pa s	Glass syringe/heat gun; 270 °C	Syringe pump; 0.05 mL/h	0.58	20 (Spinneret –ve)	40	–	SEM stub	0.84	[31]
Isotactic (i-PP), Shanghai Yishitong New Materials Development, acrylonitrile in styrene (SAN) additive (0.5, 1.0, 2.0, 5.0 wt%)	i-PP $M_w$ 7000–8000, MFI 1500 g/10 min at 230 °C; 23 wt% SAN additive MFI 2.2 g/10 min	Electrical heater ring; 210–220 °C	45 Steel piston/cylinder; polymer drawn by HV	0.2–0.7	60 (Collector +ve)	140	–	Flat wire mesh	5–10	[247]
Isotactic (i-PP) and atactic (a-PP) mixed, blend ratios of i-PP/a-PP, 100/0.75/25, 50/50, 25/75, 0/100, Sigma Aldrich	i-PP $M_w$ 12,000, a-PP $M_w$ 19,600; zero-shear viscosity at 180 °C 0.8, 1.0, 1.3, 2.0, 2.5 Pa s	Band heater around stainless syringe; 180 °C	Motor controlled extrusion; –	1	12 (Collector +ve)	20	–	–	5–60	[230]

Table 2 (Continued)

Description	Viscosity related property	Melt heating	Feed rate	Spinneret diameter [mm]	Voltage <sup>a</sup> [kV]	Collector distance [mm]	Spin zone <sup>b</sup>	Collector <sup>c</sup>	Fiber diameter [ $\mu\text{m}$ ]	Ref
Isotactic (i-PP) and atactic (a-PP) mixed, blend ratios of i-PP/a-PP, 100/0.75/25, 50/50, 25/75, 0/100, Sigma Aldrich	i-PP $M_w$ 205,000, a-PP $M_w$ 19,600; zero-shear viscosity at 200 °C 1200, 580, 140, 50, 1.6 Pas	Band heater around stainless syringe; 200 °C	Motor controlled extrusion; –	1	12 (Collector +ve)	20	–	–	5–55	[230]
Atactic, Sigma Aldrich	$M_w$ 19,600	Extruder; 200 °C	–	1.5	10–15/cm (Collector +ve)	20	–	Cu plate	21	[79]
Atactic, Sigma Aldrich	$M_w$ 14,000	Extruder; 200 °C	–	1.5	10–15/cm (Collector +ve)	20	–	Cu plate	13	[79]
Monofilament	–	CO <sub>2</sub> laser; 5 W	190 $\mu\text{m}$ fibre feed; 0.04 m/min	0.19 (filament)	20	50	–	Cu plate	38	[209]
PP6315, PP6312, PP6310, Shanghai Expert in the Developing of New Material Co.	MFR 1500 (PP6315), 1200 (PP6312), 1000 (PP6310) g/10 min	Top electrical heating ring 230 °C; bottom heating ring 210–250 °C	Stepper motor driven piston	Spray head	40–60	95–165	–	Flat wire mesh	4.47–41.72	[248]
PP6315, Shanghai Yi Shi Tong New Material Development Co.	MFR 1500 g/10 min	SS cylinder electrically heated (2 regions);	Piston	–	–	–	–	–	–	[249]
SO and NaCl additives (4–12 wt%), Expert Company, British Drug House, Merck KGaA	$M_w$ 55,509, MFI 2000 at 200 °C (PP), $M_w$ 304.44 (SO), 58.44 (NaCl) g/mol	Metal barrel electrically heated; 200 °C	Syringe pump; 0.0013 mL/min	0.2 circular protruding (die)	48 (Collector –ve)	120–150	–	Al foil	0.31–4	[161]
Synthesized, SO (British Drug House), PEG-300 (Ega Chemie) and PDMS (United Chemical Technologies Inc.) additives (4–12 wt%)	MFI 1000 at 230 °C (PP)	Metal barrel electrically heated; 200 °C	Syringe pump; 0.0013 mL/min	0.2–0.3 circular, circular protruding, trilobal (die)	48 (Collector –ve)	120–150	–	Al foil	0.88–5.25	[162]
Aldrich	$M_w$ 190,000, MFI 35 g/10 min at 200 °C	Radiant heater; 250–300 °C	Cu cup; gravity feed	1.5 hole in cup	100–3000 kV/m (Collector +ve, spinneret –ve)	20–150	Vacuum	Al plate	0.3–30	[88]
Blend with Na-stearate	$M_w$ 190,000 g/mol	Piston or extruder; 230 °C	64 nozzle spinneret; 0.2 mL/h per nozzle	–	–	–	–	–	0.552	[251]
–	–	Oil circulating jacket in heater shroud; –	Syringe pump;	–	–	–	Air (RT–100 °C)	Rotating collector	10–30	[246]

Moplen HP 456], Moplen HP 462R, Borflow HL 504FB, Basell Orlen Polyolefins	MFR 1.7–15 at 170–300 °C (Moplen HP 456J), 3–50 at 170–300 °C (Moplen HP 462R), 43.8–450 g/10 min at 170–230 °C (Borflow HL 504FB)	Extruder; spinneret 270–300 °C	Screw turn 0.1–2 rpm	0.5 (three nozzles)	15–45 (Collector +ve)	80–300 –	Rotating mandrel 11 rpm, 30 mm/s oscillation, 5 mm diameter	4.8–37 [231]
Moplen HP 456, Basell	MFI 3.4 g/min at 230 °C	Extruder; spinneret 300 °C	Screw turn 2 rpm	0.5 (three nozzles)	25–35 (Collector +ve)	100–200 –	Metallic collector	11.05–23 [352]
Moplen HP 462R	270–300 °C	Screw extruder	Screw turn 0.1–1 rpm		31–38	80–150		2–4 [243]
PP 6820	MFI 200 g/min	240 °C	15 g/h output	Needleless	20–50	260	Ring Electrode Used; Rotating Collector	3–6 [111]
i-PP, Shijiazhuang & CNTs, Sigma Aldrich i-PP, Borealis & TiO <sub>2</sub> particles	PP-H-GD-150; multi-walled CNTs	265 °C		9 g/h output	Needleless	170	Ring electrode used	1–8 [113]
Metocene MF650X & MF650Y	MFI 120 g/min & 180 g/min respectively	Glass Syringe; electrically heated 320–360 °C	Syringe pump		30 kV on top plate; 65 kV on bottom plate 60 (Collector +ve) 25	120	Al collector	1–10 [218]
				Needleless spinning disk	50–95	50		0.7 [217]
					110–160	Argon		3–14 [233]

**Table 3**

List of melt electrospun polyesters including instrument configurations/parameters and conditions, as well as resulting fiber diameter.

Polymer	Description	Viscosity related property	Melt heating	Feed rate	Spinneret diameter [mm]	Voltage <sup>a</sup> [kV]	Collector distance [mm]	Spin zone <sup>b</sup>	Collector <sup>c</sup>	Fiber diameter [μm]	Ref	
PCL	Sigma Aldrich	$M_n$ 80,000 g/mol	Glass water jacket, plastic syringe; 90 °C	Syringe pump; 5–20 μL/h	0.51	4–12	20–60	–	Microscope slides	5–33	[103]	
–	Perstorp	$M_n$ 83 kDa	–	–	–	–	–	–	–	–	[158]	
–	Perstorp	$M_w$ 50 kDa	Glass water jacket, plastic syringe; 78 °C	Syringe pump; 5–50 μL/h	0.337, 0.514	12	30	–	Al plate, computer-controlled xy stage	7.5	[234]	
Sigma-Aldrich		$M_w$ 80 kDa	Glass water jacket, plastic syringe; 70 °C	Syringe pump; 5 μL/h	0.337	12	30	–	Al plate, computer-controlled xy stage	2–45	[105]	
Shenzhen BrightChina Industrial Co., Ltd		$M_w$ 79,000 g/mol	3 × CO <sub>2</sub> laser; 4–14 mA	Rod fed; 5 mm/min	0.3 (rod)	5–25	120–200	–	Al plate, computer-controlled xy stage	20	[105]	
Sigma-Aldrich		$M_n$ 45,000 g/mol	Heating tape; 80 °C	Pneumatic syringe; 1.2–5.6 psi	0.1524, 0.051	0.825–1.05	0.17	–	Metal plate	3–12	[255]	
Perstorp, UK Ltd		$M_w$ 50 kDa	Glass water jacket, plastic syringe; 78 °C	Syringe pump; 50 μL/h	0.514	12	40	–	Glass slide on Al coated silicon wafer, XYZ precision stage on optical table; 0.8–2.4 mm/s	20–60	[106]	
Sigma-Aldrich		$M_n$ 45,000; zero shear rate viscosity 291.5 Pa s at 80 °C	Heating band, custom melting chamber; 80–120 °C	Syringe pump; 2 mL/h	0.15–1.7	10, 15, 20	50–100	–	6 mm rotating brass tube (0.306–0.919 rot/translation), lateral translating linear slide (2021–6062 mm/min)	12–220	[190]	
Sigma-Aldrich		$M_w$ 80 kDa	Glass water jacket, plastic syringe; 70 °C	Syringe pump; 5–50 μL/h	0.337, 0.514	4–12	20–60	–	Al foil, x–y stage 8.5 mm/s	5–35	[221]	
Lactel		Medical grade	Glass water jacket, plastic syringe; 80 °C	Syringe pump; 20 μL/h	–	7	40	–	Glass; porous metallic; wire mesh; translating collector	10–15	[213,236]	
Sigma Aldrich		$M_w$ 45 kDa	Electrical heated; 80 °C	Syringe pump; 2 mL/h	0.15–1.7	20	50	–	Al foil, then heat pressed onto FDM scaffolds	Translating linear slide	12–200	[239]
*PCL		$M_w$ 189,000		5 bar N <sub>2</sub> pressure	0.34	25	100	–	Translating linear slide	40	[253]	
PCL/PEG-block-PCL	80% PCL + 20% PEG <sub>5000</sub> -b-PCL <sub>5000</sub> ; Aldrich (PCL), synthesized (PEG <sub>5000</sub> -b-PCL <sub>5000</sub> )	$M_n$ 80,000 (PCL), 5000 (PEG-b-PCL) g/mol; $M_w$ 65,960	Glass water jacket, plastic syringe; 90 °C	Syringe pump; 5–50 μL/h	0.51	12	90	–	–	1.8	[103]	

	90% PCL + 10% PEG <sub>5000</sub> -b-PCL <sub>5000</sub> ; Aldrich (PCL), synthesized (PEG <sub>5000</sub> -b-PCL <sub>5000</sub> )	$M_n$ 80,000 (PCL), 5,000 (PEG-b-PCL) g/mol; $M_w$ 72,980	Glass water jacket, plastic syringe; 90 °C	Syringe pump; 5–50 µL/h	0.51	8	90	–	Al foil, SEM stub rotating at 2500 rpm, microscope slides held by hand, Stainless steel tweezers as dual collectors	2.7	[103]
	30% PCL + 70% PEG <sub>47</sub> -b-PCL <sub>95</sub> ; Aldrich (PCL), synthesized (PEG <sub>47</sub> -b-PCL <sub>95</sub> )	$M_n$ 67,000 (PCL), 10,500 (PEG <sub>47</sub> -b-PCL <sub>95</sub> ) g/mol; zero shear viscosity 49 Pa s	Glass water jacket, plastic syringe; 90 °C	Syringe pump; 0.02–0.3 mL/h	0.58	20 (spinneret –ve)	100	–	Al foil, SEM stub rotating at 2500 rpm, microscope slides held by hand, Stainless steel tweezers as dual collectors	0.27–2	[31]
	20% PCL + 80% PEG <sub>47</sub> -b-PCL <sub>120</sub> ; Aldrich (PCL), synthesized (PEG <sub>47</sub> -b-PCL <sub>120</sub> )	$M_n$ 67,000 (PCL), 12,800 (PEG-b-PCL) g/mol; shear viscosity 33 Pa s	Glass water jacket, plastic syringe; 85 °C	Syringe pump; 0.03–0.3 mL/h	0.3, 0.58, 1.19	25 (spinneret –ve)	50–300	–	Al foil	1.5–1.7	[30]
	25% PCL + 75% PEG <sub>47</sub> -b-PCL <sub>95</sub> ; Aldrich (PCL), synthesized (PEG <sub>47</sub> -b-PCL <sub>95</sub> )	$M_n$ 67,000 (PCL), 10,500 (PEG <sub>47</sub> -b-PCL <sub>95</sub> ) g/mol	Glass water jacket, plastic syringe; 75 °C	Syringe pump; 5–50 µL/h	0.33	10–23	10–100	–	Untreated or starPEG modified glass microscope slides on manual translating stage	0.7–1.2	[29]
PEG-block-PCL	PEG <sub>119</sub> -b-PCL <sub>189</sub> , PEG <sub>119</sub> -b-PCL <sub>243</sub> ; synthesized	$M_n$ 22,000 (PEG <sub>119</sub> -b-PCL <sub>189</sub> ), 26,900 (PEG <sub>119</sub> -b-PCL <sub>243</sub> ) g/mol; shear viscosity 28.1, 39.4 Pa s	Glass water jacket, plastic syringe; 60–90 °C	Syringe pump; 0.05–0.1 mL/h	1.2	20	300	–	Al foil	0.2–60	[102]
PLA	Cargill Dow	$M_w$ 186,000; zero-shear viscosity 120 Pa s at 240 °C	Syringe in shielded heating reservoir 200 °C; nozzle 185–255 °C	Syringe pump; 0.005–0.01 mL/min	0.16–0.84	5–30	100	25–80 °C	Cu plate air-cooled 25 °C	0.8–17	[83]
	Cargill Dow	$M_w$ 186,000	Syringe in shielded heating reservoir 200 °C; nozzle 175–255 °C	Syringe pump; 0.01–0.01 mL/min	–	5–25	100	25–80 °C	Cu plate air-cooled 25 °C	10–28	[245]
	Cargill Dow	$M_w$ 186,000	Syringe in shielded heating reservoir 200 °C; spinneret 210 °C; air at nozzle 210 °C	Syringe pump, pressurized air surrounding jet at nozzle (GAME); $1.67 \times 10^{-10} \text{ m}^3/\text{s}$ (PLA), 300 m/s (air)	$4.13 \times 10^{-4} \text{ m}$ (spinneret), $1.194 \times 10^{-3} \text{ m}$ (air nozzle)	20 (Collector +ve)	90	27 °C	Cu plate air-cooled 25 °C	0.18–3.5	[81]
	Cargill Dow	MFI 22.3 g/min at 210 °C	3 × CO <sub>2</sub> laser 4–20 W; N <sub>2</sub> gas blown onto melt zone	Rod fed at 2–4 mm/s	0.5 (rod)	16–41	20	–	Rotating collector tangential velocity 1 m/s	0.7–3.3	[96]

Table 3 (Continued)

Polymer	Description	Viscosity related property	Melt heating	Feed rate	Spinneret diameter [mm]	Voltage <sup>a</sup> [kV]	Collector distance [mm]	Spin zone <sup>b</sup>	Collector <sup>c</sup>	Fiber diameter [μm]	Ref
Cargill Dow		MFI 76.9 g/min at 210 °C	3 × CO <sub>2</sub> laser 5–17 W; N <sub>2</sub> gas blown onto melt zone	Rod fed at 2–4 mm/s	0.5 (rod)	16–41	20	–	Rotating collector tangential velocity 1 m/s	0.7–4	[96]
Cargill Dow		$M_w$ 186,000; zero-shear rate viscosity 1320 Pa s at 180 °C	Syringe in shielded heating reservoir 200 °C; spinneret 215–255 °C	Syringe pump; 0.02–0.06 mL/min	0.42–0.52	5–25	100	20–80 °C	Cu plate air-cooled 20–25 °C	10–25	[82]
Amorphous PLA 4060D, semicrystalline PLA 6201D, Nature Works LLC		MFR 4.8–233 (6201D), 4.7–41.7 (4060D) g/10 min at 170–230 °C	Extruder; spinneret 170–200 °C	Screw turn 0.1–2 rpm	0.5 (three nozzles)	15–40 (Collector +ve)	100–300	–	Rotating mandrel 11 rpm, 30 mm/s oscillation, 5 mm diameter	3–20	[231]
PLA 4060D, NatureWorks		MFI 15 g/min at 230 °C	Extruder; spinneret 170 °C	Screw turn 2 rpm	0.5 (three nozzles)	25–35 (Collector +ve)	100–200	–	Metallic collector	3.11–8.41	[252]
PLA 4060D			190–220 °C	Screw turn 1 rpm		30–37	60–100	–	Rotating Collector	0.9–5	[243]
Natureworks 2002D			200–250 °C		Needleless; umbellate spinneret	30–100	100–230	–	–	7.6	[114]
PLA + antioxidants	PLA + 0.1, 0.3, 0.5 wt% antioxidant; Ningbo Materials Science and Engineering Company (PLA), tris(2,4-di-tert-butylphenyl)phosphate (antioxidant 168), Tetrakis[methylene(3,5-di-tert-butyl-4-hydroxyhydrocinnamate)] methane (antioxidant 1010), Beijing Additive Institute	$M_n$ 7058–61,208 g/mol (PLA); MFR 2–7.5 at 180–220 °C	Top electrical heating ring 170 °C; Bottom heating ring 200–220 °C	Piston driven cylinder; –	Spray head	55.6	120–160	–	Al plate	–	[215]
PLA & EVOH	Pie wedge fibers, EVOH/PLA volume ratios 3/7, 5/5, 7/3	MFI 45 (PLA), 45 (EVOH) g/10 min at 230 °C	CO <sub>2</sub> laser 6–21 W	Fibre bundle fed; 7 mm/min	0.04 (300 fibers twisted together and soaked in water at 80 °C)	20–45	60–180	–	Cu plate	0.4–1.5	[101]
PLA & PEG	6350D PLA (Nature Works) & PEG 6,000 g/mol. (Kimiagaran Emrooz)		Metal barrel; electrical heating 180–200 °C	Syringe pump		50 kV (collector +ve)	10–160	–	Rotating Collector	10–25	[238]
Star-PDLLA	Four arm star-shaped PDLA synthesized, functionalized with Adenine/thymine end groups (PDLA-A,PDLA-T), PDLA-(A-T) blend	$M_n$ 45,600 g/mol	Glass pipette wrapped in heating band; 180 °C	Gravity feed	unknown	30 (Collector +ve)	60	–	Al foil	3.6 (PDLA), 4 (PDLA-A), 4.4 (PDLA-T), 9.8 PDLA-(A-T)	[240]
PLGA	PLGA 50/50, PURAC Co.	$M_w$ 47,000	Stainless steel oil jacket, glass syringe; 210 °C	Syringe pump; 1.4–5.4 mL/h	0.84	17.5 (Collector +ve)	80	–	Rotating drum	14.6–28	[206]

P(LLA-CL)	Monofilament	–	$\text{CO}_2$ laser; 7–20 W	193 $\mu\text{m}$ fibre feed; 0.02–0.04 m/min	0.193 (filament)	20	50	–	Cu plate	1–2	[209]
PLLA & P(EVOH)	PLLA dip coated in EVOH 1:0, 2:1, 1:2 (PLLA:EVOH); Cargill Dow (PLLA), Kuraray Co. (EVOH)	$M_n$ 96,080, MFI 76.9 at 210 °C (PLLA); 32 mol% Ethylene, MFI 1.6 at 190 °C (EVOH)	3 × $\text{CO}_2$ laser 8–14 W	Rod fed at 10 mm/min	0.42–0.8 (rod)	20–37	50–80	25–80 °C	Translating collector	0.845–6	[98]
PLLA + nHA particles	PLLA + 1, 3, 5, 7, 9 wt% nHA; Nature Works LLC (PLLA), Aladdin Chemistry Co., Ltd (nHA)	$M_w$ 60 kDa (PLLA)	3 × $\text{CO}_2$ laser 20 mA	Rod fed at 5 mm/min	0.5 (rod)	15	140	–	Cu plate	4.5–7.1	[216]
PI	–	$M_w$ 5000 g/mol	300–350 °C	Film	–	60	60	Vacuum	–	–	[158]
1,3,5-cyclohexane-	Derivative of cyclohexane- <i>cis,cis</i> -1,3,5-tricarboxylic acid	Columnar nematic phase (254–317 °C)	300 °C	200 $\mu\text{L}/\text{h}$	0.6	40 (spinneret –ve)	60	–	–	–	[201]
1,3,5-cyclohexane-	Derivative of cyclohexane- <i>cis,cis</i> -1,3,5-tricarboxylic acid	Optical isotropic melt (317–382 °C)	330 °C	200 $\mu\text{L}/\text{h}$	0.6	40 (spinneret –ve)	60	–	–	1.3	[201]
1,3,5-benzenetrizamide	Based on trimesic acid with n-hexyl substituents	Optical isotropic melt (218–390 °C)	250 °C	200 $\mu\text{L}/\text{h}$	0.6	30 (spinneret –ve)	60	–	–	0.9	[201]
1,3,5-benzenetrizamide	Based on 1,3,5-triaminobenzene	Optical isotropic melt (183–379 °C)	200 °C	200 $\mu\text{L}/\text{h}$	0.6	30 (spinneret –ve)	40–45	–	–	2.2	[201]
$\text{B}_2\text{O}_3$	–	Viscosity 15–26 Pa s at 850 °C	Resistance heating; 850 °C	Gravity feed	0.025 (gold wire dipped into reservoir)	250–500 ( $\times 10^{-3}$ )	$\sim 10$ ( $\times 10^{-3}$ )	–	Silicon wafer with 300 nm layer of silicon dioxide on surface	0.025–0.25	[202]
Octadecane + $\text{TiO}_2$ -PVP (co-axial)	45 wt% octadecane (ACROS Organics) in PVP/titanium tetraisopropoxide solution, Aldrich	Viscosity 1.75 cP at 70 °C, 3.8 cP at 30 °C (octadecane)	Heating tape; 68 °C (octadecane)	2 × syringe pump; 0.2 (octadecane), 0.7 ( $\text{TiO}_2$ - PVP) mL/h	0.1 polyimide- coated silica capillary inside metallic needle; $\text{TiO}_2$ -PVP in outer syringe, octadecane in inner syringe	–	–	–	Si wafers, carbon-coated Cu grids, Al foil	0.2	[258]
Hexadecane + $\text{TiO}_2$ -PVP (co-axial)	31 wt% hexadecane	–	–	–	”	–	–	–	Si wafers, carbon-coated Cu grids, Al foil	0.1	[258]
Eicosane + $\text{TiO}_2$ -PVP (co-axial)	36 wt% eicosane	–	–	–	”	–	–	–	Si wafers, carbon-coated Cu grids, Al foil	0.2	[258]

**Table 4**

List of various melt electrospun polymers not included in [Tables 2 and 3](#), with instrument configurations/parameters and conditions, as well as resulting fiber diameter.

Polymer	Description	Viscosity related property	Melt heating	Feed rate	Spinneret diameter [mm]	Voltage <sup>a</sup> [kV]	Collector distance [mm]	Spin zone <sup>b</sup>	Collector <sup>c</sup>	Fiber diameter [ $\mu\text{m}$ ]	Ref
PE	Marlex 6009 HDPE	Melt index 2.0	Electrically heated Al jacket; 200–220 °C	Air cylinder operated plunger; order of 1 m/min (spin rate)	2.2	10–23	10–30	Air, ambient temperature	Metallic plate	138–190	[58]
	LDPE	MFI 2 g/10 min	Electrical heater ring; 315–355 °C	45 Steel piston/cylinder; polymer drawn by HV	0.2–0.7	30–60 (Collector +ve)	50–200	–	Flat wire mesh	5–33	[199]
EVAL	Various ethylene contents	MFI 4.7–15.1 g/10 min	Laser; 8–16 W	Rod fed by stepper motor; 2–4 mm/s	0.2–0.5 (rod)	15	20	–	Cu plate, rotating disc	0.74–2.8	[97]
EVOH	Poly(ethylene-covinyl alcohol), Kuraray Co.	MFI 4.4 at 190 °C	Laser Line; 45 W	Sheet sample; 0.05 to 1 mm/s	N/A	40 (Spinneret +ve, collector -ve)	100	–	Cu plate	0.9–2.5	[100]
PET	Monofilament	–	$\text{CO}_2$ laser; 5–7 W	196 $\mu\text{m}$ fibre feed; 0.04 m/min	0.196 (filament)	10–25	50	–	Cu plate	4–102	[209]
	Kuraray Co.	IV 0.512–0.706 dL/g	Laser (from 3 directions); 5–11 W	Rod fed; 1–3 mm/min	0.2–0.5 (rod)	18–20	25	–	Cu plate, Al rotating disc	1.7–4	[99]
	Bottle-grade PET	IV 0.45–1.2 dL/g	– Silicon oil jacket and nozzle heater; 245–255 °C, 200–235 °C	– Pyrex piston and cylinder; gravity feed	– Unknown	–	30–90	Vacuum	– Metallic plate	2–6 10–100 <sup>d</sup>	[158] [211]
Poly(2-ethyl-2-oxazoline)	Sigma	50,000 g/mol	200–220 °C	1–3 bar	0.16–0.34	3–7	3–7	–	Al	5–125	[223]
PMMA	IH830 with (di-(2-ethylhexyl)phthalate) (DOTP) added at various mass ratios: PMMA/DOTP (60/40; 70/30)	MFI 2.3 g/10 min at 230 °C	Heating tape wrapped stainless steel tube; 210 °C	Syringe pump; feed rate not reported	0.6	15–25 (Collector +ve)	30–90	–	Al foil covered flat plate, ice water bath with 10 wt% KCl	4–34	[210]
CBT + PMMA (co-axial)	CVL-bisphenol A-1-tetradecanol mixed (1:2:20) weight ratio (CBT), Aldrich; PMMA in solution	–	Heating tape; 45 °C (CBT)	Syringe pump; 0.2–1.0 mL/h	PMMA in outer syringe, CBT in inner syringe	20–30	150–250	–	Al foil	Core 0.2–0.4, shell 0.2–0.5	[222]
EPO + Carvedilol	butylmethacrylate-(2-dimethylaminoethyl) methacrylate-methyl methacrylate copolymer (1:2:1) (EPO), Evonik; Carvedilol (CAR), Sigma-Aldrich; 80% EPO+20% CAR	$M_w$ 150,000 g/mol (EPO)	Two-zone heated stainless steel metal syringe; reservoir 130 °C, spinneret 155 °C	Microcontroller; 0.5 mL/h, (0.6 g/h deposition rate)	–	35 (Collector +ve)	100	–	Al foil	20	[237]
Polyalipate	Vectra	Apparent viscosity 3.358 Pa s at 340 °C	Laser (from 3 directions); 4–10 W	Rod fed; 1–3 mm/min	0.2–0.5 (rod)	18–20	25	–	Cu plate, Al rotating disc	2.6–10	[99]
Poly(phospholipids)	1-palmitoyl-2-oleoyl-sn-glycero-3-phosphoethanolamine (POPE)	–	Glass pipette wrapped in heating band; 200 °C	Gravity feed	Unknown	30 (Collector +ve)	60	–	Al foil	6.5	[240]

PU	Estane 58315	678.3–53.8 cP at 225–243 °C	Band heaters; 225–243 °C	Gravity feed	1	25–35 (collector between spinneret and +ve electrode)	130–210	ATM pressure	PS Petri dishes, Teflon and Pyrex, translating in concentric circles	5–18	[63]
BDI/PCL/BD	Elastollan, Renko Textile	–	MFI tester (2 resistance heaters); 205–208 °C	0.6 g/h (deposition rate)	1	4–6 kV/cm	60–150	33 °C, 30% RH	Al foil	4–8	[220]
	Elastollan 1185A	–	–	0.1 mL/h	–	50 kV	60	–	Al Collector	1–7	[205]
	Segmented block PU copolymer with 1,4-butane diisocyanate (BDI), PCL diol, 1,4-butanediol (BD) in 4/1/3 M ratio, Aldrich (PU), purified of DBTDL catalyst	$M_w$ 40 kDa (PU)	Two band heaters; 220–240 °C	Gravity feed	0.5	30 (Collector +ve)	130	–	Cu strip on glass microscope slide moving in concentric circles on xy stage	11.2	[204]
Poly(phospholipids)	Estane 58315	–	Metal sleeve; 250 °C	–	2	25 (collector at +ve 20)	160 (collector 100 from ground)	–	Phenolic board templates with inlaid Cu traces on moving stage	36.9	[208]
<i>N,N,N',N'</i> -tripropyl-1,3,5-benzenetricarboxamide	Synthesized low molecular weight compound	337 g/mol	290 °C	0.5 mL/h	0.6	–30 kV	–	–	Collected onto SEM with carbon tape	0.8	[241]
Pitch	Naphtha cracking bottom oil-based pitch Electron beam irradiated pitch	– –	200–250 °C 200–260 °C	1 mL/h 1 mL/h	0.5 0.1	10–15 0–20	– 200	– –	Rotating collector Rotating collector	8–10 5–10	[242] [200]
Nylon-6	Monofilament	–	CO <sub>2</sub> laser; 14–20 W	188 μm fibre feed; 0.04 m/min	0.188 (filament)	15–20	50	–	Cu plate	1–4	[209]
	Hyosung, Inc.	MFI 3	Heated spinneret; 270–310 °C	Syringe pump; 1.17–5.0 × 10 <sup>−10</sup> m <sup>3</sup> /s	1.07	20	100	–	Cu plate	1–10	[95]
	Hyosung, Inc.	MFI 3, zero shear rate viscosity 192.5 at 250 °C	Heating element embedded in ceramic; 250–300 °C	Syringe pump; 0.003–0.02 mL/min	0.41, 1.07	20, 28	100	Air at 25 °C	Cu plate	1–10	[80]
(Nylon 6/12) Poly(amide-6)	(hexamethylene dodecanediamide), Aldrich Stearic acid and oleic acid additives (2–10 wt%), Aldrich	– 1.5–30 Pa s	Line laser 45 W 305–345 °C	Sheet sample; 0.05 to 1 mm/s Screw extruder; feed rate not reported	N/A –	40 130 (Collector +ve)	100 450	– –	Cu plate Rotating collector	0.8–2.2 0.5–20	[100] [250]

<sup>a</sup> Positive voltage applied to spinneret and collector grounded unless otherwise specified.<sup>b</sup> Assumed ambient conditions unless otherwise specified.<sup>c</sup> Collector stationary unless otherwise specified.<sup>d</sup> Diameter not quantitatively provided—qualitative diameters provided based on figures.

Polyesters are another major class of polymers being extensively investigated, with a long history of biodegradable aliphatic polyesters researched for clinical use as both implants and for drug delivery [28]. One issue with polyurethane (PU) elastomers is that the hard segments can be composed of non-degradable units such as aromatic cycles and the products of decomposition may be toxic [203]. Alternatively, low melting point polymers such as PCL exhibit thermal stability and favorable melt electrospinning processability, where research interest is rapidly increasing [105]. Karchin et al. developed a novel, thermally stable, degradable and biocompatible aliphatic PU specifically for processing by melt electrospinning polymers containing 1,4-butane diisocyanate, PCL and 1,4-butanediol, with superior mechanical properties compared to a homopolymer such as PCL [204]. A polyether type PU elastomer has also been melt electrospun and images from above and cross-sections are shown in Fig. 4H and I [205].

An eco-friendly and biodegradable polymer such as PLA (Fig. 4B) can be hydrolyzed (or microbe digested) to produce CO<sub>2</sub> and H<sub>2</sub>O. These properties make PLA attractive in the packaging industry as well as in biomedical fields such as orthopaedic surgery, where the polymer is innocuous and biocompatible with human tissues [96]. In particular, these hydrolytically degrading polymers are attractive for the fabrication of TE scaffolds: onto which biologists can grow cells and tissue in a fibrous environment mimicking native human tissue. Such scaffolds have been manufactured by combining melt and solution electrospinning, to produce two distinct fiber populations in a single sample using PLGA (Fig. 4J) [206] or PLA (Fig. 4K) [207].

A processing technology such as melt electrospinning that does not require a volatile solvent to form ultrafine filaments is attractive for the fabrication of such medical materials as the final product remains non-toxic following melt processing [30]. The susceptibility of polyesters including PLA, poly(L-lactide) (PLLA) and poly(lactic-co-glycolic acid) (PLGA) to thermal degradation when held at elevated  $T_m$  for prolonged periods has led to the design of novel processing approaches to avoid undesired degradation by-products [96,98].

While there is a strong interest in natural polymers such as collagen for medical application, these types of polymers are not widely processed due to denaturation via heating. An exception is the melt electrospinning of a poly(phospholipid), found to form long range aggregates in the melt [208]. Therefore while biologically-derived polymers are typically not considered for melt electrospinning, their future use is possible.

Other common industrial polymers that have been melt electrospun include N6 [80,93,95,209], PE [58,199], poly(methyl methacrylate) (PMMA) [210] and PET [99,158,209,211], with a view to applications such as protective clothing, material reinforcements, separators and filtration [210]. A comprehensive list of all the reported polymers and their variants that have been melt electrospun to date is presented in Tables 2–4. The fact that less than 30 polymers are represented and notable polymers such as polystyrene (PS), polycarbonate and poly(acrylonitrile butadiene styrene) are absent from this list (with the latter one of the most frequently used

polymers in 3D printing) indicates the emerging state of melt electrospinning.

Research performed so far indicates that post-processing technologies should be transferable to melt electrospinning. Fig. 4L shows how solution electrospraying was combined with melt electrospinning to produce micro-sphere laden scaffolds [212]. Calcium phosphate (CaP) was also deposited upon melt electrospun fiber surfaces (Fig. 4M and N) with the same process that was used for solution electrospun fibers [213,214].

More extensively researched has been the used of additives in the polymer melt to provide some form of structure/function. Yang et al. found the inclusion of antioxidants improved the thermal degradation properties of PLA during melt electrospinning [114,215]. Li et al. showed that the addition of hydroxyapatite (HA) nanocrystalline particles improved PLLA fiber hydrophilicity in an attempt to combine the positive properties of organic and inorganic materials in a polymer/ceramic composite [216]. Nayak et al. increased the electrical conductivity of PP with the addition of sodium oleate (SO) and sodium chloride (NaCl). The smaller ions from NaCl (that are more mobile than SO) result in a higher net charge density, allowing the electrified molten jet to be stretched further so that fiber diameters around 300 nm were obtained [161]. The addition of PEG and poly(dimethyl siloxane) (PDMS) to PP produced a similar effect by reducing  $\eta_{melt}$  [162]. Fig. 4O shows titanium dioxide (TiO<sub>2</sub>) particles that were included into the melt and were able to absorb ultraviolet (UV) light for extended periods [217]. Multi-walled carbon nanotubes (CNTs) were also included with PP and Fig. 4P shows how they align along the direction of the fiber [218]. Inorganic particles based on strontium have also been mixed with PCL and melt electrospun so that they provide sustained nutrients to osteoclasts *in vitro* (Fig. 4Q) [219].

To date, the melt electrospinning literature is still primarily focused on exploring which thermoplastic polymers are suitable to be processed, as well as establishing appropriate processing conditions to obtain fibers with desired morphologies and functionalities [220]. While approaches used in solution electrospinning such as structured collectors (Fig. 4R) [221] and coaxial electrospinning (Fig. 4S) [222] are also translated to the melt, 3D direct writing approaches, such as with molten poly(2-oxazoline) (Fig. 4T) [223] distinguish the two techniques. Melt electrospinning involves a complex interaction and interdependency between a range of material properties, processing parameters and ambient conditions. The ability to establish a stable jet and subsequent control over the fiber diameter requires an understanding of the effects of each of these variables for subsequent process optimization. The remainder of this section examines characteristic polymer properties reported to influence the ability to successfully melt electrospin a polymer and determine the resulting fiber morphology.

### 5.1. Electrical conductivity

Studies have shown that the conductivity of the polymer melt plays a major role in the ability to form a stable jet.

Highly conductive fluids flow readily from the spinneret, however they form unstable jets that break up when  $V$  is increased. Conversely, insulating materials do not sustain surface charge and therefore minimal electrostatic drawing forces are generated on the emerging polymer extrudate [224]. For semi-conducting fluids (conductivity typically in the range of  $10^{-6}$ – $10^{-8}$  S/m) it is possible to form a stable Taylor cone [224].

In the Taylor cone, “a tangential electric field is introduced in the direction of the melt flow” [224]. Shear stresses occur on the cone due to charges that act to decrease  $d$  as the length of the jet increases, while maintaining jet stability [225]. Joo and colleagues found that low electrical conductivity ( $<10^{-10}$  S/m) is required in the polymer melt for stable jet formation [82]. They reported that “as the conductivity decreases, axial charge transport becomes primarily due to convection throughout the jet profile and the applied external electric field becomes practically unaffected by the diminishing surface charges”. The “induced electric field peak is shifted down and the electric field within the fluid jet approaches the uniform applied external electric field”. Further, decreasing conductivity dampens the significance of axial conduction and even at the beginning of jet thinning the convection current becomes significant [226].

The generation and mobility of charge carriers or ions contained within polymers dictates the electrical conductivity in the material [227]. A material such as PP, that is a good electrical insulator at RT, was shown by Nayak et al. to have electrical conductivity in the level of  $10^{-10}$  S/m in its pure form with  $T_m$  at  $200^\circ\text{C}$  [161]. The electrical conductivity increased to the level of  $10^{-7}$  S/m when 4% of SO was added, and increased to  $10^{-4}$  S/m when 12% of SO was added. Similarly, the electrical conductivity increased from  $10^{-8}$  to  $10^{-6}$  S/m when higher amounts of NaCl were used. The current flow in the melt was greater with the addition of NaCl compared to SO, where the smaller ionic size of NaCl resulted in higher mobility of the ions. Thus, the addition of NaCl produced relatively greater elongational forces on the electrified molten jet than SO, leading to smaller diameter fibers. In both cases, the increased charge-carrying capacity sufficiently increased the Coulombic charge repulsions along the jet to create bending instabilities and whipping, enabling further reduction in the diameter of the fibers [161].

## 5.2. Molecular weight

In solution electrospinning, the polymer can be diluted to a sufficiently low concentration in the solvent so that the polymer solution is able to be extruded through a fine spinneret. In melt electrospinning,  $\eta_{\text{melt}}$  can only be lowered to a limited degree by increasing  $T_m$ . Therefore, selecting an appropriate polymer molar mass (that often defines the rheological properties of the polymer melt) is required for achieving a stable and reproducible melt electrospinning process. Many properties of a polymer, such as  $\eta_{\text{melt}}$ , modulus and tensile strength, can be related to the  $M_w$  [228], often used to describe a processed polymer.

Lyons et al. showed that  $M_w$  has a significant effect on the feasibility of melt electrospinning PP fibers [79].

PP was chosen due to an extensive history of use in melt processing, a large range of available  $M_w$ , and the availability of different tacticities. Since PP is often processed through industrial machinery, the molar mass is typically above 100,000 g/mol in order to provide sufficient toughness for processing as well as for the end application [28]. At constant  $T_m$  of  $200^\circ\text{C}$ , PP with relatively too high  $M_w$  (though it could be extruded) was unable to form a Taylor cone. Instead, a fiber with a diameter reflecting the inner diameter of the spinneret ( $d_i$ ) was slowly pulled to the collector. When the  $M_w$  was reduced, a Taylor cone was formed that resulted in relatively large diameter melt electrospun fibers. As the  $M_w$  was continually decreased, there was an exponential decrease in fiber diameter, until the jet broke up due to a lack of molecular chain entanglements [79].

While the molar mass of commercially available PP is often not ideal for melt electrospinning, when the molar mass is lowered using a chain scission agent, sub-micron PP fibers are readily produced [28]. Tables 2–4 show the  $M_w$  or viscosity related parameter for all of the polymers that have been melt electrospun to date, in combination with the processing parameters that were required to deliver the reported fiber diameters.

One issue to consider for polymers such as PLA, that are susceptible to thermal degradation, is the extended exposure to relatively high temperatures if they are melted in a reservoir prior to electrospinning. Joo et al. showed that the  $M_w$  of PLA changed from 186,000 g/mol. to around 40,000 g/mol. in the first hour of melt electrospinning at  $200^\circ\text{C}$  (even though the thermal decomposition temperature of PLA is around  $330^\circ\text{C}$ ). Intramolecular transesterification reactions are the “major cause of thermal degradation for PLA below  $250^\circ\text{C}$ ” [83].

Another point to take note of is the importance of not relying solely on the  $M_w$  data provided by the manufacturer, especially when the polymer is moisture-sensitive and is in contact with air during storage. Our group has measured significant variance in the  $M_w$  of different lots of PCL from the same manufacturer using gel permeation chromatography analysis (unpublished data). Charuchinda et al. reported a similar concern where they obtained values of  $M_n$  and  $M_w$  from three different methods that were consistent with one another but varied significantly from the supplier’s value. The proposed reason for this was some hydrolytic degradation in the PCL pellets post-manufacture [229].

## 5.3. Tacticity

Lyons et al. showed that the  $M_w$  interaction was not exclusively responsible for determining the melt electrospun fiber diameter. The tacticity of the polymer was also shown to have a significant effect. It was suggested that at the same  $M_w$  the more oriented structure of isotactic poly(propylene) (i-PP) (higher tacticity) resulted in smaller fiber diameters than atactic poly(propylene) (a-PP). A-PP has a methyl group randomly placed on the polymer backbone, that negatively affects crystallization. It was proposed that this steric hindrance may result in larger fiber diameters than those obtained from similar  $M_w$  [79].

Kadomae et al. studied the significance of tacticity as a parameter to control the diameter of melt electrospun PP fibers compared to  $M_w$ , and similarly found that i-PP fibers were thinner than a-PP fibers, although the viscosities were almost the same [230]. PP samples with altered tacticity were prepared by blending different ratios of i-PP and a-PP: where the fiber diameter of the blended samples decreased as the proportion of i-PP increased (increasing the crystallinity of blended sample), and the fiber diameter distribution became narrower as the amount of i-PP increased. They considered that the difference in AFD between i-PP and a-PP cannot be directly related to crystallinity, since crystallinity is an effect of elongation and solidification during melt electrospinning. Kadomae et al. observed that the size of the a-PP Taylor cone was significantly larger than the i-PP Taylor cone. They measured little variation in the zero-shear viscosity of the polymer melt blends at 180 °C, from 0.8 Pa s at i-PP 100% to 2.5 Pa s at a-PP 100% and assumed no significant difference between the  $\gamma_s$ s in the different Taylor cones. According to the following equation to calculate  $E$  of the Taylor cone [230]:

$$E = \sqrt{\frac{4\gamma}{\varepsilon_0 R_c}} \quad (7)$$

where  $\varepsilon_0$  is the permittivity of free space; and  $R_c$  is the radius of curvature of the cone apex, they noted that  $E$  at the apex of the Taylor cone of i-PP must be stronger than that of a-PP when  $\gamma$  of i-PP is assumed to be the same as that of a-PP. However, it was confirmed that the dielectric constants of the samples were almost the same at 180 °C in the frequency range from 10 to 10,000 Hz, while  $V$  and  $TCD$  were constant. Therefore, the variations in tacticity may have caused sufficient differences in the polymer melt  $\gamma_s$ s to significantly alter the Taylor cone geometries. The parameters for PP melt electrospinning are summarized in Table 2.

Mazalevska et al. attributed the higher melt flow rate (MFR) of a semi-crystalline PLA sample compared to an amorphous PLA sample to differences in the molecular structure of the two polymers; where the number  $M_w$  was nearly the same for both the PLA specimens. The organized structure of semi-crystalline PLA was reported to have greater intermolecular interactions and therefore a resistance to flow [231]. The tacticities, and isotactic/atactic blend ratios are provided, where applicable, for each melt electrospun polyester in Table 3.

#### 5.4. Thermal properties/extensional viscosity

One of the main material properties that affects the thinning of the electrified molten jet is extensional viscosity, that is influenced by the molecular architecture and  $T_m$  [82]. Under isothermal conditions (uniform temperature in the melt electrospinning zone), Zhmayev and colleagues predicted that the jet thins faster as  $T_m$  increases, due to decreased  $\eta_{melt}$  and relaxation time. Near the spinneret, the tangential component of the electric field is dependent on the jet-thinning rate, where “the slowest thinning jet (lowest  $T_m$ ) corresponds to the highest tangential electric field” [82]. That said, the initial increase in the electric field at low  $T_m$  is dwarfed by the high viscosity and does not

result in smaller diameter fibers. Therefore,  $\eta_{melt}$  mainly influences the initial jet thinning. By increasing the initial  $T_m$  and therefore the rate of thinning, both the tensile stresses and extensional viscosity increase further away from the spinneret. Here the elongation rate declines and the surface is approximately parallel to the field lines of the applied external field, where the tangential electric fields have converged to that of the external field [82].

As opposed to the isothermal situation, most experimental configurations are characterized by non-isothermal conditions, where downstream the viscoelasticity of the jet can become quite large due to the decrease in temperature away from the heated polymer reservoir. The change in the  $d$  when it is far away from the spinneret is smaller under non-isothermal conditions as the lowering of the jet temperature restricts thinning and solidifies the airborne jet [82].

Zhou et al. investigated non-isothermal processing conditions for melt electrospinning PLA, a slow-crystallising polymer prone to thermal degradation at  $T_m$  10 °C or more above its melting temperature (200 °C) [83].  $T_m$  in the melt reservoir was maintained at 200 °C (with anti-oxidant thermal stabilizers included), and the other melt electrospinning conditions were fixed. To avoid chemical decomposition, only the temperature of the spinneret was varied above the melting temperature of PLA, since the resident time of the melt in the spinneret was estimated to be less than 0.1 s. The melt electrospinning jet zone and collector temperatures were relatively low compared to the spinneret temperature to establish non-isothermal conditions. Under these conditions, whipping was suppressed and a stable jet was sustained. It was observed that when the spinneret temperature was increased from 180 to 255 °C (below the PLA thermal decomposition temperature of 330 °C), the associated reduction in initial  $\eta_{melt}$  only caused the AFD to decrease from approximately 4 to 2  $\mu\text{m}$ . At spinneret temperatures above 255 °C, a continuous jet was not able to be maintained because the elongational viscosity was too low, and droplets were collected [83].

For PP, Dalton et al. found that the highest quality melt electrospun fibers were processed using  $\eta_{melt}$  between 30 and 55 Pa s. The addition of the viscosity-reducing additive Irgatec to PP-15 reduced  $\eta_{melt}$  from 75 to 33 Pa s at 270 °C, where the AFD decreased from 36  $\mu\text{m}$  to 840 nm [31]. Nayak and colleagues measured the shear viscosity of pure PP, as well as PP with SO and NaCl additives, over a wide range of shear rates ( $0.1\text{--}100\text{ s}^{-1}$ ) at 200 °C and 20% strain. It was observed that the viscosity of the pure PP melt increased from approximately 30 Pa s at relatively high strain rates, to 40 and 45 Pa s with the respective addition of SO and NaCl. It is interesting to note that in this case, although these additives increased the viscosity of PP, the resulting fibers were characterized by a reduction in fiber diameter: the accompanying increase in electrical conductivity due to the additives caused the jet to be sufficiently charged so that whipping instabilities developed [161]. Wang et al. observed that increasing the mass percentage of the additive (di-(2-ethylhexyl)phthalate) to PMMA reduced  $\eta_{melt}$  and increased the MFI from 5.7 g/10 min (210 °C/0.325 kg) to 12 g/10 min (210 °C/0.325 kg). The

corresponding AFDs reduced from 34 to 19.7  $\mu\text{m}$  under constant melt electrospinning conditions [210].

For a low melting point polymer such as the aliphatic polyester PCL, with relatively low  $M_w$  and low  $\eta_{\text{melt}}$ , the decrease in  $\eta_{\text{melt}}$  with increasing  $T_m$  can be described mathematically [229]. At  $T_m$  more than 100 °C above  $T_g$ , as in the case of PCL ( $T_g = -60$  °C), the  $\eta_{\text{melt}}/T_m$  dependence shows close adherence to the Arrhenius-type equation [229]:

$$\eta_{\text{melt}} = A^{E_a/R_u T_m} \quad (8)$$

where  $A$  is a constant,  $E_a$  is the activation energy for viscous flow and  $R_u$  is the universal gas constant. When plotting  $\ln \eta_{\text{melt}}$  against  $1/T_m$ , an approximate straight line with a slope of  $E_a/R_u$  is obtained. For polymers that satisfy the above criteria, this relationship usually covers a temperature range of approximately 50–150 °C [232].

Although PCL (used extensively in melt-based extrusion methods in the biopolymer field) has excellent processing properties due to a low melting point and high thermal stability, in our experience a  $T_m$  of 80–100 °C yields fibers of the greatest quality [105]. At a higher  $T_m$  heat needs to be dissipated as it cools, and there is insufficient time for in-flight fiber solidification, resulting in coalescing of the polymer on the collector surface. Investigating the viability of using a screw extruder to deliver PCL for melt electrospinning, Mota et al. demonstrated that  $\eta_{\text{melt}}$  of linear PCL ( $M_w = 50,000$  g/mol) could be reduced by more than 17 times from 829 to 48 Pa s by using a three-arm star poly( $\epsilon$ -caprolactone) (\*PCL) ( $M_w = 64,000$  g/mol) [198]. A comprehensive list of the reported thermal/viscosity properties, and viscosity reducing additives where applicable, is provided for each melt electrospun polymer in Tables 2–4.

## 6. Melt electrospinning configurations and instrument parameters

Even though the cost of establishing a melt electrospinning device is slightly more than solution electrospinning, it remains relatively low compared to many other filament fabrication technologies [233]. The majority of melt electrospinning devices are currently found in research settings where their design and instrumentation is largely customized, where the choice of components is often governed by their commercial availability. Consequently, there is no consensus on the optimal design for a melt electrospinning device, and many varied configurations have been utilized. In many research laboratories, a single spinneret system can be assembled and operated on a bench without a ventilation system. The main functions such a machine should provide include: (1) a supply zone where polymer is delivered in a molten state to a spinneret; where (2) it can become electrically charged due to a HV potential difference between this location; and (3) a fiber collection zone; where the polymer becomes sufficiently charged to form a Taylor cone that is electrostatically drawn as a polymer jet across a (4) “melt electrospinning jet zone” towards the collector zone. In this region cooling and solidification of the melt jet takes place. Fig. 5 is a schematic summary of the different melt electrospinning configurations employed so far.

### 6.1. Polymer melt supply zone

One simple and often utilized method to supply polymer to a melt electrospinning system is to load polymer pellets into a syringe (either plastic [103,105,106,108,213, 221,234–236], metal [230,237–239] or glass [31,200,205, 206,217,223,240–243]) and preheat the material to remove any pockets of air so that an uninterrupted supply of polymer can be maintained. The syringe is then placed into a heating jacket to maintain a reservoir of polymer melt at a constant  $T_m$ . The jacket can be heated directly through resistance heating [80–83,95,108,213,223,236,240,244, 245], with recirculating water [29–31,102,103,105,106, 234] or oil [205,206,211,246] or by using a heat gun [31]. Alternatively, polymer pellets can be loaded into a custom metallic heating chamber [58,153,161,162,190,199,204, 208,210,215,230,247–249]. A syringe pump connected to the syringe or to a driving piston in custom heating chambers is typically used to control the extrusion of the polymer melt [29–31,80–83,95,102–106,108,161,162, 190,200,205,206,210,213,217,221,234,236,242,245,246], although other mechanically [220,230,237,248] or pneumatically [58,223,235] driven configurations have been assembled. In some cases the polymer is heated sufficiently to flow solely under the influence of  $g$  [63,88,153, 199,202,204,208,211,240,247]. Polymer pellets have also been loaded into screw extruders, adapted for melt electrospinning [79,198,231,250–253]. For polymers that are prone to thermal degradation when stored for extended periods above their melt temperature, several groups have sought to minimize the heating time the polymer is subjected to by preparing monofilaments [209], rods [96–99, 254] or bundles [101] of solid polymer that are mechanically fed into a laser melting zone. A radiant heater has also been utilized to establish melt electrospinning in a vacuum environment [88].

#### 6.1.1. Spinneret design

In the majority of cases to date, a single, electro-conductive spinneret has been used in laboratory melt electrospinning systems. Generally this comprises a flat-tipped hypodermic needle connected to the syringe or custom heating chamber, through which the polymer melt is extruded (circular cross-section). It is also possible to change the spinneret shape to produce hollow and noncircular cross-sectional fibers [244]. Alternatively, a custom die connected to the heating chamber has been manufactured [161,162,231,252]. In some spinneret designs, the nozzle is heated independently from the melt chamber/reservoir by a second heater: the reservoir is maintained at a temperature above the polymer melting point to allow the polymer to be driven by a plunger, but as low as possible to minimize thermal degradation. The spinneret temperature is increased to lower  $\eta_{\text{melt}}$  at the point where it must flow through the fine diameter spinneret, as well as to prevent the Taylor cone from solidifying near the spinneret [80–83,95,215,237,245,248,249].

Praeger et al. report a method where a gold wire is continuously dipped into a polymer melt reservoir and the melt is electrostatically drawn from the free surface of the wire, though this is prone to low rates of production [202].

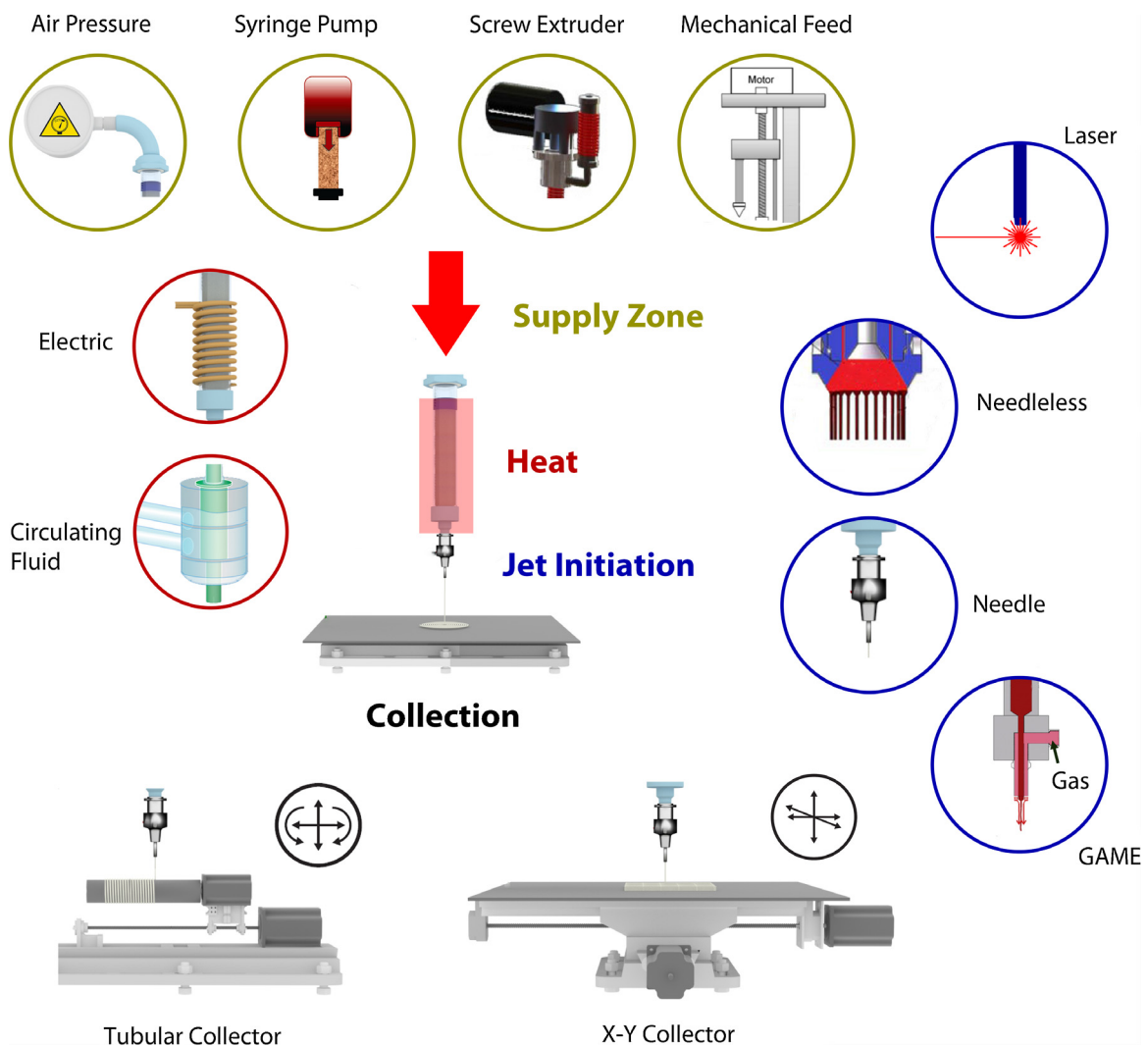


**Fig. 5.** A schematic of the many variations of melt electrospinning configurations reported in the literature. The supply zone delivers a force to the molten polymer where air pressure, syringe pumps/plungers, screw extruder and mechanical feeding mechanisms are reported. Heating of the feed polymer is achieved predominantly via direct electrical resistance sources or heated circulating fluids. A laser directed at a solid polymer filament may act both as the jet initiation point as well as the heating source. Other jet initiation systems include needles, needleless systems and also gas-assisted melt electrospinning (GAME) designs, which reduce the diameter of the collected fibers. Collectors can be stationary, however an x-y stage or rotating collector is used to perform direct writing. Unpublished Figure components provided by Felix Wunner, Queensland University of Technology, Australia.

With a view to improving the productivity of the process, several groups have investigated designs to establish multiple melt electrospinning jets. Hacker et al. designed and manufactured a 64 nozzle spinneret head [251], while several other groups have devised “needleless” spinneret designs. Shimada et al. have reported a laser line process where multiple Taylor cones can be established on a heated film of polymer [100]. Komarek et al. describe a linear “cleft” onto which a film of polymer melt flows from a reservoir [153], and Liu et al. developed an umbrella-like spray head onto the surface on which polymer melt flows and automatically forms multiple Taylor cones at the bottom edge of the head in a HV field [114,215,248]. Fang et al. designed a moving part spinneret, where a rotating metal disc partially immersed into a polymer melt bath is used as the fiber generator, underneath an inverted fiber

collector at a different HV potential. It is proposed that multiple discs can be attached along the rotating shaft to upscale this process [233].

#### 6.1.2. Application of high voltage

In many melt electrospinning devices, a positive HV source is connected to the metallic spinneret and a conductive substrate acting as the fiber collector is electrically grounded. Alternatively, negative HV sources have been applied to the spinneret [30,31,201]. Such configurations introduce the risk of arcing from the charged spinneret to other conductive metallic components in the polymer delivery mechanism if the spinneret is not shielded from these components. While the use of non-conductive glass heating jackets and plastic syringes (acting as a buffer between the spinneret and the driving syringe pump)

[103,105,106,234] is one simple strategy to avoid arcing, such designs are restricted to low melting point polymers below the temperature of the fluid circulated in the jacket. Other designs by Kong et al. [244] and Zhmayev et al. [80,82,83,95,245] have used resistive elements embedded in electrically insulating, thermally conducting ceramics to achieve higher melt reservoir and spinneret temperatures.

Another approach to protect the instrument components in the polymer delivery mechanism from electric discharge is to reverse the HV configuration in the melt electrospinning system. The spinneret and the polymer delivery device become grounded and HV (positive [79,81,199,200,204,206,208,210,218,230,231,237,238,240,247,250,252] or negative [161,162]) is applied to the collector substrate. However in these configurations for a given HV, the density of the electric charge available to charge the melt extrudate and form a Taylor cone is diminished: the extrudate must now be charged across the gap between the collector and the spinneret rather than charge be directly applied from contact with the spinneret; and mostly, the collector substrate has a significantly larger surface area compared to the spinneret, that reduces the electric charge density acting on the polymer for a given HV. The result is that increased HVs are required to be applied to the collector so that there is sufficient electrostatic drawing force on the surface of the extruded polymer to form and maintain a Taylor cone [79,198,210].

Alternatively, Shimada et al. applied a positive HV to the spinneret and a negative HV to the collector in order to generate a sufficiently strong electric field in their novel laser line melt electrospinning process [100]. Rangkupan et al. used the opposite configuration in order to melt electrospin in a vacuum [88]. In a unique arrangement, Mitchell et al. positioned the collection surface independently from the electrodes in a vacuum to avoid the influence of charge build-up on the collection surface on fiber collection [63].

## 6.2. Melt electrospinning jet zone

One aspect of melt electrospinning device design that is generally not reported is the conditions the melt jet is subjected to as it travels from the spinneret to the collector. It is assumed that in most cases when these conditions are not reported, the melt jet is subject to ambient air conditions at RT; where the effect is to rapidly quench the melt jet, inhibiting jet attenuation by rapidly increasing the jet viscosity and suppressing the development of whipping instabilities [81]. Fang et al. have reported melt electrospinning in a sealed chamber containing Argon in order to reduce the likelihood of arcing and therefore further protecting the working components [233].

Zhou et al. utilized a guiding chamber with IR heating to demonstrate that when the temperature in the melt electrospinning jet zone was raised from 25 to 80 °C during the melt electrospinning of PLA, whipping developed when the melt jet was prevented from solidifying before reaching the collector. When the jet zone temperature was raised above  $T_g$  (>55 °C for PLA), the AFD continued to decrease; where the whipping motion became stronger and extended the residence time of the jet in the melt electrospinning

zone, enabling prolonged thinning. However the stronger, though more irregular, whipping motion at higher temperatures resulted in a greater standard deviation of fiber size distribution [83].

Tian et al. found a similar result when laser melt electrospinning rods of PLLA and PLLA coated with ethylene vinyl alcohol (EVOH). Raising the jet zone temperature from 25 to 80 °C increased the jet thinning time by preventing solidification before the melt jet reached the collector, reducing the AFD [98]. Kong et al. studied the effect of the jet zone temperature on PP, by installing a ring-shaped metal heater in a guiding chamber close to the spinneret. The heating ring temperatures were controlled from 25 to 150 °C, while the rest of the melt electrospinning jet zone was exposed to RT [244]. The AFD was observed to decrease significantly when the temperature of the heating ring was increased, compared to cases where there was no heating in the jet zone. Additionally, by increasing the TCD, further time was provided for enhanced fiber thinning [244].

Zhmayev et al. reported that while IR heating can readily delay cooling of the electrified molten jet, keeping the size of the heater small is a difficult task from an engineering design point of view. Here, it is difficult to precisely control both the spinneret temperature and electrified jet temperature while not significantly degrading the polymer. To broach this issue, a gas-assisted melt electrospinning (GAME) configuration was designed, where a heated stream of gas was flowed around a PLA melt jet, supplied through the outer nozzle in a co-axial spinneret design. The gas stream transported heat from the spinneret along the outside of the polymer melt, thus delaying jet solidification. The significant flow of the heated gas added a drag force to the electrified jet, propelling it faster towards the collector with further thinning of the fibers in the absence of whipping instabilities [81].

## 6.3. Fiber collection zone

Although the majority of melt electrospinning devices are configured so that the collector lies directly below the spinneret and therefore the melt jet falls towards the collector, it has been shown that the effect of  $g$  on the jet is negligible compared to the driving electrostatic forces. Several groups have oriented the collector so that the path of the jet is horizontal, for practical reasons: where Lyons et al. [79] and Malakhov et al. [250] used a converted industrial extruder as the polymer supply system; Kim et al. supplied a second polymer, electrospun from the opposite side of a rotating collector drum [206]; as well as in cases where the spinneret to collection distance could be more conveniently modified over relatively large magnitudes [31,80–83,95,245]. Deng et al. described a system where the polymer supply chamber was gradually tilted so that the polymer melt flowed under  $g$  towards the spinneret [199], while in “needless melt electrospinning” Fang et al. described a system where a disc rotating in a polymer bath became covered in the polymer melt before being electrospun vertically towards a collector above the disc [233].

### 6.3.1. Collector material

Generally a stationary metallic substrate such as stainless steel [244], aluminum (Al) [105,213,215,217,218, 221,223,234,236,238] or copper (Cu) plate [80–82, 95–101,209,245], glass [29,221] or a plate covered in Al foil [102,161,162,190,210,221,222,237] is used to facilitate simple collection and removal of melt electrospun fibrous sheets from the device: where the conducting metal either acts to transfer the electrical charge from the collected fibers to ground or transfer charge to the jet. Solution electrosprayed particles were also incorporated into a scaffold by using melt electrospun fibers as a collecting material (Fig. 4E) [212].

Wang et al. compared collecting melt electrospun PMMA fibers onto Al foil with collecting fibers into a potassium chloride (KCl)/ice-water bath, where 10 wt% KCl improved the water conductivity. While during melt electrospinning the electric force induces chain orientation in the direction of the fiber, Wang et al. postulated that when the fibers are collected and the electric force reduces, the “molecular chains shrink and retract”. Here, the KCl/ice-water collector provided immediate resistance to polymer chain shrinkage, thereby improving molecular chain orientation and obtaining thinner fibers compared to an Al collector at RT [210]. Zhmayev et al. have similarly employed a cooled Cu plate collector [82]. Dalton et al. also demonstrated that melt electrospinning could be conducted into an aqueous substance [30]. In a method termed “direct *in vitro* electrospinning”, PCL/PEG-*b*-PCL fibers were melt electrospun onto live fibroblast cells in a PS Petri dish that was modified by inserting a metallic screw through the bottom of the dish to act as a grounded target [30].

Mitchell et al. reported that when a non-metallic collector such as a PS Petri dish, Teflon or Pyrex was placed independently between the spinneret and collector, the dielectric properties and surface area of such collector materials could be varied to distort the electric field the melt jet was subject to. Increasing the dielectric strength of the collector material “increased the resistance between the electrodes”, thereby reducing the current between the electrodes and increasing the fiber diameter. Further, there was increased residual Coulombic charge on the collected fibers that caused greater inter-fiber spacing. In contrast, increasing the surface area of the non-metallic collector caused the degree of field deflection to increase, amplifying the secondary instability of the melt jet, resulting in smaller fiber diameters [63].

Dalton et al. [29,221] and Wei et al. [235] have demonstrated that the focused deposition of melt electrospun fibers can be maintained when using thin glass microscope slides as the collector on top of a grounded metallic plate. Such substrates provide the advantage of expedient preliminary characterization of fiber morphology using optical microscopy, prior to the more involved process of scanning electron microscopy (SEM) characterization. Dalton et al. also reported that starPEG modified glass microscope slides could be used to improve the adhesion of PEG-*b*-PCL and PCL melt electrospun fibers to the slides when placed in cell culture solutions [29].

### 6.3.2. Moving collectors

One consequence of the focused melt electrospinning jet is that, although a greater volume of polymer melt will be dispensed for a given flow rate compared to solution electrospinning (due to solvent evaporation), the surface area coverage of the melt fibers will typically be less than that of a whipping solution electrospinning jet [197]. While modified spinneret designs such as multiple nozzle heads can be used to increase the surface area of fiber collection [251], researchers have also begun to employ moving collectors into their device designs. To ensure a consistent thickness of their melt electrospun meshes using a single jet, Mitchell et al. translated the collection surface in the horizontal plane in concentric circles with decreasing diameter from the outer edge of the collection surface. An average sample thicknesses of 0.3 mm was fabricated [63,204].

Dalton et al. placed a collector onto a manually moving x-y stage to collect lines of coiled fibers over areas up to 15 mm<sup>2</sup>. Using a computer controlled x-y stage, Mota et al. were able to collect 20 mm<sup>2</sup> square sheets of coiled fibers [198] and Ko et al. demonstrated similar 100 mm<sup>2</sup> sheets with 2 mm thickness. Karchin et al. mounted 25 × 75 mm phenolic boards and Cu plates as collectors onto an automatic x-y stage, that was programmed to translate in a raster pattern to ensure the boards were completely covered with melt electrospun fibers. The phenolic boards were inlaid with Cu traces 0.15 mm wide and spaced 2.5 mm apart to create parallel and diamond templated patterns [208]. Melt electrospun fibers were observed to deposit randomly as a nonwoven mesh on the uniform Cu plate, while on the phenolic boards the fibers deposited preferentially towards the conductive Cu traces. The result was that meshes with controlled regions of fiber concentration, according to the template design, were fabricated showing a degree of fiber alignment [208].

Another common approach that has been used by melt electrospinning researchers to fabricate highly structured sheets of fibers is to use a rotating mandrel collector and then remove the wound mesh and flatten it out [97,206,246,250]. Or alternatively, nonwoven tubular constructs can be fabricated for biomedical applications such as vascular prostheses [231]. When the tangential speed of the rotating collector is increased above that of the speed of the melt electrospinning jet, the fibers will be mechanically drawn straight, to create sheets of aligned fibers in the direction of rotation [96]. Larrondo et al. showed that the additional mechanical winding force could be used to further reduce the fiber diameter of PE, where at higher  $T_{ms}$  the fiber reduction was more significant [58].

## 6.4. Instrument parameters

To date, nearly all melt electrospinning journal articles have reported on experiments conducted to establish appropriate processing conditions for a polymer to be melt electrospun, where the resulting fiber morphologies are characterized using techniques such as SEM. While the conductivity of the polymer melt is a major factor in determining the ability to form a stable jet, as previously

discussed, by far the most important polymer property to control the diameter of melt electrospun fibers is the extensional viscosity. This is largely determined by the  $M_w$  of the polymer, as well as the presence of additives [247,248]. For example, in the first paper by Larrondo et al. where engineering-grade (i.e., high  $M_w$ ) PP was melt electrospun as received, the resulting fibers were up to hundreds of microns in diameter [58]. Dalton et al. showed that the addition of viscosity-reducing additives to such PP reduced the polymer chain length and therefore the viscosity, resulting in a significant reduction in fiber diameter from 36  $\mu\text{m}$  to 840 nm [31].

Extended heating times for polymers such as PLA, susceptible to thermo-oxidative degradation, will also lead to decreased  $M_w$  without the addition of anti-oxidant additives [215]. Increasing the temperature at the spinneret [31,58,72,80–83,95,102,105,114,198,199,201,204,211,215,231,244,245,247,248,250], as well as in the spinning zone [72,83,98,190,244] over suitable ranges has also been observed to promote thinning of the melt jet by reducing and maintaining reduced extensional viscosity and jet viscoelasticity. As the spinneret temperature increases the AFD decreases, and importantly, the standard deviation for the AFD is reduced [83].

In addition to controlling the extensional viscosity, once a melt electrospinning jet is formed, many studies have demonstrated that the fiber diameter can be influenced by varying “in process” operating parameters, that are controlled by the instruments used to build the machine. Such parameters include  $d_i$  (where used),  $Q$ ,  $V$  and TCD. The values of these parameters vary over finite ranges that are limited by both the ability to form and maintain a melt jet as well as the physical characteristics of the equipment chosen [30,58,72,79–82,95–105,161,162,198,199,202,206,209–211,215,220,231,235,244,245,248,255].

Liu et al. conducted an orthogonal design study showing that the influence of several instrument parameters on melt electrospun PP AFD was not as significant as the MFR, an indirect measure of the  $M_w$  [248]. The significance of the adjusted parameters on fiber diameter diminished in the following order: MFR >  $V$  > TCD >  $T_m$ . Whereas the influence on the fiber diameter SD occurred in the following order: MFR >  $T_m$  > TCD >  $V$ . It should be noted that while it was acknowledged in this study that  $T_m$  has the most significant effect on  $\eta_{\text{melt}}$  at a particular  $M_w$ , the varied temperature scale was conducted significantly above the melting point of PP and so a change in  $T_m$  did not lead to a significant change in  $\eta_{\text{melt}}$  for the different  $M_w$  PPs [248].

It is important to note that the configuration and dimensions of a melt electrospinning instrument impacts the processing of the polymer. Since to date melt electrospinning systems are designed and built largely “in-house”, there are many differences in how the devices function from a polymer processing point of view. This makes it challenging to quantitatively compare the effect on fiber morphology of varying an instrument parameter between devices, complicating the ability to derive definitive relationships between all of the instrument parameters acting in combination for each polymer. For example, different spinneret geometries and collector geometries will affect

charge transport to the polymer as well as the electric field profile to which the Taylor cone is subjected. Furthermore, according to Mitchell et al. the “the practice of grounding the collection surface to the lower electrode does not allow the manufacturing features to be independently controlled”. [63].

Typically in the literature, one instrument parameter is varied at a time while the other parameters remain fixed and the effect on fiber diameter is characterized. However, the interdependence between instrument parameters and the melt electrospinning conditions is illustrated in the following example by Dasdemir et al., where the electrostatic forces ( $f_e$ ) that act to stretch the melt electrospinning jet were defined as [220]:

$$f_e = \frac{e(t)V}{h(t)} \quad (9)$$

where  $e$  is the jet charge,  $V$  is the applied voltage, and  $h$  is the TCD. According to this model, the magnitude of  $f_e$  can be controlled by changing the electrostatic field strength ( $V/h$ ). A higher  $V/h$  could result in more stretching and therefore a decrease in fiber diameter. Higher  $V/h$  can be achieved either by increasing the applied HV or by reducing the TCD, or both [220]; Dasdemir observed the general trend that the AFD of melt electrospun PU fibers decreased with increasing  $V/h$  [220], while this was also reported for PE [58], PP [58,79] and PEG-*b*-PCL with PCL [30].

Deng et al. showed that AFD of LDPE continuously decreased when  $V$  was raised at fixed  $h$  [199]. When  $V$  was fixed and  $h$  decreased, there was not the expected monotonic decrease in AFD as a function of increasing  $f_e$ . Although the AFD initially decreased as  $h$  was reduced, there was a pronounced increase in AFD at low values of  $h$ . These results suggested that at too short TCDs, the melt jet did not have sufficient time to elongate. When the TCD was too long, the reduced  $f_e$  also resulted in thicker fibers [199]. Then  $V$  and  $h$  were simultaneously adjusted so that  $f_e$  remained constant. At low  $V$  and low  $h$ , relatively thick fibers were produced. As  $V$  and  $h$  were simultaneously increased, the AFD initially decreased until a point where it started to increase again, despite the constant  $f_e$  [199]. Unfortunately in this study, the authors neglected the power law relationship between  $V$  and  $h$ , where Coulomb's law states that  $f_e$  is directly proportional to  $V$  and inversely proportional to  $h^2$  [190]. Instead, the values of  $V$  and  $h$  were varied linearly to maintain a constant  $f_e$ .

Of the instrument parameters, material delivery rate is generally reported to have the most significant influence on fiber diameter; where increased supply of polymer to the Taylor cone will reduce the charge density and therefore the electrostatic drawing effect [28,245]. However, the mechanism to supply polymer to the Taylor cone influences the manner and therefore the unit used to describe the material delivery rate: for screw extruders units of “screw turns” (rpm) [198,231,252] are used; compared to the programmed flow rate (L/h) when a syringe pump is used to directly plunge molten polymer through a syringe [29–31,80–82,93,95,102,103,105,106,206,234,245]; the linear feed rate (m/s) is reported when a stepper motor is used to feed solid polymer rods to a melting zone [96–101,209,216,254]; and in other devices no  $Q$  is reported,

where the polymer melt flows to the spinneret under the influence of  $g$  and is drawn through the spinneret by the electrostatic force [63,88,153,202,204,211,240].

In addition to affecting the density of charge transported to the polymer,  $d_i$  also effects the fluid flow rate to the Taylor cone [82]. Interestingly, during the development of a non-isothermal model, Zhmayev et al. showed in a plot of dimensionless  $d_i$  versus distance from the spinneret that while the initial electrified jet profiles are changed with  $d_i$ , the final fiber diameters were not influenced. They proposed that their previous observations of decreasing final fiber diameters with decreasing  $d_i$  [83] can be attributed to an inadvertent lowering of mass flow to the spinneret. Similarly, studies by Kirichenko et al. with lower viscosity fluids concluded that the asymptotic fiber diameter limit is due to the MFR and not  $d_i$  [256]. In practice, experiments are often conducted using TCDs significantly shorter than the asymptotic limit of the melt electrospinning jet. In these cases, when all of the other instrument parameters are held constant, using a smaller  $d_i$  has been reported to result in smaller fiber diameters [190].

During the fabrication of melt electrospun PLGA fibers, Kim et al. studied the influence of certain instrument parameters: the AFD decreased with increasing  $T_m$  due to the lower  $\eta_{melt}$ ; the AFD increased gradually with increasing  $Q$  and increased  $d_i$ ; while  $V$  and TCD were observed to have a negligible effect on the AFD of the melt electrospun fibers. The significance of the effects of these processing parameters on the AFD of melt electrospun PLGA fibers was reported in the order  $Q > T_m > d_i > \text{TCD} > V$  [257]. Using a suitable combination of these processing parameters, the AFD of PLGA fibers could be controlled. A significant decrease in AFD was measured at lower  $Q$ , potentially due to the formation of a smaller Taylor cone with the decreased volume of polymer melt supplied [257]. In contrast, during the melt electrospinning of PCL Ko et al. reported that increasing  $T_m$  led to a significant increase in AFD when  $d_i$  was held constant, due to the accompanying decrease in polymer  $\rho$  [190].

These reports highlight that the effects of varying instrument parameters are not independent of the thermal profile of the melt electrospinning jet, where under non-isothermal conditions a series of complex nonlinear relationships will combine to affect quenching and thinning of the jet at differing rates. At this stage, in order to obtain high-quality melt electrospun fibers, it appears a degree of “tuning” of the instrument parameters is required to determine the optimum TCD [28]. While one approach to obtain fine fibers is by increasing  $V$  and reducing  $h$  to induce a large electrostatic drawing force on the jet, the speed of the jet may be sufficiently high so that it has not cooled to a solid state before reaching the collector, causing molten fibers to coalesce on the collector [220]. Higher quality fibers with solid, uniform morphology may be achieved by increasing  $h$  [30], however this may reduce the amount of fusion between fibers at their crossover points, and therefore weaken the overall fibrous structure [220].

In summary, several groups have built in-house melt electrospinning apparatuses with very diverse design characteristics, having been designed for research settings where much of the focus is on characterizing the

processability and suitability of various polymers to be processed into sub-micron and micron-scale fibers. While low cost single spinneret and static collector designs provide sufficient data for such preliminary proof of principle and characterization work, applications involving translating collectors to produce defined 3D structures will move the field forward. To deliver the fiber yields required for industrial applications, such configurations may be incorporated into designs that generate multiple melt jets. As melt electrospinning becomes more widespread and standardized machines are developed and used across many laboratories, the complex relationships between melt electrospinning jet material properties and environmental conditions will become better defined and controlled through instrument variables. Sub-micron diameter fibers have been produced from numerous melt electrospinning configurations in different laboratories [29,31,81,83,88,100–102,161,162,201,202,251,258], with the smallest diameter reported thus far for non-mechanically drawn fibers being between 25 and 250 nm [202]. For reference, Tables 2–4 provides a comprehensive summary of all the reported processing conditions for each polymer melt electrospun to date and the resulting fiber diameters, as well as comments on the configuration of the machine used.

## 7. Melt electrospinning and direct writing

Another group of fiber-based techniques based on micro-extrusion, that allow the formation of complex constructs, include melt extrusion-based direct writing [143] and fused deposition modeling (FDM). Based on the newest ASTM norms, such techniques have their roots in AM, which allow the fabrication of complex structures with high resolution and reliable precision [259]. In AM, data is read in from computer-aided design (CAD), converted into a series of computer generated cross-sectional layers and then created automatically as a solid object matching the CAD using layer-by-layer deposition [32,35]. In AM a broad range of polymers, ceramics, and metals can be used while the layer-by-layer deposition falls into three categories: powder-based; liquid-based, and solid-based systems [35]. AM – the industrial version of 3D printing – has tremendous potential in numerous scientific and industrial applications, since it allows designers and engineers to rapidly design, fabricate and test multiple prototype iterations including highly customized parts.

The suitability of a material to each AM process is largely distinguished by the state in which the material can be supplied, as well as the mechanism required to bond and solidify the successive layers. For example, material that can be delivered in a powdered form and will fuse under a laser beam is used in selective laser sintering (SLS) [260,261]. Alternatively, powders can be bonded together by a liquid adhesive in 3D printing. Stereolithography (SLA) [33] is a liquid-based AM method in which a photopolymer is cured by a UV laser beam [33]. Although objects with sub-micron resolutions are achievable with SLA [262], the limited number of commercially available resins that rapidly solidify upon illumination with light is currently recognized as a limitation of the technique [33].

Solid-based AM processes provide the advantage that thermoplastic polymers can be processed in their pure form by melting and subsequent shaping [263]. Industrial extrusion processes, typically used for injection molding or to feed melt spinning, have recently been miniaturized and adapted to AM [159,160,263]. In micro-extrusion, polymer pellets are inserted into a reservoir and melted, then driven by pressurized air into an auger-type screw, that transports the melt forward. Alternatively direct plunge methods can be used [264,265]. Eventually the polymer is extruded through a nozzle as a continuous filament, with the diameter largely dependent on the nozzle  $d_i$  [263].

In melt extrusion-based direct writing, the nozzle is located in close proximity to a collector platform. The extruded filament is deposited directly onto the collector, according to the pattern described by the computer-generated layer. The deposited material thermally bonds with the previous layers and then solidifies. For each layer of deposition, the collector is moved downwards by the height of one filament, so the next layer can be deposited. This layer-by-layer deposition is repeated until the desired 3D object is fabricated [266].

One limitation to melt extrusion processes is the thermal vulnerability of some polymers, including PLA, that degrade due to chain scission when they are heated for an extended periods above their  $T_m$  in the feed reservoir [267,268]. In contrast, FDM uses a solid polymer filament that is fed by motorized drive wheels to a heated FDM extrusion head. By regulating the temperature of the extrusion head to slightly above the  $T_m$  of the polymer, the filament is only melted just prior to being dispensed directly onto the collector, where a support material is dispensed in parallel. Furthermore, the solid filament acts as a piston to push the polymer melt towards the opening of the orifice [269]. This reduces the residence time of the polymer in the heating compartment and allows continuous production without the need to replace the feedstock. One disadvantage, however is that complicated filament preparation is necessary [270]. Although these processes allow excellent placement resolution, currently the lower limit of the filament diameter achievable is restricted to approximately 50  $\mu\text{m}$ . This is due to the high pressures required to extrude relatively high viscosity polymer melts through small diameter nozzles [234].

In many aspects, melt electrospinning can be considered an extension to such melt extrusion-based AM techniques. Whereas in direct writing the extruded polymer is applied directly to a collector surface, or previous layers of the build object, in melt electrospinning a separation distance is established between the dispense head and the collector. The addition of HV to the spinneret and subsequent electrostatic drawing of the charged polymer jet over this distance allows further reduction in the filament diameter, i.e. the potential for an improved resolution polymer melt direct writing process [32]. Alternatively, the nozzle diameter can be much larger than in AM while still achieving comparable filament resolutions without the high pressures required for direct melt extrusion and associated issues with damage to the polymer due to shearing as it flows through the nozzle [32].

Our group recently reported the development of a melt electrospinning-based direct writing technique (Fig. 6A) that allows the controlled fabrication of PCL structures up to 10 mm in height, over relatively large build areas, approaching single micron filament resolutions and 20  $\mu\text{m}$  placement resolutions [105]. The process relies on a stable electrified molten jet that directly ejects to the collector, without bending instabilities (Fig. 6B). If the melt electrospinning collector is stationary or translated at speeds below that of the melt jet elongation, the compressive buckling force as the jet impacts the collector results in coiling of the fiber to create a nonwoven substrate [29,105]. However when the collector speed approaches that of the jet, the tensile drag force between the cooling jet and the collector balances the compressive impact force (Fig. 6C). The result is that the characteristic fiber deposition buckling is damped and a continuous filament void of coiling can be collected with remarkable control: using computer-controlled translating collectors to print CAD data as achieved in other AM processes (Fig. 6D–I) [188]. More recently, Wei et al. showed subsequently that by reducing the TCD, the placement resolution could be improved to 10  $\mu\text{m}$  [235].

Solution electrospinning researchers have also sought improved control over the predictability of solution electrospun fiber deposition [32]. This has been achieved by reducing the length of the jet to below that at which bending instabilities develop, i.e. maintaining a straight jet flight path [235–240]. Scanning tip electrospinning [237] and near-field electrospinning [239] have used a computer-controlled translating collector to show relatively predictable control over the location of sub-micron fibers. However, both of these methods involve supplying the fluid as a droplet on a fine conductive tip that has been dipped into the polymer solution. This limits the total length of the fiber that can be deposited, and fiber thickness is non-uniform since the consumption of the polymer on the tip is not constant. Therefore, such approaches are limited to small amounts/areas of deposition, and their ability to develop 3D constructs is unproven. Although Chang et al. [238] and Hellman et al. [240] reported a similar method to control the location of fibers over a larger area, only a single layer of oriented fibers was demonstrated. Such techniques may find 2D applications, however solvent and charge accumulation issues may restrict the ability to create 3D objects.

The convergence between electrospinning and AM processes is highlighted in recent examples where tissue engineers have combined micro- (FDM) and nano-scale (solution electrospun) elements in the fabrication of porous constructs [271–273]. In this approach, following the printing of each FDM layer, the process was paused to deposit an electrospun fiber mesh, thus creating multimodal TE scaffolds. The larger FDM filaments created the overall architecture with large pores for cell invasion and provided the mechanical stability of the scaffold, while the electrospun nanofibers provided suitably fine structures and large specific surface areas for cell adhesion [32]. A melt electrospinning direct writing approach provides the potential to bridge these two magnitudes of scale, where melt electrospun fiber diameters can be controlled from

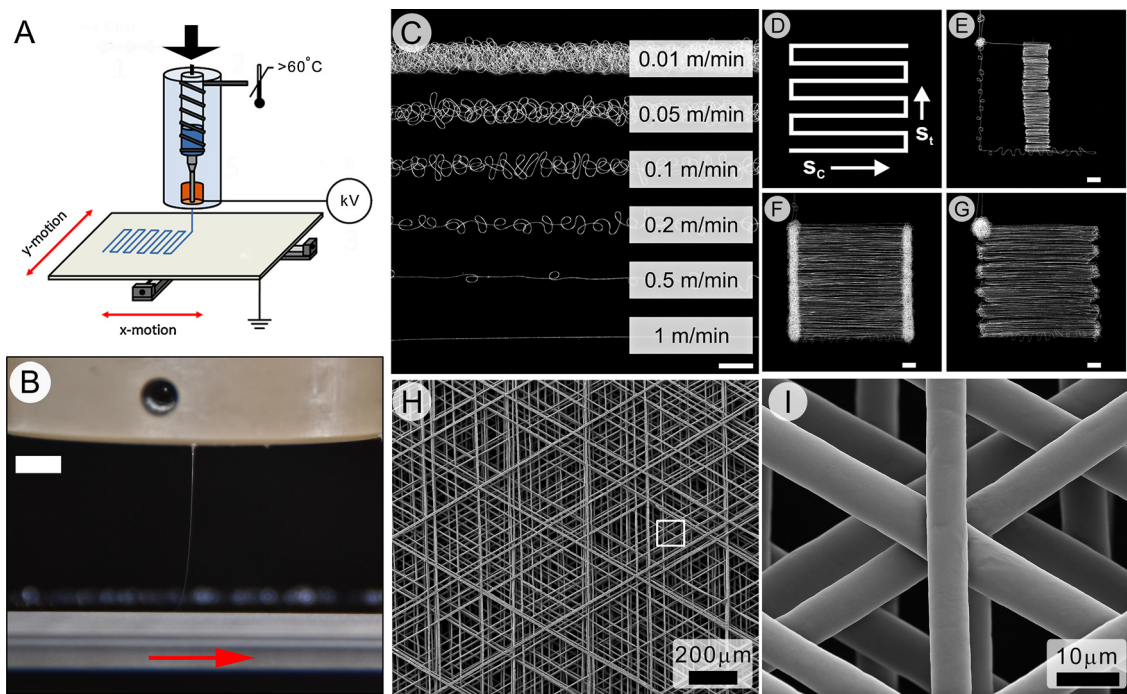


**Fig. 6.** (A) Schematic demonstrating melt electrospinning direct writing, where a collector is placed onto a computer-controlled x-y stage and translated laterally under the melt jet, according to a pre-programmed pattern [223]. So far as there is an electrical potential difference between the spinneret and collector, there are numerous permutations of how the voltage may be applied to the system to create the potential difference. (B) Photograph showing a stable PCL melt electrospinning jet in direct writing mode, where the collector is translating in the direction of the red arrow [107]. (C) When the collector is translated at relatively slow speeds compared to the melt jet (0.01 m/min), the fibers coil due to viscous buckling of the depositing jet. As the collection speed increases, the compressive  $\omega$  diminishes until the jet deposits as a straight fibre (1 m/min). (D) Schematic representing a programmed square wave pattern translated by the collector to direct write one layer of a TE scaffold. ((E)–(G)) PCL fibers written with constant straight line speed ( $s_c$  matching the melt jet speed) while the turning speed ( $s_t$ ) is varied (E) above, (F) below and (G) to match the melt jet speed, causing different results in fibre collection. ((H) and (I)) More complex collector translation patterns can be programmed to create TE scaffolds which are cell invasive. Copyright Permission Sources: (A) [223], Copyright 2014, Elsevier Ltd; (B) [107], Copyright 2014, Mary Ann Liebert Inc; ((C)–(I)) [105], Copyright 2011, John Wiley & Sons Inc. (For interpretation of the references to color in this figure legend, the reader is referred to the web version of this article.)

several hundred microns down to sub-micron ranges. Furthermore, since  $Q$  is a key determinant of AFD in melt electrospinning, it is possible to create a gradient of filament resolutions in a single process by varying only one process parameter.

With increasing interest in the ability to print periodic thermoplastic structures with sub-10  $\mu\text{m}$  resolution [274–276], improvements in polymer extrusion, control over the melt electrospinning jet characteristics, as well as fiber placement resolution, will accelerate the industrial application of melt electrospinning in a direct writing mode as an addition to AM [277]. One key property of this process is that it remains stable over periods of days of constant printing. Fig. 2 shows a PCL scaffold containing 150  $\mu\text{m}$  wide boxes produced using 8  $\mu\text{m}$  AFD filaments. The highly ordered micro-structure is repeated across the scaffold over centimeter dimensions with minimal defects. While such defined structures are available with other light based technologies, the low cost to establish melt electrospinning is an advantage.

## 8. Research translation and industrial potential

There are currently more than 50 companies worldwide marketing products manufactured from nonwoven

ultrafine solution electrospun fibers, that offer high specific surface areas to trap materials [20]. The predominant industrial application of such products is in gas and liquid filtration, including: dust/diesel particulate/smoke/aerosol removal in air intake systems for turbomachinery, transport cabins and cleanrooms; gas diffusion and turbine gas cartridges; as well as fuel/water separation and air/oil separation in waste water and engines. Other applications include composite membranes, reverse osmosis membranes and fuel cell catalyst technologies [20], textiles, separator and biomedical applications [247].

Donaldson Company Inc. have focused on the development of filtration media in areas such as cabin air cleaning, fuel, or oil filters, while DuPont market similar products, with the addition of medical device filters. Industrial scale fiber production devices such as the NanoSpider™ (Elmarco) or Ultra Web™ (Donaldson Company Inc.) are already marketed and used around the globe. With the continuous development and need for ultrafine fiber technology combined with the high industry demand for new filtration systems, we predict that the areas of application will rapidly expand.

To date there is no reported industrial use of melt electrospinning, where typically the polymer delivery rates required to achieve comparable fiber diameters are

significantly lower than in solution electrospinning. However, 100% of the melt electrospun polymer is collected compared to 2–10% of the total volume processed in solution electrospinning [218]. Dasdemir et al. showed that the deposition rate of melt electrospun PU was four times higher than when it was solution electrospun under the same processing conditions, though the AFD of solution electrospun fibers was much lower than those melt electrospun [220]. Achieving similar fibrous volume delivery rates with comparable fiber diameters to solution electrospinning will increase process efficiency and allow melt electrospinning to become industrially widespread. Currently, modified and multi-spinneret designs [114,153,215,248,251], as well as needleless polymer melt dispensing systems [153,233] are being developed, that demonstrate that multiple Taylor cones can be established simultaneously.

Increasing the quantity of samples is a common requirement for industrialization of a processing technology. Melt electrospinning operates at low flow rates ( $\mu\text{g}/\text{h}$  to  $\text{g}/\text{h}$ ) and research has been performed that tackles this challenge. One approach is to increase the number of spinnerets used, such as in Fig. 7A. Another approach is to use needleless systems, although this also results in HVs applied between the collector and melt. Needleless melt electrospinning configurations are a key aspect of scale-up for solution electrospinning and also have produced the greatest quantities of melt electrospun fibers. First performed using a laser system to melt a sheet of polymer (Fig. 7B and C), the highest output (36 g/h) has been achieved with so called umbellate spinnerets that result in up to 60 defined jets ejected towards the collector (Fig. 7D–F) [110].

Although melt electrospinning requires equipment not found in solution electrospinning, such as heating and cooling systems in order to maintain precise in-process temperature control, solvent recovery and treatment costs are eliminated. This will ultimately prove more attractive for industrial applications because materials can

be processed that are environmentally benign [237]. An important technological advantage compared to its solution counterpart, is that melt electrospinning can be coupled with a screw extruder to supply the polymer melt and thus continuous manufacturing is feasible [79,198,250,253]. As previously described, melt electrospinning is a fiber spinning process that allows the user great flexibility in the type of substrate manufactured. The device configuration, processing conditions and fiber collection method can be modified to resemble a variety of fiber spinning processes such as melt blowing and melt spinning to create: nonwoven fibrous mats with bonded or unbonded fibers; as well as aligned fibrous mats and tubular constructs with precisely-controlled porous architectures. Additionally, melt electrospinning can be conducted in a direct writing mode to produce complex 3D fibrous devices from micron-scale fibers that will allow new applications for this process.

Melt electrospinning enables a wide selection of thermoplastic polymers to be processed, including PE and PP that are not readily dissolved [245]. As more and more polymers are demonstrated to be compatible with processing by melt electrospinning, the list of potential applications will rapidly expand. Currently, proposed applications for melt electrospun polymers range from molecular templates [211], glass cleaning [87], chemical catalysis [202] and high-temperature gas filters [99], as well as solar sails in space [79,88]. This review concludes with a discussion of the diverse range of applications for which melt electrospun fibers are currently being investigated, in fields including: energy; environmental, filtration and separation applications; textiles; and biomedical engineering.

### 8.1. Energy

Cho et al. demonstrated the super-hydrophobicity of PP fibers melt electrospun at elevated temperatures, that can be deposited upon solar cells to reduce contamination and

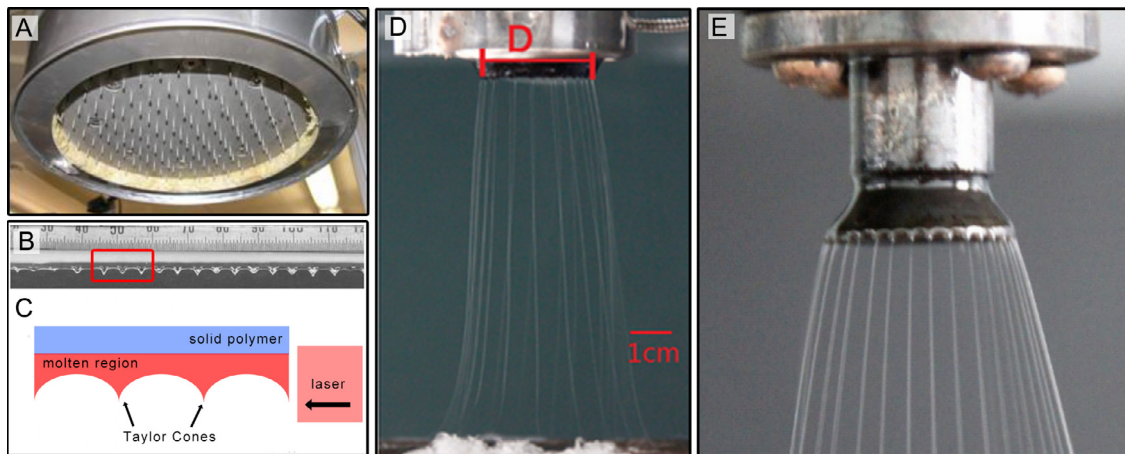


**Fig. 7.** Various melt electrospinning spinneret designs to generate multiple Taylor cones which are simultaneously electrostatically drawn towards a collector to form nonwoven material. (A) A multi-nozzle melt electrospinning design concept [28,251]. (B) Multiple jets developed (C) during laser melt electrospinning [100]. Similarly two electrically heated “umbellate” large (D) or small (E) deposit increased quantities of fibers, [111] and [110], resp. Copyright Permission Sources: (A) [28], Copyright 2008; (B) [100], Copyright 2010; ((D) and (E)) [110], Copyright 2014, John Wiley & Sons Inc.

increase their effective lifetime [94]. It was noted that the major requirement for such hydrophobicity is that the fiber diameters should be less than 10  $\mu\text{m}$ . Improved performance over commercially available nonwoven mats was demonstrated due to the reduced diameters of the electrospun fibers [94]. Other potential energy applications that are currently being investigated by melt electrospinning researchers include: electronic circuit design [218]; organic electronics [161,162,275]; piezoelectrics [201]; battery separation [99,218,230,247,255]; microelectromechanical systems [275]; as well as micro/nano optical [88,211], thermal and chemical sensors [81–83,95,218,275].

While many of these energy applications can be served by polymeric materials, the ability to produce ultrafine fibers readily from glass, with its accompanying thermal, optical, mechanical, and chemical properties, will prove very useful, particularly in hostile (high temperature, corrosive) environments [202]. Electrospinning of glass fibers direct from the melt may also potentially unlock areas of interest such as on-chip production of sub-wavelength optical interconnects [278]. Although there have been reports demonstrating electrospun glass or glassy fibers, these have invariably required the use of a host polymer solution, with subsequent post-processing steps involving heat/chemical treatment to form the glassy material [279,280].

To date, the direct production of sub-micron diameter glass fibers has relied on mechanical drawing techniques [281]. However, Praeger et al. recently reported the experimental realization of glass nanofibers by electrospinning directly from molten  $\text{B}_2\text{O}_3$ , demonstrating the viability of electrospinning fibers from non-polymer materials with high melting temperatures and higher  $\gamma$ . The resulting solid glass fibers had diameters around 100 nm and no post-processing was required [202].

Another feature of melt electrospinning is the ability to create coaxial fibers from polymer blends, mirroring that of coaxial solution electrospinning. In this manner, an inner “core” material can be supplied through a capillary that is located concentrically inside the spinneret, and delivered inside a stable “sheath” material. This approach significantly expands the applications of these materials by changing their performance [250]. Sahoo et al. noted that nanocomposite fibers with improved electrical and mechanical properties can be obtained by incorporating CNTs into melt electrospun thermoplastic polymers [282], where these fibers can readily be employed in energy applications such as electrodes in solar cells [88,218]. Although solution electrospinning was used to disperse and align CNTs within a polymer matrix, the extended  $\pi$  conjugation was disrupted resulting in reduced conductivity of the functionalized CNTs [282].

Cao et al. recently demonstrated the melt electrospinning of a multi-walled CNT/PP conductive membrane, containing fiber diameters between 1 and 3  $\mu\text{m}$  [218]. To increase the dispersion of CNTs and the spinnability of PP, the CNTs were initially mixed in paraffin liquid prior to melt-blending with PP. Compared with traditional fibrous membranes, this was reported to provide significant processing advantages and resulted in good electric conductivity, excellent tensile strength, modulus

and hydrophobicity. Reported potential applications are wide ranging, including the preparation of electric devices, antistatic protective clothing, coatings on solar cells, TE scaffolds, biosensors, and electrochemical detectors [218].

## 8.2. Environment, filtration and separation

Filtration and separation processes using fine porous membranes are becoming more important and finding increasing applications in process industries, including: gas and liquid filtration [31,63,79–83,87,88,102,104,162,201,202,209,211,215,218,220,230,247,250,251,283–286]; petrochemical [287]; as well as previously mentioned electronic, fuel cell, and clean energy systems [284,288]. Demand for novel, efficient, and long-life filtering and separation media is very high [20,88]. Compared to traditionally used materials, ultrafine fibers can provide several advantages such as high surface energy, fine porous structures and relatively high strength, which implies less energy consumption during the filtration process [20], as well as drastic enhancement in collection efficiency of sub-micron sized particles [83]. Depending on the membrane structure, various fundamental processes can be achieved: particles of different sizes can be separated from each other; immobilized to improve specific separation or filtration behavior; or contact membranes can be used as mediators to promote contact between two reactive components [20].

Ultrafine fibers can be used in water filtration to pre-treat waste water before reverse osmosis, significantly reducing power consumption and system maintenance costs, while providing the ability to operate with higher flux [289]. Melt electrospun fibers may be useful in the production of large quantities of filters for such industrial and domestic applications, reducing the large volumes of toxic solvent and waste associated with solution electrospinning. Polymers such as N6 [80,93,95,100,209,250], PE [58,97,199] and PP [31,58,79,88,153,161,162,209,218,230,231,233,244,246–249,251,252], that are used in industrial filtration, have been processed using melt electrospinning. Dalton et al. have demonstrated that melt electrospun fibers from such polymers can have diameters small enough to be used as nanofiltration membranes [31].

PET has been melt electrospun by groups including Ogata et al. [99,158,209,211] into membranes that may be applicable to the food industry in applications such as apple juice clarification [290]. Rajabinejad et al. demonstrated that melt electrospinning of used PET bottle plastic into ultrafine fibers is a viable technique to increase the degradation rate of the polymer and improve recycling, therefore reducing environmental pollution [211].

In addition to biomedical applications where it is innocuous and biocompatible with human tissues, PLA is a biodegradable polymer commonly used in daily applications, such as: disposable cutlery, plates, cups, lids, films, and containers for liquid foods [114]; as well as being widely employed in packaging and agricultural materials [254]. PLA is an aliphatic polyester that can be hydrolyzed, degraded by microbes, with the eventual degradation products being  $\text{CO}_2$  and  $\text{H}_2\text{O}$  [96]. As such,

many investigations have recently been conducted on PLA fibers [81–83,96,231,245,252] where fibers with diameters down to 180 nm have been produced by melt electrospinning [81] for applications including dust particle capture in air [83,215].

### 8.3. Textiles

Melt electrospun fibers may also find application in specialty textiles [31,95,161,220], including: non-wetting textile surfaces [79]; artificial leather [209]; wiping cloths [209]; composite materials reinforcement in military and construction [79,202,220,247]; as well as protective clothing from chemical warfare agents [88,220,255] and from pesticides in agriculture [63,162,211,218,247,250]. For any textile to be used to prevent liquid penetration for personal protective equipment (PPE), the surface chemistry of the selected polymer is a critical factor. While membrane hydrophobicity is important to repel liquid, protective clothing made of impermeable materials may be hazardous, causing issues such as hyperthermia at higher temperatures. Thus, the breathability of a material for wearer comfort in hot, humid conditions must be considered in combination with providing high barrier performance [291].

PP is one of the widely used nonwovens for PPE due to low cost, its light weight nature, chemical resistance and low surface energy. Lee and Obendorf demonstrated a breathable textile made from melt electrospun PP fibers, where water vapor was allowed through the fabric, while the hydrophobic surface created high barrier performance to water in liquid state. Such protective clothing provided high levels of comfort while protecting workers from chemicals such as pesticides [27]. Schreuder-Gibson et al. showed increased aerosol protection by using a fine layer of electrospun fibers. Electrospun N6,6, polybenzimidazole, polyacrylonitrile, and PU provided good aerosol particle protection, while maintaining moisture vapor transport [292].

Schreuder-Gibson reported that one major advantage of electrospinning in the manufacture of PPE is that fibers can be applied directly to garment systems, in particular onto 3D forms [292]. With the added control over the melt electrospinning jet permitting focused deposition of fibers, this would allow regional differences in the coating thickness. This was proposed as useful in producing “zoned” materials, eliminating costly manufacturing steps as well as solving seam-sealing challenges for PPE [291,292].

### 8.4. Biomedical engineering

The interest of the biomedical community in electrospinning started in the early 2000s and the number of papers published on this subject increased exponentially, particularly for the biomaterials and TE & RM fields. Both synthetically prepared and biologically derived polymers have been used for more than two decades in the electrospinning of TE scaffolds. The selection of the biomaterial is influenced by the application, physical and chemical properties of the polymer as well as the scientific question being asked. The polymer properties and the rate of

degradation are tuneable by modifying the polymer composition and  $M_w$  while most biodegradable implants are made of aliphatic polyesters, polyorthoesters, polyanhydrides, polycarbonates and their copolymers [293]. The most important aspect determining the suitability of a polymer for use in biomedical applications is its purity, defined by a so called “Material Master File”; the quantitative and qualitative presence of leakage substances, processing aids, surfactants and catalysts that affect the potential for adverse effects, such as local and systemic toxicity distinguish medical grade from common grade polymers. Since melt electrospinning allows medical grade polymers to be processed “as received”, this provides a significant advantage to gain regulatory approval over devices fabricated using processes such as solution electrospinning, where the removal of toxic solvents through post-processing proves technically challenging and expensive [80–83,95,101,161,162,202,220,230,240,251].

#### 8.4.1. Growth factor/drug delivery

In drug delivery, there is a need for controlled release systems where sustained and/or booster drug release is often preferred for drug-loaded implants [294], and wound dressings [295] for adequate long-term effect. In addition to sustained drug release, oral dosage forms often require enhanced dissolution to achieve sufficient bioavailability, since many drugs possess poor water solubility [237]. Nagy et al. recently demonstrated the improved release of a drug with poor water solubility, loaded into a cationic methacrylate copolymer that was melt electrospun [237].

The potential for melt extrusion to increase the drug dissolution is widely demonstrated in the literature [296–298], and marketed products such as Kaletra® and Isoptin-SRE® (Abbott, Chicago, Illinois) are being prepared using this method [299]. Recently Nagy et al. demonstrated the preparation of Eudragit® melt electrospun fibers with the release of Carvedilol (a poorly water soluble drug). The release rate from the melt electrospun fibers was greater than that of the extrudate, likely due to the increase in surface area. In another study the advantages of pharmaceutical melt extrusion manufacturing (e.g. solvent-free, continuous process, and effective amorphization) were combined with solution electrospinning (large product surface area) to achieve enhanced dissolution. It was noted that while the productivity of using a single spinneret was limited, this can be significantly improved using multi-spinneret heads or needless approaches [237].

Another approach for the fabrication of scaffolds for biomedical applications is the stabilization of small particles, proteins, or molecules in paraffin droplets that are incorporated into a fibrous matrix, allowing release of the molecules at a controlled rate [20,258]. Bock et al. recently demonstrated the fabrication of biodegradable PCL microfibers coated with high densities of PLGA microparticles, encapsulating a model protein, bovine serum albumin. This technique enabled control over the physical and protein release parameters that may ultimately be tailored to fit any protein delivery purpose, and may be particularly suited as a template for growth factor delivery therapies for skin, cartilage and bone [212]. Coaxial melt electrospinning has also been widely proposed as a promising method for

the microencapsulation and controlled release of growth factors and drugs [237].

#### 8.4.2. Biosensors

Melt electrospinning with a coaxial spinneret is also being explored as a method for “the encapsulation of solids in a composite or polymer matrix to generate nanofiber-based phase change materials (PCM)” [258]. While attracting interest for “their phase-transformation reversibility and energy-storage and management properties” [222], the translation into real-world products of phase change thermochromic materials (PCTM) has been limited due to their fluidity after melting [222]. Since PCMTs melt and crystallise with thermal cycling, it is necessary to stabilize them in a solid matrix. Recently Li et al. described the fabrication of thermochromic core–shell fibers by coaxial melt electrospinning, where a PCTM was encapsulated in PMMA fibers. Using a transparent PMMA shell with a thermo-responsive core (Fig. 4S) made of a mixture of crystal violet lactone, bisphenol A, 1-tetradecanol (CBT), the fibers had promising properties for this application [222].

One traditional PCTM system with stable thermochromic properties involves crystal violet lactone (CVL) as a dye and bisphenol A as a developer, mixed with a fatty alcohol or fatty acid: where the thermochromic temperature can be adjusted by changes in the concentrations. While the phase-change temperature of 1-tetradecanol matches the human body temperature. The CBT system was shown to have an absorption and release process at the melting point of 37–39 °C combined with a fluorescent change at the phase-change temperature. The fabrication of PCTM encapsulated ultrafine fibers has further potential in the preparation of body-temperature thermal materials and thermoresponsive sensors [222].

McCann et al. developed a similar method based on melt coaxial electrospinning to fabricate phase change fibers consisting of long-chain hydrocarbon cores and composite sheaths [258]. They used nonpolar solids such as paraffins for electrospinning and adopted a one-step procedure for encapsulation. Such PCM fibers are able to “absorb, hold, and release large amounts of thermal energy” due to the heat of fusion of long-chain hydrocarbons [258]. This study focused on compounds with melting points near RT and body temperature as these temperature ranges are most valuable in practice [258].

In summary, the electrospinning of stimuli-responsive compounds into micro/nanostructures is an emerging field with the potential to generate new research directions for the biofunctional materials community [202,247].

#### 8.4.3. Tissue engineering & regenerative medicine

RM, and in particular TE, is a field of biomaterials where the development of applications based on electrospinning is rapidly gaining interest [12]. In fact, a significant proportion of the melt electrospinning literature is currently focused towards developing viable fibrous synthetic biomaterials onto which cells can be grown into tissues [29,31,63,79,88,97,98,102–106,190,198,199,202,204,206,208,216,218,220,230,231,234,235,240,247,252,253,255,300] for: artificial vascular grafts/blood vessels [79,88,

211,220,231,234,248,252]; wound dressings [79,82,87,88,199,202,248,253] and dermal substitutes [199,234]; as well as for implant interfaces [63,214] and establishing disease models [108].

The central concept of TE is to “combine a scaffold or matrix, with living cells, and/or biologically active molecules to form a tissue engineering construct (TEC) to promote the repair and/or regeneration of tissues” [34]. Although the functions provided by a TEC should be tailored to assist the repair and/or replace the function of specific tissues in a unique state of health and/or injury, there are general properties expected from all TECs, including: appropriate mechanical properties; non-toxic degradation products; as well as biochemical properties and an architecture that supports cell attachment, migration, growth, and ultimately tissue maturation [28]. The importance of an open and interconnected pore network throughout the TEC has been identified as a critical element to ensure that cells invade the entirety of the TEC. Furthermore, this allows the transfer of nutrients and waste throughout the cellular network, as well as tissue ingrowth, vascularization, and eventually integration of the TEC with the host tissue. Ideally, the gross size and shape of the TEC should also be customized to the patient [301].

The design and manufacture of scaffolds for TE & RM was initiated over four decades ago and is constantly being improved upon. In addition to developing biocompatible materials as raw materials for scaffolds, there are practical manufacturing considerations that must meet the complex and numerous requirements for a TEC. For example, the manufacture must be reproducible, in a sterile environment at an economic cost and speed while meeting the requirements for regulatory approval of a medical device. If the fabrication process requires biological components, such as growth factors and/or cells to be added, then these must be accommodated within the regulatory framework [302]. Ideal TECs are inherently complex and have been part of the exploration of innovative manufacturing techniques including AM [28] as well as conventional chemical methods [301]. However, many current approaches lack the resolution or control of placement of structures, and thus porosity, in a 3D environment that has volume relevant to a biomedical device for tissue replacement or repair (at least 1 mm in all directions) [28].

Conventional scaffold fabrication techniques are based on chemical processes and include: solvent casting and particulate leaching [303–305]; gas foaming [306–308]; and phase separation [309,310]. However, these processes are unable to precisely control key scaffold properties such as pore size, geometry, interconnectivity and anisotropic morphologies [35]. In addition, many of these techniques require organic solvents to dissolve polymers, so an additional requirement of manufacture is to ensure that cells are not exposed to toxic and carcinogenic residual solvents [30].

Solid freeform fabrication (SFF) technologies have recently been introduced within TE and include 3D printing [311–313], SLA [314–316], FDM [266,269,270,317], SLS [318–320] and direct writing [321,322]. As reviewed in detail by Melchels et al. and previously described, SFF is often used to describe AM techniques [34].

Many AM techniques that are based on the controlled deposition of molten material extruded through a nozzle/orifice [321] are relevant for comparison with melt electrospinning. Although these techniques involving biocompatible/degradable polymers provide precise control over key scaffold architectural features such as pore size, pore geometry and interconnectivity to create an environment promoting cell-invasiveness and growth [323], they currently lack the filament resolution ( $50\text{ }\mu\text{m}$ ) and thus high specific area required when trying to mimic the physical microenvironment of native extracellular matrix (ECM).

As previously mentioned, solution electrospinning has been heavily researched since the turn of the 21st century for the fabrication of TE constructs [324], providing a user-friendly approach (compared to other fiber manufacturing technologies) to fabricate macro- to nanoscaled fibrous constructs with a variety of properties that encourage cellular adhesion, migration, and proliferation: fiber diameters within the size range of the fibrils in native ECM, as well as high porosity and surface-area-to-volume ratios [1,325]. Furthermore, electrospinning allows the surface chemistry of fibers to be tailored, the fabrication of aligned structures to direct cell growth, and the incorporation of bioactive molecules through methods such as encapsulation [326–328].

Although solution electrospun nonwovens provide a dense network of interconnected ultrafine fibers, more often than not, the ability of cells cultured on such constructs to invade throughout the TEC is limited since the pore sizes are smaller than that of the cells [329–334]. Depending on the tissue, the optimal pore size can vary [335]. For example, pore sizes of  $>300\text{ }\mu\text{m}$  have been recommended for the cellular growth into and vascularization of bone, [336], while fibroblasts appear to benefit with a smaller diameter pore size of approximately  $6\text{--}20\text{ }\mu\text{m}$  [337]. The inherently small pore diameters of solution electrospun scaffolds (reported as low as  $100\text{ nm}$  [338–340]) are smaller than that of cells and as such act as a barrier to cellular infiltration and tissue ingrowth [341] where cells cultured on solution electrospun substrates often remain only on the surface. Unfortunately, this incongruity in scaffold design is not frequently discussed in the electrospinning literature. A study by Mikos and colleagues demonstrated that, assuming randomly deposited fibers on a flat stationary collector, fiber diameters must be at least  $4\text{ }\mu\text{m}$  to create an electrospun scaffold with a minimum pore size of  $20\text{ }\mu\text{m}$  in order to promote cell invasion *in vitro* [189], while to ensure vascularization of relevant tissues *in vivo*, pore sizes larger than  $100\text{ }\mu\text{m}$  are required [342].

With this in mind, recently there has been a move away from using nonwoven solution electrospun substrates, where the fibers are randomly deposited, in order to develop cell invasive scaffolds. It has been observed that ordered and aligned fibers are preferential in TE, amounting to guided cell growth [328]. Various device configurations have been explored with varying degrees of success to accurately place fibers in specific locations. As well as guiding cell growth, this opens up opportunities to increase the pore sizes of such constructs, and therefore promote cellular infiltration while using sub-micron diameter fibers [343].

**Fig. 8** shows TECs after seeding cells onto melt electrospun scaffolds fabricated using an AM direct writing approach. These scaffolds were constructed on either flat (Fig. 8A–D) or curved (Fig. 8E–G) collector surfaces. Such scaffolds have pores large enough to promote cell invasion and seeded cells have been shown to produce key ECM components such as collagen and fibronectin. Indeed, a core aspect of such scaffolds is that fiber placement can be controlled independently from fiber diameter. This may permit the rational design of scaffolds where varied combinations of pore size and fiber diameter can be investigated for optimal conditions for the growth of various cells/tissues.

Methods investigated by electrospinning researchers to improve fiber alignment have included: manipulating the electric field in an attempt to control the flight of the charged electrospinning jet [104,344–347]; introducing a rotating collector/mandrel into the experimental setup and then removing the wound mesh and flattening it out [206,348–357]; or combining these two approaches [65,328,350,358–361]. Specific approaches to increase pore size include: the use of patterned electroconductive collectors, with ridges, indentations, grids or pores, that act as templates to form patterned 2D solution electrospun meshes [362–364]; collecting fibers onto liquid media [365–367]; or post-electrospinning modifications, that involve the adaptation of hydrogel modification techniques, including sacrificial polymers [21,368–370].

Although scaffolds with improved fiber alignment and a broad range of pore sizes from  $10$  to  $931\text{ }\mu\text{m}$  [343] have been fabricated, precise control over inter-fiber spacing or the ability to create complex patterns remains elusive as there is still a degree of randomness in the approaches described above [250,363,371]. In solution electrospinning, the build-up of electrostatic charges on the deposited fibers and/or the collector causes a loss of control of fiber location over time before the structures obtain any relevant thickness to be classed as a truly 3D TE scaffold [70]. Furthermore, the fibers forming these structures are poorly connected, with poor structural integrity [70]. Thus, the ability to additively manufacture a defined 3D structure using solution electrospinning alone is still unclear.

Recently, improved control over solution electrospun fiber deposition has been achieved by adopting AM principles with a computer-controlled translating collector and short TCDs to avoid bending instabilities in the jet [188,352,372,373]. However, these methods have been limited to extremely small deposition areas/thicknesses and the removal of accumulated solvent is a significant issue for mass production, becoming more challenging as the TCD is reduced. Hence the difficulty to fabricate constructs with a thickness relevant to TE applications remains, while the chemicals used to dissolve the biopolymers may leave residues that can affect the biocompatibility of the TEC and induce an undesirable host response. These factors create a challenge to establish acceptable integration between the TEC and the host tissue [28].

Using biodegradable polymers such as PCL, melt electrospun fibers have recently been assembled using a bottom-up AM approach to create 3D constructs with well-controlled porous architectures. By precisely controlling

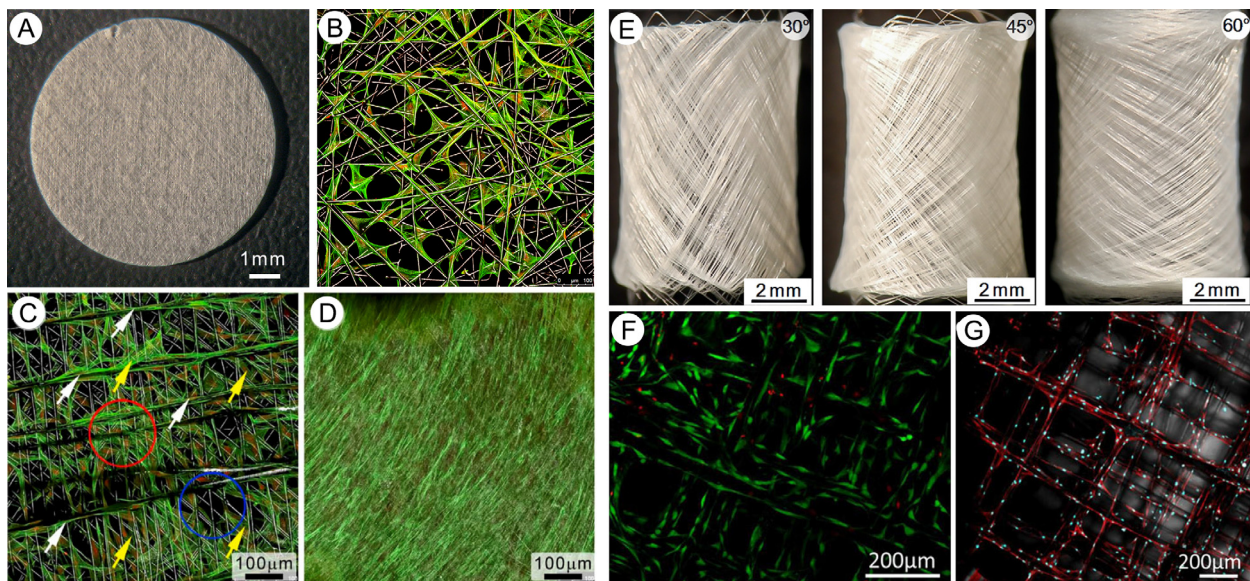


**Fig. 8.** Cell adhesion on TE scaffolds formed using melt electrospinning writing. (A) Scaffold fabricated with a change in fibre pitch of 30° in both x and y directions and (B–D) subsequent seeding of fibroblasts onto the scaffold, with good adhesion and full confluence after 7 and 14 days *in vitro*, respectively [234]. (E) Direct writing onto tubular collectors has also been performed, with the fibre pitch changed depending on the desired morphology [106]. (F) Live/dead staining showed that >90% of the seeded hOBs were alive after 2 weeks of culture, while (G) shows the hOBs, fixed and stained for f-actin (red) and nuclei (blue), elongated and oriented along the fibers. Copyright Permission Sources: (A) and (C) [234], Copyright 2013, IOP Publishing; (B) [32], Copyright 2013, the Royal Society of Chemistry; (D) [234], Copyright 2013, IOP Publishing; ((E)–(G)) [106], Copyright 2012, AIP Publishing. (For interpretation of the references to color in this figure legend, the reader is referred to the web version of this article.)

the spacing between adjacent fibers as each layer is written, the pore sizes of the structure can be designed with size and control over geometry so far not demonstrated in solution electrospinning. Such TECs have been demonstrated to be cell invasive when using simple top-seeding approaches [32,105,106,234].

With the prevalence of tubular anatomical structures throughout the human body, varying approaches to tubular scaffold fabrication have been investigated [106]. Recently, using PCL, our group demonstrated that the melt electrospinning jet can be wound continuously onto a rotating tubular collector in a manner similar to melt spinning [83]. Adjusting the take-up speed (at speeds above the jet speed) allowed control over the AFD due to induced drawing, as well as controlled fiber alignment. At relatively low  $T_m$ , there was no bonding between the wound fibers at the points where it crossed over itself. By increasing  $T_m$ , the wound fiber bonded at the crossover points to create a porous tubular structure. When the rotating tubular collector was translated back and forth laterally to the jet path, controlling the relative speed between the rotational and translational speeds allowed the winding angle of the melt electrospun fiber to be controlled. By defining the winding angle, tubular structures with controllable micro-patterns and mechanical properties could be fabricated using micron diameter fibers (Fig. 8E). In particular, the porous architecture of the tubular structure could be designed in terms of parameters including: number of pores; pore size and geometry; as well as total porosity [106].

Since melt electrospinning can take place in a sterile sealed environment without the requirement for evaporation of toxic solvents, the underlying biocompatibility of the fibers is dictated by the bulk material, its purity and whether toxic products result from thermal degradation during melt processing. For PCL, which is available in medical grades, a combination of relatively low  $T_m$  ( $\sim 60^\circ\text{C}$ ) and long degradation time results in cell compatible fibers, despite prolonged elevated temperatures. Fig. 9A shows how melt electrospun PCL fibers, which together form a TE scaffold interact with a bone chip (white arrow) that has been caught at the convergence of fibers. Mesenchymal stromal cells (MSCs) are migrating out of this bone chip and adhering well to fibers (red arrows). Fig. 9B–E demonstrate MSCs top seeded and cultured for periods above a week, dividing and forming rounded tissue structures prior to filling the pores with more cells and ECM.

The melt electrospinning of non-water soluble polymers allows fibers to be collected onto water or directly onto cells [30]. Dalton et al. melt electrospun fibers from a blend of PEG-*b*-PCL/PCL directly onto *in vitro* cultured fibroblasts. Cell vitality was maintained throughout melt electrospinning and after 6 days fibroblasts were shown to migrate and proliferate within the fiber network. The fibroblasts formed long and spindle-shaped morphologies when adhering to the fibers. Such results demonstrate an important step towards producing layer-on-layer TECs for TE [30].

A fundamental advantage of AM is the ability to fabricate multiphasic scaffolds that contain different process

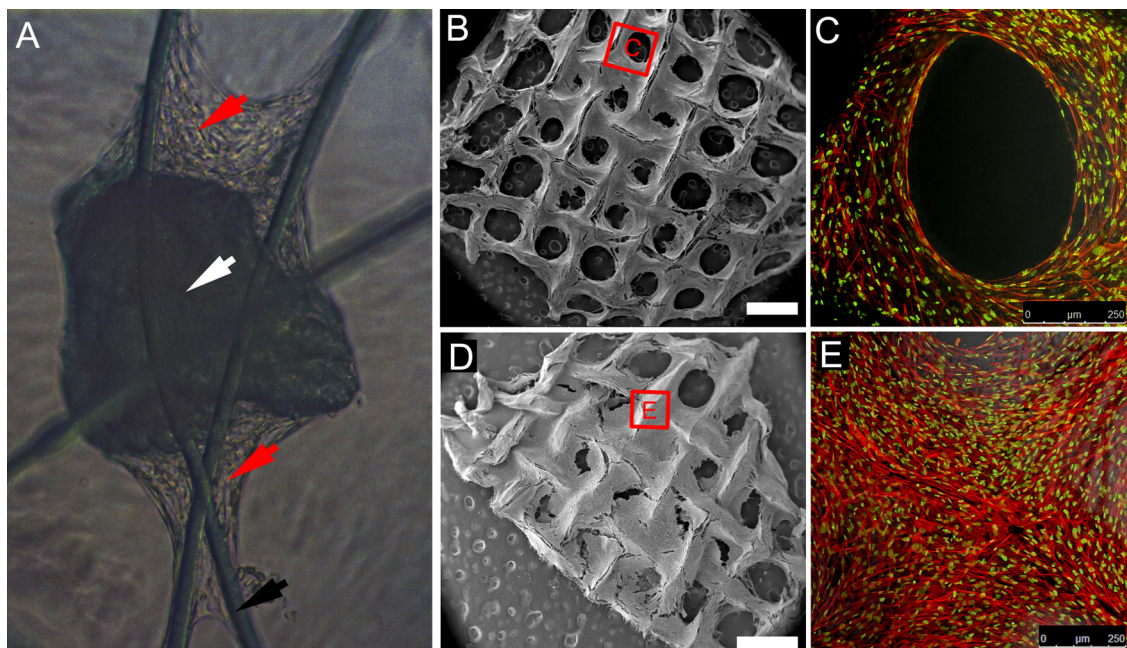


**Fig. 9.** Cell migration and ECM production on melt electrospun TE scaffolds. (A) Photograph of a small bone chip (white arrow) caught between fibre junctions. Cells are migrating out of the bone chip and are migrating along and bridging the gap between fibers (red arrow). ((B) and (C)) A scaffold fabricated using 90° fibre turns and seeded with hOBs. After adhesion to the fibers where the cells organize along the fibre directions, cells divide and begin to fill the square pores, spanning across the perpendicular fibre junctions at the corners of the pores. ((D) and (E)) With time the circular voids become filled by cells until they close each pore. Sources: All Figures unpublished and are courtesy Dietmar W. Hutmacher from Queensland University of Technology, Australia.

components, where each component provides a unique regenerative function. This is shown in Fig. 10 where scaffolds containing sub-micron and micron scale elements are combined [108,213,236], and planted in an ectopic (subcutaneous) animal model. Another approach is to manufacture scaffolds that integrate different material zones, where varied tissues interface. Such designs depend on whether the goal is to generate a multi-phasic tissue such as an osteochondral, bone-ligament or bone muscle graft. In this respect, melt electrospun fibers comprise only one region in the scaffold structure, where three examples are demonstrated in Fig. 10.

Periodontal ligament regeneration is the first application where melt electrospun fibers were used to form a membrane between a dentin block and an FDM-fabricated PCL core scaffold, as part of a multiphasic scaffold [213]. The FDM and melt electrospun sections were heated and pressed together (Fig. 10A). The nonwoven melt electrospun scaffold was fabricated by depositing fibers onto a static collector (Fig. 10B). A histological section (Fig. 10C) illustrates the significant difference in size between the filaments (white voids labeled FDM and MES respectively) produced using the two fiber forming methods. The SEM image in Fig. 10D shows the interface between the FDM/melt electrospun filaments in the composite structure, where red arrows indicate stacked melt electrospun fibers. This multiphasic structure was seeded with osteoblast (bone-forming) cells (hOBs), fixed against a dentin block and subcutaneously implanted into rodents.

Vascularization is seen close to the melt electrospun substrate (Fig. 10E).

FDM and melt electrospun scaffolds were combined in a second multiphasic scaffold design, as part of the development of an ectopic osteochondral defect model (Fig. 10F). Using both chondrocytes (cartilage forming) and osteoblasts (bone forming), the TECs were placed subcutaneously in rodents. The subcutaneous implantation promotes vascularization and tissue maturation. In this application, the melt electrospun sections sealed off the ends of a tube formed from FDM filaments (shaded in pink) that was filled with a hydrogel [236].

The final example of implantation into an animal model is a melt electrospun tube filled with cells/alginate/bone morphogenic protein, placed subcutaneously (Fig. 10G–J). In this instance, human bone constructs are intended to be formed in the back of mice so that breast cancer metastasis can be studied. After implantation for 12 weeks subcutaneously (Fig. 10G), a bone-like tubular tissue is formed, including marrow formed within the lumen (Fig. 10H and I), and neobone formed within the tubular scaffold (Fig. 10J). When human breast cancer cells are injected into the heart of the mouse, they target the humanized bone construct. This leads to both understanding cancer metastases and developing the most appropriate treatment strategy for cancer patients [108].

While acceptance of melt electrospinning as a highly suitable scaffold fabrication technology within the TE & RM community is expected to increase, the rate at which

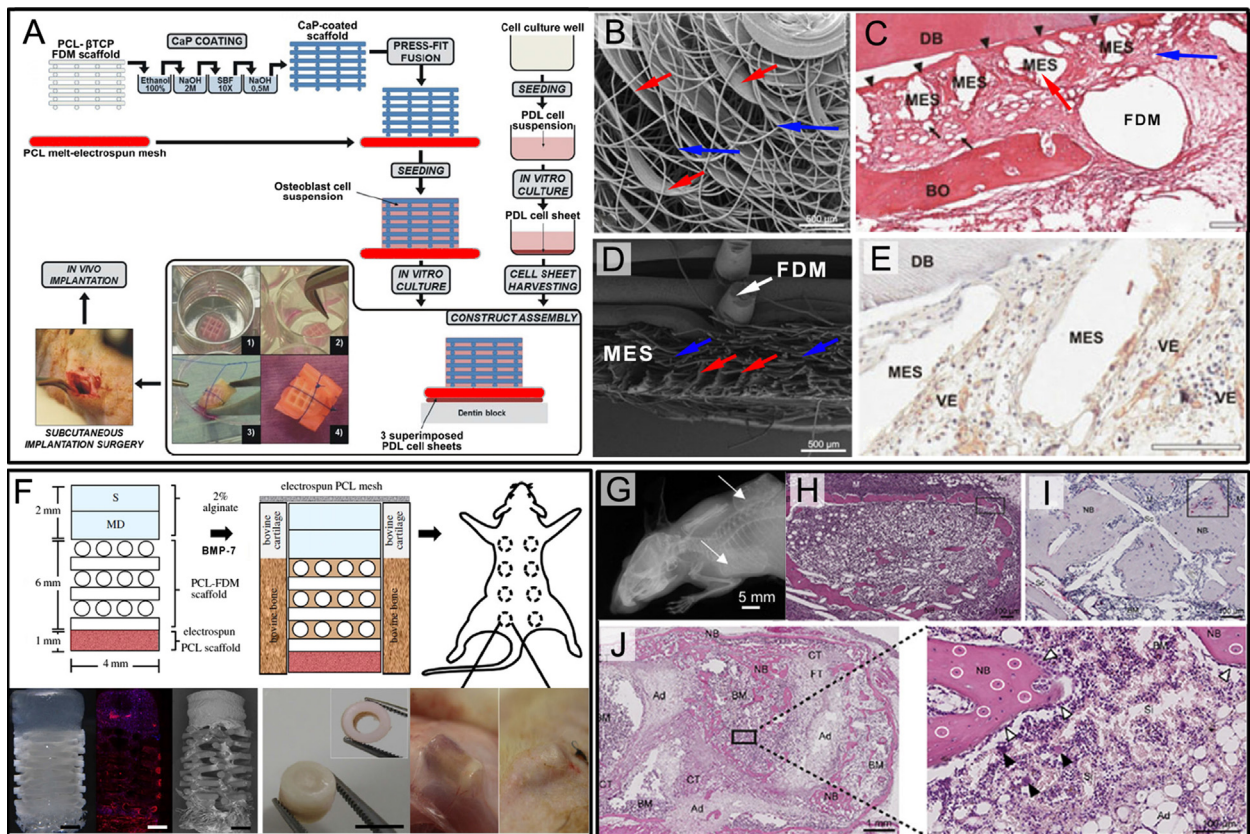


**Fig. 10.** Three *in vivo* models involving melt electrospinning: ((A)–(E)) periodontal ligament [213]; (F) osteochondral TECS [236]; and ((G)–(J)) ectopic bone formation for cancer metastasis research [108]. (A) Schematic showing the manufacture of a multiphasic periodontal ligament scaffold, where a CaP-coated FDM scaffold is heat pressed onto a melt electrospun substrate (red) prior to *in vivo* implantation. (B) Due to viscous thread deposition phenomena, the repeated stacking of certain fibrous elements (red arrows) occurs during the formation of a melt electrospun nonwoven, interspersed amongst the “regular” random fibers (blue arrows). (C) Histological section (stained for blood vessels) where the white voids illustrate the significant difference in AFD between melt electrospun fibers (blue arrows) and “FDM” filaments. Red arrows signify white regions occupied by melt electrospun fibre stacks (“MES”). (D) SEM image showing similar cross-section of the FDM/melt electrospun fibre interface to (C). These stacked and individual fibre zones are indicated using their respective colored arrows. (E) Vascularization is shown close to the melt electrospun fibers. (F) Melt electrospun scaffolds were used to prevent excess tissue penetrating an osteochondral defect that is implanted ectopically. (G) Tubular melt electrospun scaffolds were also implanted ectopically, where ((H) and (I)) neo-bone formed in the tube walls, while (J) the lumen was filled with a bone-marrow structure. Copyright Permission Sources: ((A)–(E)) [213], Copyright 2014, John Wiley & Sons Inc; (F) [236], Copyright 2014, the Royal Society of Chemistry; ((G)–(J)) [108], Copyright 2014, Elsevier Ltd. (For interpretation of the references to color in this figure legend, the reader is referred to the web version of this article.)

products are translated into RM strategies and implanted into patients will be largely governed by both the economics of TE and performance *in vivo* [28]. In the meantime, we expect that products manufactured from melt electrospinning will be commercialized in far reaching applications as the range of melt electrospun polymers increases, alongside improved control over 3D arrangements of melt electrospun fibers.

## 9. Conclusions & future perspectives

A recent and rapidly growing list of research publications is demonstrating that melt electrospinning enables the fabrication of ultrafine polymer fibers in the absence of solvents, providing benefits including: allowing a new variety of polymers to be processed which are not soluble in solvents; avoiding toxicity issues that may affect the collector substrate and intended application outcome; eliminating the costly and hazardous

need to collect solvent fumes and recycle them; as well as faster and less complicated material preparation, amounting to higher and more cost-effective throughput. Finally, the ability to accurately electrospin fibers directly onto a specific substrate in a direct writing mode has significant implications for substrate design and material properties. Such factors are particularly pertinent for biomedical engineering, where approved medical grade polymers can be processed as received, potentially reducing device development approval timelines in fields such as TE & RM and one day may allow fibers to be directly applied onto a patient as part of a treatment strategy. Promising integration and also vascularization of melt electrospun scaffolds *in vivo* is already shown. Melt electrospinning as an AM technique is likely to be used within new treatment approaches using high-performance multiphasic scaffold materials, as well as innovative approaches such as the encapsulation of functional materials within composite fibers.

Progress has also been recently made in the fundamental understanding and modeling of the melt electrospinning process, as well as the development of a broad range of melt electrospinning devices and instruments. Although there are cases where extended heating times can lead to polymer degradation and high processing temperatures may not be suitable for the processing of specific drugs or bioactive molecules, evolving machine designs are demonstrating improved control over the parameters (including temperature profiles and accurate melt supply) which govern fiber formation and control over AFD. Coupled with strategies such as the addition of viscosity reducing additives to the bulk polymer prior to processing, the continual manufacture of significant quantities of melt electrospun fibers with AFDs approaching nanofiber magnitudes has been readily demonstrated for a range of polymers. Importantly, in-process operating parameters can be varied to control the magnitude of AFD from 100 s of  $\mu\text{m}$  down to 100 s of nm without ceasing the process. Further advances in the computational modeling of the process and its parameters will enhance our theoretical understanding and inform future experimental work to study the heat transfer, stress response, in-flight crystallization, charge transfer and dissipation mechanisms for viscoelastic melt electrospun polymer materials. Coupled with knowledge of their behavioral response over varied operating parameters and spinning zone conditions, this will assist in improved process optimization, performance and applications of melt electrospun fibers.

From a translational research point of view, the market for electrospinning equipment and electrospun materials with high surface areas and porosities is expected to grow significantly. For both laboratory research and industrial production, sub-micron fibers maintain advantages in diverse areas such as energy and electronics, environment, filtration and separation, as well as textiles. In the 21<sup>st</sup> century melt electrospinning is emerging as a fiber fabrication process that offers solutions to some of the issues limiting the industrial implementation of its counterpart process, solution electrospinning. While the ability to upscale is a key challenge for industry, and based on existing literature melt electrospinning often requires relatively low material delivery rates [31,102,105,223], recent device designs such as multiple needle and needless configurations have demonstrated a roadmap to upscale fiber production. For industrial implementation, value-added and high-performance materials will likely justify the first melt electrospun products. The ability to accurately place melt electrospun fibers to create reproducible ordered scaffold architectures using filament resolutions improved by several orders of magnitude compared to traditional melt-extrusion based direct writing processes will drive the rapid development of novel strategic applications, particularly in advanced biomedical applications such as TE & RM, where cell alignment, guidance or protection is important [235].

As the range of melt electrospun thermoplastic and functional polymer materials increases, particularly with well-controlled structures and improved filament resolutions, research will shift towards applications suited to the particular properties of each material, as well as

the manner in which the fibers are assembled. In AM machines, one current trend is to incorporate multiple material dispense heads to enable the fabrication of complex multicomponent materials. We anticipate that melt electrospinning will soon be integrated as an alternative processing technology in such approaches, for example with cell/hydrogel printing, where the fibers may act to provide physical/chemical cues for the migration of cells through the hydrogel. As well as finding applications as a standalone process, we predict that melt electrospinning principles will be incorporated into other fiber forming processes to facilitate process improvements, particularly as these technologies evolve and their distinguishing features overlap to meet the processing demands of new functional materials and the assembly methods of novel structures.

## Acknowledgements

Financial assistance from the EU Project HYDROZONES (FP7/2007–2013; Grant # 309962), the Australian Research Council (Grant # DP110103890 and Future Fellowship to Dietmar W. Hutmacher), the National Health and Medical Research Council and the National Breast Cancer Foundation Australia (RM # 2014001080) is appreciated in preparing this manuscript. Support in design of figures by Mr. Felix Wunner and the assistance with formatting of references by Ms Patrina Poh is appreciated.

## References

- [1] Li D, Xia Y. Electrospinning of nanofibers: reinventing the wheel? *Adv Mater* 2004;16:1151–70.
- [2] Greiner A, Wendorff JH. Electrospinning: a fascinating method for the preparation of ultrathin fibers. *Angew Chem Int Ed* 2007;46:5670–703.
- [3] Frenot A, Chronakis IS. Polymer nanofibers assembled by electrospinning. *Curr Opin Colloid Interface Sci* 2003;8:64–75.
- [4] Reneker DH, Chun I. Nanometre diameter fibres of polymer, produced by electrospinning. *Nanotechnology* 1996;7:216–23.
- [5] Gopal R, Kaur S, Ma Z, Chan C, Ramakrishna S, Matsuura T. Electrospun nanofibrous filtration membrane. *J Membr Sci* 2006;281:581–6.
- [6] Okuda T, Tominaga K, Kidoaki S. Time-programmed dual release formulation by multilayered drug-loaded nanofiber meshes. *J Control Release* 2010;143:258–64.
- [7] Hong Y, Chen X, Jing X, Fan H, Guo B, Gu Z, Zhang X. Preparation, bioactivity, and drug release of hierarchical nanoporous bioactive glass ultrathin fibers. *Adv Mater* 2010;22:754–8.
- [8] Agarwal S, Wendorff JH, Greiner A. Use of electrospinning technique for biomedical applications. *Polymer* 2008;49:5603–21.
- [9] Sill TJ, von Recum HA. Electrospinning: applications in drug delivery and tissue engineering. *Biomaterials* 2008;29:1989–2006.
- [10] Grafairend D, Heffels K-H, Beer MV, Gasteier P, Möller M, Boehm G, Dalton PD, Groll J. Degradable polyester scaffolds with controlled surface chemistry combining minimal protein adsorption with specific bioactivation. *Nat Mater* 2010;10:67–73.
- [11] Kanani AG, Bahrami SH. Review on electrospun nanofibers scaffold and biomedical applications. *Trends Biomater Artif Organs* 2010;24:93–115.
- [12] Pham QP, Sharma U, Mikos AG. Electrospinning of polymeric nanofibers for tissue engineering applications: a review. *Tissue Eng* 2006;12:1197–211.
- [13] Xia Y, Yang P, Sun Y, Wu Y, Mayers B, Gates B, Yin Y, Kim F, Yan H. One-dimensional nanostructures: synthesis, characterization, and applications. *Adv Mater* 2003;15:353–89.
- [14] Kim FS, Ren G, Jenekhe SA. One-dimensional nanostructures of  $\pi$ -conjugated molecular systems: assembly, properties, and applications from photovoltaics, sensors, and nanophotonics to nanoelectronics. *Chem Mater* 2010;23:682–732.

- [15] Agarwal S, Greiner A, Wendorff JH. Functional materials by electrospinning of polymers. *Prog Polym Sci* 2013;38:963–91.
- [16] Ikegami M, Tajima K, Aida T. Template synthesis of polypyrrole nanofibers insulated within one-dimensional silicate channels: hexagonal versus lamellar for recombination of polarons into bipolarons. *Angew Chem Int Ed* 2003;42:2154–7.
- [17] Hong Y, Legge RL, Zhang S, Chen P. Effect of amino acid sequence and pH on nanofiber formation of self-assembling peptides EAK16-II and EAK16-IV. *Biomacromolecules* 2003;4:1433–42.
- [18] Ellison CJ, Phatak A, Giles DW, Macosko CW, Bates FS. Melt blown nanofibers: fiber diameter distributions and onset of fiber breakup. *Polymer* 2007;48:3306–16.
- [19] Pisignano D, Maruccio G, Mele E, Persano L, Di Benedetto F, Cingolani R. Polymer nanofibers by soft lithography. *Appl Phys Lett* 2005;87, 123109/1–123109/3.
- [20] Góra A, Sahay R, Thavasi V, Ramakrishna S. Melt-electrospun fibers for advances in biomedical engineering, clean energy, filtration, and separation. *Polym Rev* 2011;51:265–87.
- [21] Zhang Y, Ouyang H, Lim CT, Ramakrishna S, Huang Z-M. Electrospinning of gelatin fibers and gelatin/PCL composite fibrous scaffolds. *J Biomater Sci Mater Res*, B 2005;72:156–65.
- [22] Bognitzki M, Czado W, Frese T, Schaper A, Hellwig M, Steinhart M, Greiner A, Wendorff JH. Nanostructured fibers via electrospinning. *Adv Mater* 2001;13:70–2.
- [23] Persano L, Camposeo A, Tekmen C, Pisignano D. Industrial upscaling of electrospinning and applications of polymer nanofibers: a review. *Macromol Mater Eng* 2013;298:504–20.
- [24] Deitzel JM, Kleinmeyer JD, Hirvonen JK, Beck Tan N. Controlled deposition of electrospun poly(ethylene oxide) fibers. *Polymer* 2001;42:8163–70.
- [25] Huang Z-M, Zhang YZ, Kotaki M, Ramakrishna S. A review on polymer nanofibers by electrospinning and their applications in nanocomposites. *Compos Sci Technol* 2003;63:2223–53.
- [26] Cui W, Chang J, Dalton PD. Electrospun fibers for drug delivery. In: Ducheyne P, editor. *Comprehensive biomaterials*. Amsterdam: Elsevier Ltd; 2011. p. 445–62.
- [27] Hutmacher DW, Woodfield T, Dalton PD. Scaffold design and fabrication. In: De Boer J, Van Blitterswijk C, editors. *Tissue engineering*. 2nd ed. Amsterdam: Elsevier; 2014. p. 583–625.
- [28] Hutmacher DW, Dalton PD. Melt electrospinning. *Chem Asian J* 2011;6:44–56.
- [29] Dalton PD, Joergensen NT, Groll J, Moeller M. Patterned melt electrospun substrates for tissue engineering. *Biomed Mater* 2008;3, 034109/1–034109/11.
- [30] Dalton PD, Klinkhammer K, Salber J, Klee D, Möller M. Direct *in vitro* electrospinning with polymer melts. *Biomacromolecules* 2006;7:686–90.
- [31] Dalton PD, Grafarend D, Klinkhammer K, Klee D, Möller M. Electrospinning of polymer melts: phenomenological observations. *Polymer* 2007;48:6823–33.
- [32] Dalton PD, Vaquette C, Farrugia BL, Dargaville TR, Brown TD, Hutmacher DW. Electrospinning and additive manufacturing: converging technologies. *Biomater Sci* 2013;1:171–85.
- [33] Melchels FP, Feijen J, Grijpma DW. A review on stereolithography and its applications in biomedical engineering. *Biomaterials* 2010;31:6121–30.
- [34] Melchels FPW, Domingos MAN, Klein TJ, Malda J, Bartolo PJ, Hutmacher DW. Additive manufacturing of tissues and organs. *Prog Polym Sci* 2012;37:1079–104.
- [35] Peltola SM, Melchels FP, Grijpma DW, Kellomäki M. A review of rapid prototyping techniques for tissue engineering purposes. *Ann Med* 2008;40:268–80.
- [36] Tucker N, Stanger JJ, Staiger MP, Razzaq H, Hofman K. The history of the science and technology of electrospinning from 1600 to 1995. *J Eng Fibers Fabrics* 2012;7:63–73.
- [37] Gilbert W, Translator Mottelay PF. *De magnete. Mineola, NY: Dover Publications*; 1958. p. 368. Repr 1893 Ed. New York: John Wiley & Sons Inc.
- [38] Gilbert W. *De Magnetis magnetisque corporibus, et de magno magneti tellure, physiologia nova, plurimis & argumentis & experimentis demonstrata*. London: Petrus Short; 1600. p. 240.
- [39] Rayleigh JW. On the conditions of instability of electrified drops, with applications to the electric discharge from liquid points. *Proc R Soc* 1879;29:71–83.
- [40] Rayleigh XX JW. On the equilibrium of liquid conducting masses charged with electricity. London, Edinburgh, Dublin. *Philos Mag J Sci* 1882;14:184–6.
- [41] Böse GM. *Recherches sur le cause et sur véritable théorie de l'électricité*. Wittenberg: de J. F. Slomac; 1745. p. 56.
- [42] Zeleny J. The electrical discharge from liquid points, and a hydrostatic method of measuring the electric intensity at their surfaces. *Phys Rev* 1914;3:69–91.
- [43] Zeleny J. Instability of electrified liquid surfaces. *Phys Rev* 1917;10:1–7.
- [44] Cooley JF. Apparatus for electrically dispersing fluids. US 692631, 1902.
- [45] Morton WJ. Method of dispersing fluids. US 705691 A, 1902.
- [46] Cooley JF. Electrical method of dispersing fluids. US 745276 A, 1903.
- [47] Hagiwara K. Process for manufacturing artificial silk and other filaments by applying electric current. US 1699615 A, 1929.
- [48] Formhals A. Process and apparatus for preparing artificial threads. US 1975504, 1934.
- [49] Barhate R, Ramakrishna S. Nanofibrous filtering media: filtration problems and solutions from tiny materials. *J Membr Sci* 2007;296:1–8.
- [50] Luo C, Stoyanov SD, Stride E, Pelan E, Edirisinghe M. Electrospinning versus fibre production methods: from specifics to technological convergence. *Chem Soc Rev* 2012;41:4708–35.
- [51] Filatov Y, Budyka A, Kirichenko V. Electrospinning of micro-and nanofibers: fundamentals in separation and filtration processes. Redding, CT: Begell House Inc; 2007. p. 488.
- [52] Lukáš D, Sarkar A, Martinová L, Vodseďáková K, Lubasova D, Chaloupek J, Pokorný P, Mikeš P, Chvojka J, Komárek M. Physical principles of electrospinning (electrospinning as a nano-scale technology of the twenty-first century). *Textile Prog* 2009;41:59–140.
- [53] Jirsák O, Petrik S. Recent advances in nanofibre technology: needleless electrospinning. *Int J Nanotechnol* 2012;9:836–45.
- [54] Andrade AL. *Science and technology of polymer nanofibers*. Hoboken, NJ: John Wiley & Sons Inc; 2008. p. 404.
- [55] Srinivasan G, Reneker DH. Structure and morphology of small diameter electrospun aramid fibers. *Polym Int* 1995;36:195–201.
- [56] Doshi J, Reneker DH. Electrospinning process and applications of electrospun fibers. *J Electrostat* 1995;35:151–60.
- [57] Taylor G. Electrically driven jets. *Proc R Soc Lond A* 1969;313:453–75.
- [58] Larroondo L, St. John Manley R. Electrostatic fiber spinning from polymer melts. I. Experimental observations on fiber formation and properties. *J Polym Sci Polym Phys Ed* 1981;19:909–20.
- [59] Spivak A, Dzenis Y. Asymptotic decay of radius of a weakly conductive viscous jet in an external electric field. *Appl Phys Lett* 1998;73:3067–9.
- [60] Shin Y, Höhman M, Brenner M, Rutledge G. Electrospinning: a whipping fluid jet generates submicron polymer fibers. *Appl Phys Lett* 2001;78:1149–51.
- [61] Shin Y, Höhman M, Brenner M, Rutledge G. Experimental characterization of electrospinning: the electrically forced jet and instabilities. *Polymer* 2001;42:09955–9967.
- [62] Yarin A, Koombhongse S, Reneker D. Bending instability in electrospinning of nanofibers. *J Appl Phys* 2001;89:3018–26.
- [63] Mitchell S, Sanders J. A unique device for controlled electrospinning. *J Biomater Sci Mater Res*, A 2006;78:110–20.
- [64] Pagliara S, Camposeo A, Mele E, Persano L, Cingolani R, Pisignano D. Enhancement of light polarization from electrospun polymer fibers by room temperature nanoimprint lithography. *Nanotechnology* 2010;21, 215304/1–215304/6.
- [65] Katta P, Alessandro M, Ramsier R, Chase G. Continuous electrospinning of aligned polymer nanofibers onto a wire drum collector. *Nano Lett* 2004;4:2215–8.
- [66] Isakov DV, de Matos Gomes E, Vieira LG, Dekola T, Belsley MS, Almeida BG. Oriented single-crystal-like molecular arrangement of optically nonlinear 2-methyl-4-nitroaniline in electrospun nanofibers. *ACS Nano* 2010;5:73–8.
- [67] Li D, Wang Y, Xia Y. Electrospinning of polymeric and ceramic nanofibers as uniaxially aligned arrays. *Nano Lett* 2003;3:1167–71.
- [68] Deitzel J, Kleinmeyer J, Harris Dea, Beck Tan N. The effect of processing variables on the morphology of electrospun nanofibers and textiles. *Polymer* 2001;42:261–72.
- [69] Zhou FL, Gong RH, Porat I. Mass production of nanofibre assemblies by electrostatic spinning. *Polym Int* 2009;58:331–42.
- [70] Ramakrishna S, Fujihara K, Teo W, Lim T-C, Ma Z. An introduction to electrospinning and nanofibers. Singapore: World Scientific Publishing Co Pte Ltd; 2005. p. 382.
- [71] Ngiam M, Ramakrishna S, Raghunath M, Chan CK. Nanofiber patent landscape. *Recent Pat Nanotechnol* 2007;1:137–44.
- [72] Lee S, Obendorf SK. Use of electrospun nanofiber web for protective textile materials as barriers to liquid penetration. *Text Res J* 2007;77:696–702.

- [73] Ye H, Lam H, Titchenal N, Gogotsi Y, Ko F. Reinforcement and rupture behavior of carbon nanotubes–polymer nanofibers. *Appl Phys Lett* 2004;85:1775–7.
- [74] Teo W, Ramakrishna S. A review on electrospinning design and nanofibre assemblies. *Nanotechnology* 2006;17:R89–106.
- [75] Gao K, Hu X, Dai C, Yi T. Crystal structures of electrospun PVDF membranes and its separator application for rechargeable lithium metal cells. *Mater Sci Eng B* 2006;131:100–5.
- [76] Yang C, Jia Z, Guan Z, Wang L. Polyvinylidene fluoride membrane by novel electrospinning system for separator of Li-ion batteries. *J Power Sources* 2009;189:716–20.
- [77] Choi S-S, Lee YS, Joo CW, Lee SG, Park JK, Han K-S. Electrospun PVDF nanofiber web as polymer electrolyte or separator. *Electrochim Acta* 2004;50:339–43.
- [78] Cho T, Sakai T, Tanase S, Kimura K, Kondo Y, Tarao T, Tanaka M. Electrochemical performances of polyacrylonitrile nanofiber-based nonwoven separator for lithium-ion battery. *Electrochim Solid State Lett* 2007;10:A159–62.
- [79] Lyons J, Li C, Ko F. Melt-electrospinning Part I: Processing parameters and geometric properties. *Polymer* 2004;45:7597–603.
- [80] Zhamayev E, Cho D, Joo YL. Modeling of melt electrospinning for semi-crystalline polymers. *Polymer* 2010;51:274–90.
- [81] Zhamayev E, Cho D, Joo YL. Nanofibers from gas-assisted polymer melt electrospinning. *Polymer* 2010;51:4140–4.
- [82] Zhamayev E, Zhou H, Joo YL. Modeling of non-isothermal polymer jets in melt electrospinning. *J NonNewton Fluid Mech* 2008;153:95–108.
- [83] Zhou H, Green TB, Joo YL. The thermal effects on electrospinning of polylactic acid melts. *Polymer* 2006;47:7497–505.
- [84] Norton CL. Method of and apparatus for producing fibrous or filamentary material. US 2048651 A, 1936.
- [85] Larrendo L, St John Manley R. Electrostatic fiber spinning from polymer melts. II. Examination of the flow field in an electrically driven jet. *J Polym Sci Polym Phys Ed* 1981;19:921–32.
- [86] Larrendo L, St John Manley R. Electrostatic fiber spinning from polymer melts. III. Electrostatic deformation of a pendant drop of polymer melt. *J Polym Sci Polym Phys Ed* 1981;19:933–40.
- [87] Kim J-S, Lee DS. Thermal properties of electrospun polyesters. *Polymer J* 2000;32:616–8.
- [88] Rangkupan R, Reneker DH. Electrospinning process of molten polypropylene in vacuum. *J Met Mater Miner* 2003;12:81–7.
- [89] Yarin AL. Electrospinning of Nanofibers from Polymer Solutions and Melt. In: The Fiber Society: New Frontiers in Fiber Science Conference. 2001. p. 10–1.
- [90] Bowlin GM, Matthews JA, Simpson DG, Kenawy ER, Wnek GE. Electrospinning of Biomaterials. In: The Fiber Society: New Frontiers in Fiber Science Conference. 2001. p. 5–6.
- [91] Reneker DH, Yarin AL, Zussman E, Xu H. Electrospinning of nanofibers from polymer solutions and melts. *Adv Appl Mech* 2007;41:143–195, 345–346.
- [92] Lyons J, Pastore C, Ko F. Developments in melt-electrospinning of thermoplastic polymers. *Polym Prepr* 2003;44(2):122–3.
- [93] Cho D, Zhamayev E, Joo YL. Structural studies of electrospun nylon 6 fibers from solution and melt. *Polymer* 2011;52:4600–9.
- [94] Cho D, Zhou H, Cho Y, Audus D, Joo YL. Structural properties and superhydrophobicity of electrospun polypropylene fibers from solution and melt. *Polymer* 2010;51:6005–12.
- [95] Zhamayev E, Cho D, Joo YL. Electrohydrodynamic quenching in polymer melt electrospinning. *Phys Fluids* 2011;23, 073102/1–073102/8.
- [96] Ogata N, Yamaguchi S, Shimada N, Lu G, Iwata T, Nakane K, Ogihara T. Poly(lactide)nanofibers produced by a melt-electrospinning system with a laser melting device. *J Appl Polym Sci* 2007;104:1640–5.
- [97] Ogata N, Lu G, Iwata T, Yamaguchi S, Nakane K, Ogihara T. Effects of ethylene content of poly(ethylene-co-vinyl alcohol) on diameter of fibers produced by melt-electrospinning. *J Appl Polym Sci* 2007;104:1368–75.
- [98] Tian S, Ogata N, Shimada N, Nakane K, Ogihara T, Yu M. Melt electrospinning from poly(L-lactide) rods coated with poly(ethylene-co-vinyl alcohol). *J Appl Polym Sci* 2009;113:1282–8.
- [99] Ogata N, Shimada N, Yamaguchi S, Nakane K, Ogihara T. Melt-electrospinning of poly(ethylene terephthalate) and polyalipate. *J Appl Polym Sci* 2007;105:1127–32.
- [100] Shimada N, Tsutsumi H, Nakane K, Ogihara T, Ogata N. Poly(ethylene-co-vinyl alcohol) and Nylon 6/12 nanofibers produced by melt electrospinning system equipped with a line-like laser beam melting device. *J Appl Polym Sci* 2010;116:2998–3004.
- [101] Shimada N, Ogata N, Nakane K, Ogihara T. Spot laser melt electrospinning of a fiber bundle composed of poly(lactide)/poly(ethylene-co-vinyl alcohol) pie wedge fibers. *J Appl Polym Sci* 2012;125:E384–9.
- [102] Dalton PD, Lleixà Calvet J, Mourran A, Klee D, Möller M. Melt electrospinning of poly(ethylene glycol-block-ε-caprolactone). *Biotechnol J* 2006;1:998–1006.
- [103] Detta N, Brown TD, Edin FK, Albrecht K, Chiellini F, Chiellini E, Dalton PD, Hutmacher DW. Melt electrospinning of polycaprolactone and its blends with poly(ethylene glycol). *Polym Int* 2010;59:1558–62.
- [104] Dalton PD, Klee D, Möller M. Electrospinning with dual collection rings. *Polymer* 2005;46:611–4.
- [105] Brown TD, Dalton PD, Hutmacher DW. Direct writing by way of melt electrospinning. *Adv Mater* 2011;23:5651–7.
- [106] Brown TD, Slotosch A, Thibaudeau L, Taubenberger A, Loessner D, Vaquette C, Dalton PD, Hutmacher DW. Design and fabrication of tubular scaffolds via direct writing in a melt electrospinning mode. *Biointerphases* 2012;7:1–16.
- [107] Muerza-Cascante ML, Haylock D, Hutmacher DW, Dalton PD. Melt electrospinning and its technologization in tissue engineering. *Tissue Eng. B* 2014;21:187–202.
- [108] Thibaudeau L, Taubenberger AV, Holzapfel BM, Quent VM, Fuehrmann T, Hesami P, Brown TD, Dalton PD, Power CA, Holler BG, Hutmacher DW. A tissue-engineered humanized xenograft model of human breast cancer metastasis to bone. *Dis Model Mech* 2014;7:299–309.
- [109] Li HY, Wu WF, Bubakir MM, Chen HB, Zhong XF, Liu ZX, Ding Y, Yang WM. Polypropylene fibers fabricated via a needleless melt-electrospinning device for marine oil-spill cleanup. *J Appl Polym Sci* 2014;131, 40080/1–40080/9.
- [110] Li H, Chen H, Zhong X, Wu W, Ding Y, Yang W. Interjet distance in needleless melt differential electrospinning with umbrella nozzles. *J Appl Polym Sci* 2014;131:8, <http://dx.doi.org/10.1002/app.40515>.
- [111] Li XH, Zhang YC, Li HY, Chen HB, Ding YM, Yang WM. Effect of oriented fiber membrane fabricated via needleless melt electrospinning on water filtration efficiency. *Desalination* 2014;344:266–73.
- [112] Li HY, Bubakir MM, Xia T, Zhong XF, Ding YM, Yang WM. Mass production of ultra-fine fibre by melt electrospinning method using umbrella spinneret. *Mater Res Innov* 2014;18(S4):921–5.
- [113] Ma S, Li H, Chen S, Ding Y, Yang W. Hydrophilic modification of ultrafine fibres produced by melt differential electrospinning device. *Mater Res Innov* 2014;18:914–20.
- [114] Liu Y, Zhao F, Zhang C, Zhang J, Yang W. Solvent-free preparation of polylactic acid fibers by melt electrospinning using umbrella-like spray head and alleviation of problematic thermal degradation. *J Srb Chem Soc* 2012;77:1071–82.
- [115] Gupta B, Revagade N, Hilborn J. Poly(lactic acid) fiber: an overview. *Prog Polym Sci* 2007;32:455–82.
- [116] Hearle JWS, Woodings C. Fibers related to cellulose. In: Woodings C, editor. *Regenerated cellulose fibres*. Amsterdam: Elsevier Ltd; 2001. p. 156–73.
- [117] Rupprecht A. Preparation of oriented DNA by wet spinning. *Acta Chem Scand* 1966;20:494–504.
- [118] Watson JD, Crick FHC. Molecular structure of nucleic acids. *Nature* 1953;171:737–8.
- [119] Guenthner AJ, Khomhongse S, Liu W, Dayal P, Reneker DH, Kyu T. Dynamics of hollow nanofiber formation during solidification subjected to solvent evaporation. *Macromol Theory Simul* 2006;15:87–93.
- [120] Nain AS, Sitti M, Jacobson A, Kowalewski T, Amon C. Dry spinning based spinneret based tunable engineered parameters (STEP) technique for controlled and aligned deposition of polymeric nanofibers. *Macromol Rapid Commun* 2009;30:1406–12.
- [121] Ingersoll H. Fibrillated strand. US 3081519 A, 1963.
- [122] Shin H, Samuels SL. Flash-spinning polymeric plexifilaments. US 5147586 A, 1992.
- [123] Kwolek SL. Process of making wholly aromatic polyamides. US 3063966 A, 1962.
- [124] Rey AD. Capillary models for liquid crystal fibers, membranes, films, and drops. *Soft Matter* 2007;3:1349–68.
- [125] Van Dingenen JLJ. Gel-spun high-performance polyethylene fibres. In: Hearle JW, editor. *High-performance fibres*, vol. 15. Cambridge: Woodhead Publishing; 2001. p. 62–92.
- [126] Erdem N, Erdogan U. Recent advances in the spinning processes used for high performance fibers. Book of abstracts. In: The Fiber Society 2003 Spring Symposium. 2003. p. 2.

- [127] Plunkett RJ. Tetrafluoroethylene polymers. US 2230654 A, 1941.
- [128] Curran DJG. A method of making a composite ceramic fiber from pre-ceramic polymers. US 5705122 A, 1998.
- [129] Tsuji T, Korematsu M. Highly flame-retardant shaped articles comprising a halogen containing polymer and polyvinyl alcohol. US 3859390 A, 1975.
- [130] Yarin A. Coaxial electrospinning and emulsion electrospinning of core-shell fibers. *Polym Adv Technol* 2011;22:310–7.
- [131] Shambaugh RL. A macroscopic view of the melt-blowing process for producing microfibers. *Ind Eng Chem Res* 1988;27:2363–72.
- [132] Uyttendaele MA, Shambaugh RL. Melt blowing: general equation development and experimental verification. *AIChE J* 1990;36:175–86.
- [133] Majumdar B, Shambaugh RL. Air drag on filaments in the melt blowing process. *J Rheol* 1990;34:591–601.
- [134] Rao RS, Shambaugh RL. Vibration and stability in the melt blowing process. *Ind Eng Chem Res* 1993;32:3100–11.
- [135] Eian G, Cheney PG. Durable melt-blown fibrous sheet material. US 4681801 A, 1987.
- [136] Pourdeyhimi B, Fedorova N, Dondero W, Gorga RE, Michielson S, Ghosh T, Chhaparwal S, Barrera C, Rinaldi C, Satcher M, Hinesstroza JP. Textile nanotechnologies. In: Goddard III WA, Brenner DW, Lyshevski SE, Iafrate GJ, editors. *Handbook of nanoscience, engineering, and technology*. 2nd ed. Boca Raton, FL: CRC Press; 2007. p. 21.1–66.
- [137] Podgócki A, Bałazy A, Gradoń L. Application of nanofibers to improve the filtration efficiency of the most penetrating aerosol particles in fibrous filters. *Chem Eng Sci* 2006;61:6804–15.
- [138] Brang JE, Wilkie A, Haggard JS. Method and apparatus for production of meltblown nanofibers. US 20080023888 A1, 2008.
- [139] Hassounah I. Melt electrospinning of thermoplastic polymers. Aachen, Germany: RWTH Aachen University; 2012. p. 127. PhD Thesis.
- [140] Cicero JA, Dorgan JR, Garrett J, Runt J, Lin J. Effects of molecular architecture on two-step, melt-spun poly(lactic acid) fibers. *J Appl Polym Sci* 2002;86:2839–46.
- [141] Na B, Tian N, Lv R, Zou S, Xu W, Fu Q. Annealing-induced oriented crystallization and its influence on the mechanical responses in the melt-spun monofilament of poly(L-lactide). *Macromolecules* 2009;43:1156–8.
- [142] Ellä V, Annala T, Länsman S, Nurminen M, Kellomäki M. Knitted polylactide 96/4 L/D structures and scaffolds for tissue engineering: shelf life, *in vitro* and *in vivo* studies. *Biomater* 2011;1:102–13.
- [143] Tamayol A, Akbari M, Annabi N, Paul A, Khademhosseini A, Juncker D. Fiber-based tissue engineering: progress, challenges, and opportunities. *Biotechnol Adv* 2012;31:669–87.
- [144] Huang T, Marshall LR, Armantrout JE, Yembrick S, OConnor JM, Mueller T, Avgousti M, Wetzel MD. Production of nanofibers by melt spinning. US 20080242171 A1, 2008.
- [145] Weitz R, Harnan L, Rauschenbach S, Burghard M, Kern K. Polymer nanofibers via nozzle-free centrifugal spinning. *Nano Lett* 2008;8:1187–91.
- [146] Ren L, Pandit V, Elkin J, Denman T, Cooper JA, Kotha SP. Large-scale and highly efficient synthesis of micro- and nano-fibers with controlled fiber morphology by centrifugal jet spinning for tissue regeneration. *Nanoscale* 2013;5:2337–45.
- [147] Huang T, Marshall LR, Armantrout JE, Yembrick S, Dunn WH, O'Connor JM, Mueller T, Avgousti M, Wetzel MD. Collection of polyolefin nanofibers. EP 2,527,503, 2012.
- [148] Turaga U, Singh V, Lalagiri M, Kiekens P, Ramkumar SS. Nanomaterials for defense applications. In: Kickens P, Jayaraman S, editors. *Intelligent textiles and clothing for ballistic and NBC protection*. Dordrecht, NL: Springer; 2012. p. 197–218.
- [149] Li H, Ke Y, Hu Y. Polymer nanofibers prepared by template melt extrusion. *J Appl Polym Sci* 2006;99:1018–23.
- [150] Zuo F, Tan DH, Wang Z, Jeung S, Macosko CW, Bates FS. Nanofibers from melt blown fiber-in-fiber polymer blends. *ACS Macro Lett* 2013;2:301–5.
- [151] Nakata K, Fujii K, Ohkoshi Y, Gotoh Y, Nagura M, Numata M, Kamiyama M. Poly(ethylene terephthalate) nanofibers made by sea-island-type conjugated melt spinning and laser-heated flow drawing. *Macromol Rapid Commun* 2007;28:792–5.
- [152] Hartman R, Brunner D, Camelot D, Marijnissen J, Scarlett B. Electrohydrodynamic atomization in the cone-jet mode physical modeling of the liquid cone and jet. *J Aerosol Sci* 1999;30:823–49.
- [153] Komarek M, Martinova L. Design and evaluation of melt-electrospinning electrodes. In: Proc 2nd NANOCOM Int Confer. 2010. p. 72–7.
- [154] Yarin A, Koombhongse S, Reneker D. Taylor cone and jetting from liquid droplets in electrospinning of nanofibers. *J Appl Phys* 2001;90:4836–46.
- [155] Yarin A, Kataphinan W, Reneker D. Branching in electrospinning of nanofibers. *J Appl Phys* 2005;98, 064501/1–064501/12.
- [156] Bousfield D, Keunings R, Marrucci G, Denn M. Nonlinear analysis of the surface tension driven breakup of viscoelastic filaments. *J NonNewton Fluid Mech* 1986;21:79–97.
- [157] Saville D. Stability of electrically charged viscous cylinders. *Phys Fluids* 1971;14:1095–9.
- [158] Reneker DH, Yarin AL. Electrospinning jets and polymer nanofibers. *Polymer* 2008;49:2387–425.
- [159] Domingos M, Chiellini F, Gloria A, Ambrosio L, Bartolo P, Chiellini E. Effect of process parameters on the morphological and mechanical properties of 3D bioextruded poly(3-caprolactone) scaffolds. *Rapid Prototyp J* 2012;18:56–67.
- [160] Domingos M, Chiellini F, Gloria A, Ambrosio L, Bartolo P, Chiellini E. BioExtruder: Study of the influence of process parameters on PCL scaffolds properties. In: da Silva Bártoolo PJ, et al., editors. *Innovative developments in design and manufacturing*. London: Taylor & Francis Group; 2009. p. 67–73, 14 other.
- [161] Nayak R, Kyratzis IL, Truong YB, Padhye R, Arnold L. Melt-electrospinning of polypropylene with conductive additives. *J Mater Sci* 2012;47:6387–96.
- [162] Nayak R, Padhye R, Kyratzis IL, Truong YB, Arnold L. Effect of viscosity and electrical conductivity on the morphology and fiber diameter in melt electrospinning of polypropylene. *Text Res J* 2013;83:606–17.
- [163] Zhang J, Gupta A, Baker J. Effect of relative humidity on the prediction of natural convection heat transfer coefficients. *Heat Transf Eng* 2007;28:335–42.
- [164] Still M, Venzke H, Durst F, Melling A. Influence of humidity on the convective heat transfer from small cylinders. *Exp Fluids* 1998;24:141–50.
- [165] Go DB, Maturana RA, Fisher TS, Garimella SV. Enhancement of external forced convection by ionic wind. *Int J Heat Mass Transf* 2008;51:6047–53.
- [166] Bandyopadhyay A, Sen S, Sarkar A, Bhattacharyya S. Investigation of forced convective heat transfer enhancement in the presence of an electric field—a finite element analysis. *Int J Numer Method Heat Fluid Flow* 2004;14:264–84.
- [167] Molki M, Damronglerd P. Electrohydrodynamic enhancement of heat transfer for developing air flow in square ducts. *Heat Transf Eng* 2006;27:35–45.
- [168] Pascual C, Stromberger J, Jeter S, Abdel-Khalik S. An empirical correlation for electrohydrodynamic enhancement of natural convection. *Int J Heat Mass Transf* 2000;43:1965–74.
- [169] Djuric Z, Balachandran W, Wilson C. Electrical field and space charge modelling in a viscous fluid flow in a nozzle. *J Phys D* 1998;31:2132–42.
- [170] Goldman M, Goldman A, Sigmund R. The corona discharge, its properties and specific uses. *Pure Appl Chem* 1985;57:1353–62.
- [171] Jewell-Larsen N, Hsu C, Krichatovitch I, Montgomery S, Dibene J, Mamishev A. CFD analysis of electrostatic fluid accelerators for forced convection cooling. *IEEE Trans 2008*;15:1745–53.
- [172] Laohalertdecha S, Naphon P, Wongwises S. A review of electrohydrodynamic enhancement of heat transfer. *Renew Sustain Energy Rev* 2007;11:858–76.
- [173] Ould Ahmedou SA, Havet M. Effect of process parameters on the EHD airflow. *J Electrostat* 2009;67:222–7.
- [174] Collins G, Federici J, Imura Y, Catalani LH. Charge generation, charge transport, and residual charge in the electrospinning of polymers: a review of issues and complications. *J Appl Phys* 2012;111, 044701/1–044701/18.
- [175] Coe G, Hughes J, Secker P. High-current injection into liquid hexane using field emitters. *Br J Appl Phys* 1966;17:885–90.
- [176] Higuera F. Electrohydrodynamic flow of a dielectric liquid due to autonomous injection of charge by a needle electrode. *Phys Fluids* 2002;14:423–6.
- [177] Melcher J, Taylor G. Electrohydrodynamics: a review of the role of interfacial shear stresses. *Annu Rev Fluid Mech* 1969;1:111–46.
- [178] Saville D. Electrohydrodynamics: the Taylor-Melcher leaky dielectric model. *Annu Rev Fluid Mech* 1997;29:27–64.
- [179] Van Turnhout J. Thermally stimulated discharge of electrets. In: Sessler GM, editor. *Electrets*. 2nd ed. Heidelberg: Springer-Verlag; 1987. p. 81–215.
- [180] Yamashita T, Ikezaki K. A method for correlating charge traps of polypropylene to its morphology. *J Electrostat* 2005;63:559–64.

- [181] Mohmeyer N, Behrendt N, Zhang X, Smith P, Altstädt V, Sessler GM, Gerhard M, Schmidt H-W. Additives to improve the electret properties of isotactic polypropylene. *Polymer* 2007;48:1612–9.
- [182] Arita Y, Sha Shiratori S, Ikezaki K. A method for detection and visualization of charge trapping sites in amorphous parts in crystalline polymers. *J Electrostat* 2003;57:263–71.
- [183] Mishra A. Studies of polymer electrets. II. Factors governing the stabilities of homoelectrets obtained from polystyrene and its derivatives. *J Appl Polym Sci* 1982;27:1107–18.
- [184] Sessler GM. Polymeric electrets. In: Seanor DA, editor. *Electrical properties of polymers*. New York, NY: Academic Press; 1982. p. 241–84.
- [185] Hayashi K, Yoshino K, Inuishi Y. Temperature dependence of carrier mobility in polyethylene terephthalate. *Jpn J Appl Phys* 1973;12:1089–90.
- [186] Lowell J. Absorption and conduction currents in polymers: a unified model. *J Phys D* 1990;23:205–10.
- [187] Han T, Reneker DH, Yarin AL. Pendulum-like motion of straight electrified jets. *Polymer* 2008;49:2160–9.
- [188] Han T, Reneker DH, Yarin AL. Buckling of jets in electrospinning. *Polymer* 2007;48:6064–76.
- [189] Pham QP, Sharma U, Mikos AG. Electrospun poly( $\epsilon$ -caprolactone) microfiber and multilayer nanofiber/microfiber scaffolds: characterization of scaffolds and measurement of cellular infiltration. *Biomacromolecules* 2006;7:2796–805.
- [190] Ko J, Mohtaram NK, Ahmed F, Montgomery A, Carlson M, Lee PC, Willerth S, Jun MBG. Fabrication of poly( $\epsilon$ -caprolactone) microfiber scaffolds with varying topography and mechanical properties for stem cell-based tissue engineering applications. *J Biomater Sci Polym Ed* 2014;25:1–17.
- [191] Eichhorn SJ, Sampson WW. Statistical geometry of pores and statistics of porous nanofibrous assemblies. *J R Soc Interface* 2005;2:309–18.
- [192] Tan E, Ng S, Lim C. Tensile testing of a single ultrafine polymeric fiber. *Biomaterials* 2005;26:1453–6.
- [193] Williamson MR, Coombes AG. Gravity spinning of polycaprolactone fibres for applications in tissue engineering. *Biomaterials* 2004;25:459–65.
- [194] Liao T, Adanur S, Drean J-Y. Predicting the mechanical properties of nonwoven geotextiles with the finite element method. *Text Res J* 1997;67:753–60.
- [195] Lee KH, Kim HY, Ryu YJ, Kim KW, Choi SW. Mechanical behavior of electrospun fiber mats of poly(vinyl chloride)/polyurethane polyblends. *J Polym Sci, B: Polym Phys* 2003;41:1256–62.
- [196] Croisier F, Duwez A-S, Jérôme C, Léonard A, Van der Werf K, Dijkstra P, Bennink ML. Mechanical testing of electrospun PCL fibers. *Acta Biomater* 2012;8:218–24.
- [197] Heikkilä P, Söderlund I, Uusimäki J, Kettunen L, Harlin A. Exploitation of electric field in controlling of nanofiber spinning process. *Polym Eng Sci* 2007;47:2065–74.
- [198] Mota C, Puppi D, Gazzarri M, Bártolo P, Chiellini F. Melt electrospinning writing of three-dimensional star poly( $\epsilon$ -caprolactone) scaffolds. *Polym Int* 2013;62:893–900.
- [199] Deng R, Liu Y, Ding Y, Xie P, Luo L, Yang W. Melt electrospinning of low-density polyethylene having a low-melt flow index. *J Appl Polym Sci* 2009;114:166–75.
- [200] Jung JY, Lee YS. Preparation of pitch from pyrolyzed fuel oil by electron beam radiation and its melt-electrospinning property. *Carbon Lett* 2014;15:129–35.
- [201] Singer JC, Giesa R, Schmidt H-W. Shaping self-assembling small molecules into fibres by melt electrospinning. *Soft Matter* 2012;8:9972–6.
- [202] Praeger M, Saleh E, Vaughan A, Stewart W, Loh W. Fabrication of nanoscale glass fibers by electrospinning. *Appl Phys Lett* 2012;100, 063114/1–063114/3.
- [203] Marcos-Fernández A, Abraham GA, Valentín J, Román JS. Synthesis and characterization of biodegradable non-toxic poly(ester-urethane-urea)s based on poly( $\epsilon$ -caprolactone) and amino acid derivatives. *Polymer* 2006;47:785–98.
- [204] Karchin A, Simonovsky FI, Ratner BD, Sanders JE. Melt electrospinning of biodegradable polyurethane scaffolds. *Acta Biomater* 2011;7:3277–84.
- [205] Hacker C, Karahaliloglu Z, Seide G, Denkbas EB, Gries T. Functionally modified, melt-electrospun thermoplastic polyurethane mats for wound-dressing applications. *J Appl Polym Sci* 2014;131:12, <http://dx.doi.org/10.1002/app.40132>.
- [206] Kim SJ, Jang DH, Park WH, Min B-M. Fabrication and characterization of 3-dimensional PLGA nanofiber/microfiber composite scaffolds. *Polymer* 2010;51:1320–7.
- [207] Yoon YI, Park KE, Lee SJ, Park WH. Fabrication of microfibrous and nano-/microfibrous scaffolds: melt and hybrid electrospinning and surface modification of poly(L-lactic acid) with plasticizer. *Biomed Res Int* 2013;2013, 309048/1–309048/10.
- [208] Karchin A, Wang YN, Sanders J. Modulation of gene expression using electrospun scaffolds with templated architecture. *J Biomater Sci Mater Res, A* 2012;100:1605–14.
- [209] Takasaki M, Fu H, Nakata K, Ohkoshi Y, Hirai T. Ultra-fine fibers produced by laser-electrospinning. *Sen-i Gakkaishi* 2008;64:29–31.
- [210] Wang X-F. Melt-electrospinning of PMMA. *Chin J Polym Sci* 2010;28:45–53.
- [211] Rajabinejad H, Khajavi R, Rashidi A, Mansouri N, Yazdanshenas M. Recycling of used bottle grade poly ethyleneterephthalate to nanofibers by melt-electrospinning method. *Int J Environ Res* 2009;3:663–70.
- [212] Bock N, Woodruff MA, Steck R, Hutmacher DW, Farrugia BL, Dargaville TR. Composites for delivery of therapeutics: combining melt electrospun scaffolds with loaded electrosprayed microparticles. *Macromol Biosci* 2013;14:202–14.
- [213] Costa PF, Vaquette C, Zhang QY, Reis RL, Ivanovski S, Hutmacher DW. Advanced tissue engineering scaffold design for regeneration of the complex hierarchical periodontal structure. *J Clin Periodontol* 2014;41:283–94.
- [214] Vaquette C, Fan W, Xiao Y, Hamlet S, Hutmacher DW, Ivanovski S. A biphasic scaffold design combined with cell sheet technology for simultaneous regeneration of alveolar bone/periodontal ligament complex. *Biomaterials* 2012;33:5560–73.
- [215] Zhao F, Liu Y, Yuan H, Yang W. Orthogonal design study on factors affecting the degradation of polylactic acid fibers of melt electrospinning. *J Appl Polym Sci* 2012;125:2652–8.
- [216] Li X, Liu H, Wang J, Li C. Preparation and characterization of PLLA/nHA nonwoven mats via laser melt electrospinning. *Mater Lett* 2012;73:103–6.
- [217] Karahaliloglu Z, Hacker C, Demirbilek M, Seide G, Denkbas EB, Gries T. Photocatalytic performance of melt-electrospun polypropylene fabric decorated with TiO<sub>2</sub> nanoparticles. *J Nanopart Res* 2014;16, 2615/1–2615/14.
- [218] Cao L, Su D, Su Z, Chen X. Fabrication of multi-walled carbon nanotube/polypropylene conductive fibrous membranes by melt electrospinning. *Ind Eng Chem Res* 2014;53:2308–17.
- [219] Ren J, Blackwood KA, Doustgani A, Poh PP, Steck R, Stevens MM, Woodruff MA. Melt-electrospun polycaprolactone-strontium substituted bioactive glass scaffolds for bone regeneration. *J Biomater Sci Mater Res, A* 2013;41, <http://dx.doi.org/10.1002/jbma.34985>.
- [220] Dasdemir M, Topalbekiroglu M, Demir A. Electrospinning of thermoplastic polyurethane microfibers and nanofibers from polymer solution and melt. *J Appl Polym Sci* 2013;127:1901–8.
- [221] Brown TD, Edin F, Detta N, Skelton AD, Hutmacher DW, Dalton PD. Melt electrospinning of poly( $\epsilon$ -caprolactone) scaffolds: phenomenological observations associated with collection and direct writing. *Mater Sci Eng C* 2014;45:698–708.
- [222] Li F, Zhao Y, Wang S, Han D, Jiang L, Song Y. Thermochromic core-shell nanofibers fabricated by melt coaxial electrospinning. *J Appl Polym Sci* 2009;112:269–74.
- [223] Hochleitner G, Hummer JF, Luxenhofer R, Groll J. High definition fibrous poly(2-ethyl-2-oxazoline) scaffolds through melt electrospinning writing. *Polymer* 2014;55:5017–23.
- [224] Lyons J, Ko F. Melt electrospinning of polymers: a review. *Polym News* 2005;30:170–8.
- [225] Hayati I, Bailey A, Tedros TF. Mechanism of stable jet formation in electrohydrodynamic atomization. *Nature* 1986;319:41–3.
- [226] Melcher J, Warren E. Electrohydrodynamics of a current-carrying semi-insulating jet. *J Fluid Mech* 1971;47:127–43.
- [227] Kim D, Yoshino K. Morphological characteristics and electrical conduction in syndiotactic polypropylene. *J Phys D* 2000;33:464–71.
- [228] Chung CI. *Extrusion of polymers: theory and practice*. 2nd ed. Munich: Hanser Verlag; 2010. p. 483.
- [229] Charuchinda A, Molloy R, Siripitayananon J, Molloy N, Sriyai M. Factors influencing the small-scale melt spinning of poly( $\epsilon$ -caprolactone) monofilament fibres. *Polym Int* 2003;52:1175–81.
- [230] Kadomae Y, Maruyama Y, Sugimoto M, Taniguchi T, Koyama K. Relation between tacticity and fiber diameter in melt-electrospinning of polypropylene. *Fibers Polym* 2009;10:275–9.
- [231] Mazalevska O, Struszczuk MH, Krucinska I. Design of vascular prostheses by melt electrospinning—structural characterizations. *J Appl Polym Sci* 2013;129:779–92.

- [232] Progelhof RC, Throne JL, Progelhof R. *Polymer engineering principles: properties, processes, and tests for design*. Munich: Hanser Gardner Pubns; 1993. p. 935.
- [233] Fang J, Zhang L, Sutton D, Wang X, Lin T. Needleless melt-electrospinning of polypropylene nanofibres. *J Nanomater* 2012;2012, 16/1-16/9.
- [234] Farrugia BL, Brown TD, Upton Z, Hutmacher DW, Dalton PD, Dar-gaville TR. Dermal fibroblast infiltration of poly( $\epsilon$ -caprolactone) scaffolds fabricated by melt electrospinning in a direct writing mode. *Biofabrication* 2013;5, 025001/1-025001/11.
- [235] Wei C, Dong J. Direct fabrication of high-resolution three-dimensional polymeric scaffolds using electrohydrodynamic hot jet plotting. *J Micromech Microeng* 2013;23, 025017/1-025017/9.
- [236] Jeon JE, Vaquette C, Theodoropoulos C, Klein TJ, Hutmacher DW. Multiphasic construct studied in an ectopic osteochondral defect model. *J R Soc Interface* 2014;11, 20140184/1-20140184/14.
- [237] Nagy ZK, Balogh A, Drávavölgyi G, Ferguson J, Pataki H, Vajna B, Marosi G. Solvent-free melt electrospinning for preparation of fast dissolving drug delivery system and comparison with solvent-based electrospun and melt extruded systems. *J Pharm Sci* 2013;102:508–17.
- [238] Nazari T, Garmabi H. Polylactic acid/polyethylene glycol blend fibres prepared via melt electrospinning: effect of polyethylene glycol content. *Micro Nano Lett* 2014;9:686–90.
- [239] Ko J, Bhullar SK, Mohtaram NK, Willerth SM, Jun MBG. Using mathematical modeling to control topographical properties of poly(epsin-caprolactone) melt electrospun scaffolds. *J Micromech Microeng* 2015;25, 045018/1-045018/13.
- [240] Hunley MT, Karikari AS, McKee MG, Mather BD, Layman JM, Fornof AR, Long TE. Taking advantage of tailored electrostatics and complementary hydrogen bonding in the design of nanostructures for biomedical applications. *Macromolecular Symp Wiley Online Libr* 2008;279:1–7.
- [241] Kluge D, Singer JC, Neugirg BR, Neubauer JW, Schmidt HW, Fery A. Top-down meets bottom-up: a comparison of the mechanical properties of melt electrospun and self-assembled 1,3,5-benzenetrisamide fibers. *Polymer* 2012;53:5754–9.
- [242] Kim J, Lee SH, Park SJ, Lee YS. Preparation and gas-sensing properties of pitch-based carbon fiber prepared using a melt-electrospinning method. *Res Chem Intermediat* 2014;40:2571–81.
- [243] Chrzanowska O, Struszczyk MH, Krucinska I. Small diameter tubular structure design using solvent-free textile techniques. *J Appl Polym Sci* 2014;131:14, <http://dx.doi.org/10.1002/app.40147>.
- [244] Kong C, Jo K, Jo N, Kim H. Effects of the spin line temperature profile and melt index of poly(propylene) on melt-electrospinning. *Polym Eng Sci* 2009;49:391–6.
- [245] Carroll CP, Zhmayev E, Kalra V, Joo YL. Nanofibers from electrically driven viscoelastic jets: modeling and experiments. *Korea Aust Rheol J* 2008;20:153–64.
- [246] Warner S, Fowler A, Jaffe M, Patra P, Ugbolue S, Coates J, Subramanian C. Cost effective nanofiber formation: melt electrospinning. *US Nat Text Cent Annu Rep* 2005:6.
- [247] Cao L, Dong M, Zhang A, Liu Y, Yang W, Su Z, Chen X. Morphologies and crystal structures of styrene-acrylonitrile/isotactic polypropylene ultrafine fibers fabricated by melt electrospinning. *Polym Eng Sci* 2013;53:2674–82.
- [248] Liu Y, Deng R, Hao M, Yan H, Yang W. Orthogonal design study on factors effecting on fibers diameter of melt electrospinning. *Polym Eng Sci* 2010;50:2074–8.
- [249] Liu Y, Liu ZX, Deng L, Wang KJ, Yang WM. Effect of different factors on falling process of melt electrospinning jet. *Mater Sci Forum* 2013;745–6:407–11.
- [250] Malakhov S, Khomenko AY, Belousov S, Prazdnichnyi A, Chvalun S, Shepelev A, Budyka AK. Method of manufacturing nonwovens by electrospinning from polymer melts. *Fibre Chem* 2009;41:355–9.
- [251] Hacker CJ, Seide G, Gries T, Thomas H, Moeller M. Electrospinning of polymer melt: steps toward an upscaled multi-jet process. In: Proc Int Confer Latest Advances in High Tech Textiles and Textile-Based Materials. 2009. p. S71–6.
- [252] Mazalevska O, Struszczyk MH, Chrzanowski M, Krucińska I. Application of electrospinning for vascular prothesis design—preliminary results. *Fibres Text East Eur* 2011;19:46–52.
- [253] Gazzari M, Bartoli C, Mota C, Puppi D, Dinucci D, Volpi S, Chiellini F. Fibrous star poly( $\epsilon$ -caprolactone) melt-electrospun scaffolds for wound healing applications. *J Bioact Compat Polym* 2013;28:492–507.
- [254] Li X, Liu H, Liu J, Wang J, Li C. Preparation and experimental parameters analysis of laser melt electrospun poly(L-lactide) fibers via orthogonal design. *Polym Eng Sci* 2012;52:1964–7.
- [255] Li X, Liu H, Wang J, Li C. Preparation and characterization of poly( $\epsilon$ -caprolactone) nonwoven mats via melt electrospinning. *Polymer* 2012;53:248–53.
- [256] Kirichenko V, Petryanov-Sokolov I, Suprun N, Shutov A. Asymptotic radius of a slightly conducting liquid jet in an electric field. *Soviet Phys Dokl* 1986;31:611–3.
- [257] Kim SJ, Jeong L, Lee SJ, Cho D, Park WH. Fabrication and surface modification of melt-electrospun poly(D, L-lactic-co-glycolic acid) microfibers. *Fibers Polym* 2013;14:1491–6.
- [258] McCann JT, Marquez M, Xia Y. Melt coaxial electrospinning: a versatile method for the encapsulation of solid materials and fabrication of phase change nanofibers. *Nano Lett* 2006;6:2868–72.
- [259] Hutmacher DW, Sittiger M, Risbud MV. Scaffold-based tissue engineering: rationale for computer-aided design and solid free-form fabrication systems. *TRENDS Biotechnol* 2004;22:354–62.
- [260] Chua C, Leong K, Sudarmadji N, Liu M, Chou S. Selective laser sintering of functionally graded tissue scaffolds. *MRS Bull* 2011;36:1006–14.
- [261] Niino T, Hamajima D, Montagne K, Oizumi S, Naruke H, Huang H, Sakai Y, Kinoshita H, Fujii T. Laser sintering fabrication of three-dimensional tissue engineering scaffolds with a flow channel network. *Biofabrication* 2011;3, 034104/1-034104/10.
- [262] Maruo S, Ikuta K. Submicron stereolithography for the production of freely movable mechanisms by using single-photon polymerization. *Sens Actuators, A: Phys* 2002;100:70–6.
- [263] Ragaert K, Cardon L, Dekeyser A, Degrieck J. Machine design and processing considerations for the 3D plotting of thermoplastic scaffolds. *Biofabrication* 2010;2, 014107/1-014107/8.
- [264] Shor L, Gücüri S, Chang R, Gordon J, Kang Q, Hartsock L, An Y, Sun W. Precision extruding deposition (PED) fabrication of polycaprolactone (PCL) scaffolds for bone tissue engineering. *Biofabrication* 2009;1, 015003/1-015003/10.
- [265] Wei C, Cai L, Sonawane B, Wang S, Dong J. High-precision flexible fabrication of tissue engineering scaffolds using distinct polymers. *Biofabrication* 2012;4, 025009/1-025009/12.
- [266] Sun Q, Rizvi G, Bellehumeur C, Gu P. Effect of processing conditions on the bonding quality of FDM polymer filaments. *Rapid Prototyp J* 2008;14:72–80.
- [267] Ragaert K, Dekeyser A, Cardon L, Degrieck J. Quantification of thermal material degradation during the processing of biomedical thermoplastics. *J Appl Polym Sci* 2011;120:2872–80.
- [268] Tsuji H, Fukui I. Enhanced thermal stability of poly(lactide)s in the melt by enantiomeric polymer blending. *Polymer* 2003;44: 2891–6.
- [269] Ramanath H, Chua C, Leong K, Shah K. Melt flow behaviour of poly( $\epsilon$ -caprolactone in fused deposition modelling. *J Mater Sci Mater Med* 2008;19:2541–50.
- [270] Zein I, Hutmacher DW, Tan KC, Teoh SH. Fused deposition modeling of novel scaffold architectures for tissue engineering applications. *Biomaterials* 2002;23:1169–85.
- [271] Park SH, Kim TG, Kim HC, Yang D-Y, Park TG. Development of dual scale scaffolds via direct polymer melt deposition and electrospinning for applications in tissue regeneration. *Acta Biomater* 2008;4:1198–207.
- [272] Kim G, Son J, Park S, Kim W. Hybrid process for fabricating 3D hierarchical scaffolds combining rapid prototyping and electrospinning. *Macromol Rapid Commun* 2008;29:1577–81.
- [273] Moroni L, De Wijn J, Van Blitterswijk C. Integrating novel technologies to fabricate smart scaffolds. *J Biomater Sci Polym Ed* 2008;19:543–72.
- [274] Ahn SH, Lee HJ, Kim GH. Polycaprolactone scaffolds fabricated with an advanced electrohydrodynamic direct-printing method for bone tissue regeneration. *Biomacromolecules* 2011;12:4256–63.
- [275] He G, Zheng G, Zheng J, Lin Y, Wei J, Liu H, Wang B, Sun D. Micro/nano structure written via sheath gas assisted EHD jet. In: IEEE Int Conf Nano/Micro Eng Molecular Syst. 2013. p. 625–8.
- [276] Wang X, Zheng G, He G, Wei J, Liu H, Lin Y, Zheng J, Sun D. Electrohydrodynamic direct-writing ZnO nanofibers for device applications. *Mater Lett* 2013;109:58–61.
- [277] Sun DH, Lin YH, He GQ, Liu HY, Zheng JY, Zheng GF, Wei J. Electrohydrodynamic Printing via Spinneret with Conductive Probe. *Key Eng Mater* 2013;562:1155–60.
- [278] Kessick R, Tepper G. Microscale electrospinning of polymer nanofiber interconnections. *Appl Phys Lett* 2003;83:557–9.
- [279] Clark JE, Olesik SV. Electrospun glassy carbon ultra-thin layer chromatography devices. *J Chromatogr A* 2010;1217:4655–62.
- [280] Wang M, Jing N, Su CB, Kameoka J, Chou C-K, Hung M-C, Chang K-A. Electrospinning of silica nanochannels for single molecule detection. *Appl Phys Lett* 2006;88, 033106/1-033106/3.

- [281] Tong L, Gattass RR, Ashcom JB, He S, Lou J, Shen M, Maxwell I, Mazur E. Subwavelength-diameter silica wires for low-loss optical wave guiding. *Nature* 2003;426:816–9.
- [282] Sahoo NG, Rana S, Cho JW, Li L, Chan SH. Polymer nanocomposites based on functionalized carbon nanotubes. *Progr Polym Sci* 2010;35:837–67.
- [283] Goncharuk V, Kavitskaya A, Skil'skaya M. Nanofiltration in drinking water supply. *J Water Chem Technol* 2011;33:37–54.
- [284] Ramakrishna S, Jose R, Archana P, Nair A, Balamurugan R, Venugopal J, Teo WE. Science and engineering of electrospun nanofibers for advances in clean energy, water filtration, and regenerative medicine. *J Mater Sci* 2010;45:6283–312.
- [285] Sutherland K. Air filtration: using filtration to control industrial air pollution. *Filtration Sep* 2008;45:16–9.
- [286] Sutherland K. Developments in filtration: what is nanofiltration? *Filtration Sep* 2008;45:32–5.
- [287] Takht Ravanchi M, Kaghazchi T, Kargari A. Application of membrane separation processes in petrochemical industry: a review. *Desalination* 2009;235:199–244.
- [288] Shabani I, Hasani-Sadrabadi MM, Haddadi-Asl V, Soleimani M. Nanofiber-based polyelectrolytes as novel membranes for fuel cell applications. *J Membr Sci* 2011;368:233–40.
- [289] Van der Bruggen B, Määntäri M, Nyström M. Drawbacks of applying nanofiltration and how to avoid them: a review. *Sep Purif Technol* 2008;63:251–63.
- [290] Veleirinho B, Lopes-da-Silva J. Application of electrospun poly(ethylene terephthalate) nanofiber mat to apple juice clarification. *Process Biochem* 2009;44:353–6.
- [291] Lee S, Kay Obendorf S. Developing protective textile materials as barriers to liquid penetration using melt-electrospinning. *J Appl Polym Sci* 2006;102:3430–7.
- [292] Schreuder-Gibson H, Gibson P, Senecal K, Sennett M, Walker J, Yeomans W, Ziegler D, Tsai PP. Protective textile materials based on electrospun nanofibers. *J Adv Mater* 2002;34:44–55.
- [293] Felix Lanao RP, Jonker AM, Wolke JG, Jansen JA, van Hest JC, Leeuwenburgh SC. Physicochemical properties and applications of poly(lactic-co-glycolic acid) for use in bone regeneration. *Tissue Eng, B* 2013;19:380–90.
- [294] Weinberg BD, Blanco E, Gao J. Polymer implants for intratumoral drug delivery and cancer therapy. *J Pharm Sci* 2008;97:1681–702.
- [295] Boateng JS, Matthews KH, Stevens HN, Eccleston GM. Wound healing dressings and drug delivery systems: a review. *J Pharm Sci* 2008;97:2892–923.
- [296] Verreck G, Six K, Van den Mooter G, Baert L, Peeters J, Brewster ME. Characterization of solid dispersions of itraconazole and hydroxypropylmethylcellulose prepared by melt extrusion—Part I. *Int J Pharm* 2003;251:165–74.
- [297] Breitenbach J. Melt extrusion: from process to drug delivery technology. *Eur J Pharm Biopharm* 2002;54:107–17.
- [298] Saucet M, Fages J, Common A, Nikitine C, Rodier E. New challenges in polymer foaming: a review of extrusion processes assisted by supercritical carbon dioxide. *Progr Polym Sci* 2011;36:749–66.
- [299] Vajna B, Pataki H, Nagy Z, Farkas I, Marosi G. Characterization of melt extruded and conventional Isoptin formulations using Raman chemical imaging and chemometrics. *Int J Pharm* 2011;419:107–13.
- [300] Lee H, Ahn S, Choi H, Cho D, Kim G. Fabrication, characterization, and in vitro biological activities of melt-electrospun PLA micro/nanofibers for bone tissue regeneration. *J Mater Chem B* 2013;1:3670–7.
- [301] Dalton P, Woodfield T, Hutmacher D. Snapshot: Polymer scaffolds for tissue engineering. *Biomaterials* 2009;30:701–2.
- [302] Zhou Y, Chen F, Ho ST, Woodruff MA, Lim TM, Hutmacher DW. Combined marrow stromal cell-sheet techniques and high-strength biodegradable composite scaffolds for engineered functional bone grafts. *Biomaterials* 2007;28:814–24.
- [303] Mikos AG, Sarakinos G, Leite SM, Vacanti JP, Langer R. Laminated three-dimensional biodegradable foams for use in tissue engineering. *Biomaterials* 1993;14:323–30.
- [304] Mikos AG, Thorsen AJ, Czerwonka LA, Bao Y, Langer R, Winslow DN, Vacanti JP. Preparation and characterization of poly(L-lactic acid) foams. *Polymer* 1994;35:1068–77.
- [305] Ochi K, Chen G, Ushida T, Gojo S, Segawa K, Tai H, Ueno K, Ohkawa H, Mori T, Yamaguchi A. Use of isolated mature osteoblasts in abundance acts as desired-shaped bone regeneration in combination with a modified poly-D,L-lactic-co-glycolic acid (PLGA)-collagen sponge. *J Cell Physiol* 2003;194:45–53.
- [306] Harris LD, Kim BS, Mooney DJ. Open pore biodegradable matrices formed with gas foaming. *J Biomater Sci Mater Res* 1998;42:396–402.
- [307] Mooney DJ, Baldwin DF, Suh NP, Vacanti JP, Langer R. Novel approach to fabricate porous sponges of poly(D, L-lactic-co-glycolic acid) without the use of organic solvents. *Biomaterials* 1996;17:1417–22.
- [308] Yoon JJ, Park TG. Degradation behaviors of biodegradable macro-porous scaffolds prepared by gas foaming of effervescent salts. *J Biomater Sci Mater Res* 2001;55:401–8.
- [309] Borden M, Attawa M, Khan Y, Laurencin CT. Tissue engineered microsphere-based matrices for bone repair: design and evaluation. *Biomaterials* 2002;23:551–9.
- [310] Guan J, Fujimoto KL, Sacks MS, Wagner WR. Preparation and characterization of highly porous, biodegradable polyurethane scaffolds for soft tissue applications. *Biomaterials* 2005;26:3961–71.
- [311] Leukers B, Gülkán H, Irsen SH, Milz S, Tille C, Schieker M, Seitz H. Hydroxyapatite scaffolds for bone tissue engineering made by 3D printing. *J Mater Sci Mater Med* 2005;16:1121–4.
- [312] Seitz H, Rieder W, Irsen S, Leukers B, Tille C. Three-dimensional printing of porous ceramic scaffolds for bone tissue engineering. *J Biomater Sci Mater Res, B* 2005;74:782–8.
- [313] Pfister A, Landers R, Laib A, Hübner U, Schmelzeisen R, Mülhaupt R. Biofunctional rapid prototyping for tissue-engineering applications: 3D bioplotting versus 3D printing. *J Polym Sci, A: Polym Chem* 2004;42:624–38.
- [314] Cooke MN, Fisher JP, Dean D, Rimmac C, Mikos AG. Use of stereolithography to manufacture critical-sized 3D biodegradable scaffolds for bone ingrowth. *J Biomater Sci Mater Res, B* 2003;64:65–9.
- [315] Dhariwala B, Hunt E, Boland T. Rapid prototyping of tissue-engineering constructs, using photopolymerizable hydrogels and stereolithography. *Tissue Eng* 2004;10:1316–22.
- [316] Sodian R, Loebe M, Hein A, Martin DP, Hoerstrup SP, Potapov EV, Hausmann EV, Leuth T, Hetzer R. Application of stereolithography for scaffold fabrication for tissue engineered heart valves. *ASAIO J* 2002;48:12–6.
- [317] Hutmacher DW, Schantz T, Zein I, Ng KW, Teoh SH, Tan KC. Mechanical properties and cell cultural response of polycaprolactone scaffolds designed and fabricated via fused deposition modeling. *J Biomater Sci Mater Res* 2001;55:203–16.
- [318] Chua C, Leong K, Tan K, Wiria F, Cheah C. Development of tissue scaffolds using selective laser sintering of polyvinyl alcohol/hydroxyapatite biocomposite for craniofacial and joint defects. *J Mater Sci Mater Med* 2004;15:1113–21.
- [319] Tan KH, Chua CK, Leong KF, Cheah CM, Gui WS, Tan WS, Wiria FE. Selective laser sintering of biocompatible polymers for applications in tissue engineering. *Biomater Eng* 2005;15:1113–24.
- [320] Williams JM, Adewunmi A, Schek RM, Flanagan CL, Krebsbach PH, Feinberg SE, Hollister SJ, Das S. Bone tissue engineering using polycaprolactone scaffolds fabricated via selective laser sintering. *Biomaterials* 2005;26:4817–27.
- [321] Lewis JA, Gratson GM. Direct writing in three dimensions. *Mater Today* 2004;7:32–9.
- [322] Gratson GM, Xu M, Lewis JA. Microperiodic structures: direct writing of three-dimensional webs. *Nature* 2004;428:386–96.
- [323] Hutmacher DW. Scaffold design and fabrication technologies for engineering tissues—state of the art and future perspectives. *J Biomater Sci Polym Ed* 2001;12:107–24.
- [324] Zeugolis DI, Khew ST, Yew ES, Ekaputra AK, Tong YW, Yung LY, Hutmacher DW, Sheppard C, Raghunath M. Electro-spinning of pure collagen nano-fibres—just an expensive way to make gelatin? *Biomaterials* 2008;29:2293–305.
- [325] Boudriot U, Dersch R, Greiner A, Wendorff JH. Electrospinning approaches toward scaffold engineering—a brief overview. *Artif Organs* 2006;30:785–92.
- [326] He W, Yong T, Teo WE, Ma Z, Ramakrishna S. Fabrication and endothelialization of collagen-blended biodegradable polymer nanofibers: potential vascular graft for blood vessel tissue engineering. *Tissue Eng* 2005;11:1574–88.
- [327] McCann JT, Li D, Xia Y. Electrospinning of nanofibers with core-sheath, hollow, or porous structures. *J Mater Chem* 2005;15:735–8.
- [328] Xu C, Inai R, Kotaki M, Ramakrishna S. Aligned biodegradable nanofibrous structure: a potential scaffold for blood vessel engineering. *Biomaterials* 2004;25:877–86.
- [329] He W, Ma Z, Yong T, Teo WE, Ramakrishna S. Fabrication of collagen-coated biodegradable polymer nanofiber mesh and its potential for endothelial cells growth. *Biomaterials* 2005;26:7606–15.

- [330] Jin H-J, Chen J, Karageorgiou V, Altman GH, Kaplan DL. Human bone marrow stromal cell responses on electrospun silk fibroin mats. *Biomaterials* 2004;25:1039–47.
- [331] Min B-M, Lee G, Kim SH, Nam YS, Lee TS, Park WH. Electro-spinning of silk fibroin nanofibers and its effect on the adhesion and spreading of normal human keratinocytes and fibroblasts in vitro. *Biomaterials* 2004;25:1289–97.
- [332] Mo X, Xu C, Kotaki Mea, Ramakrishna S, Electrospun P. (LLA-CL) nanofiber: a biomimetic extracellular matrix for smooth muscle cell and endothelial cell proliferation. *Biomaterials* 2004;25:1883–90.
- [333] Shin HJ, Lee CH, Cho IH, Kim Y-J, Lee Y-J, Kim IA, Park K-D, Yui N, Shin J-W. Electrospun PLGA nanofiber scaffolds for articular cartilage reconstruction: mechanical stability, degradation and cellular responses under mechanical stimulation in vitro. *J Biomater Sci Polym Ed* 2006;17:103–19.
- [334] Venugopal JR, Zhang Y, Ramakrishna S. In vitro culture of human dermal fibroblasts on electrospun polycaprolactone collagen nanofibrous membrane. *Artif Organs* 2006;30:440–6.
- [335] Yang S, Leong K-F, Du Z, Chua C-K. The design of scaffolds for use in tissue engineering. Part I. Traditional factors. *Tissue Eng* 2001;7:679–89.
- [336] Karageorgiou V, Kaplan D. Porosity of 3D biomaterial scaffolds and osteogenesis. *Biomaterials* 2005;26:5474–91.
- [337] Lowery JL, Datta N, Rutledge GC. Effect of fiber diameter, pore size and seeding method on growth of human dermal fibroblasts in electrospun poly( $\epsilon$ -caprolactone) fibrous mats. *Biomaterials* 2010;31:491–504.
- [338] Li WJ, Laurencin CT, Caterson EJ, Tuan RS, Ko FK. Electrospun nanofibrous structure: a novel scaffold for tissue engineering. *J Biomater Sci Mater Res* 2002;60:613–21.
- [339] Schindler M, Ahmed I, Nur-E-Kamal A, Grafe TH, Young Chung H, Meiners S. A synthetic nanofibrillar matrix promotes in vivo-like organization and morphogenesis for cells in culture. *Biomaterials* 2005;26:5624–31.
- [340] Keun Kwon I, Kidoaki S, Matsuda T. Electrospun nano-to microfiber fabrics made of biodegradable copolymers: structural characteristics, mechanical properties and cell adhesion potential. *Biomaterials* 2005;26:3929–39.
- [341] Blakeney BA, Tamburri A, Anderson JM, Andukuri A, Lim D-J, Dean DR, Jun H-W. Cell infiltration and growth in a low density, uncompressed three-dimensional electrospun nanofibrous scaffold. *Biomaterials* 2011;32:1583–90.
- [342] Ekapatra AK, Prestwich GD, Cool SM, Hutmacher DW. The three-dimensional vascularization of growth factor-releasing hybrid scaffold of poly( $\epsilon$ -caprolactone)/collagen fibers and hyaluronic acid hydrogel. *Biomaterials* 2011;32:8108–17.
- [343] Rnjak-Kovacina J, Weiss AS. Increasing the pore size of electrospun scaffolds. *Tissue Eng, B* 2011;17:365–72.
- [344] Jha BS, Colello RJ, Bowman JR, Sell SA, Lee KD, Bigbee JW, Bowlin GL, Chow WN, Mathern BE, Simpson DG. Two pole air gap electro-spinning: fabrication of highly aligned, three-dimensional scaffolds for nerve reconstruction. *Acta Biomater* 2011;7:203–15.
- [345] Li D, Wang Y, Xia Y. Electrospinning nanofibers as uniaxially aligned arrays and layer-by-layer stacked films. *Adv Mater* 2004;16:361–6.
- [346] Li D, Ouyang G, McCann JT, Xia Y. Collecting electrospun nanofibers with patterned electrodes. *Nano Lett* 2005;5:913–6.
- [347] Teo W, Ramakrishna S. Electrospun fibre bundle made of aligned nanofibres over two fixed points. *Nanotechnology* 2005;16:1878–84.
- [348] Matthews JA, Wnek GE, Simpson DG, Bowlin GL. Electrospinning of collagen nanofibers. *Biomacromolecules* 2002;3:232–8.
- [349] Subramanian A, Vu D, Larsen GF, Lin H-Y. Preparation and evaluation of the electrospun chitosan/PEO fibers for potential applications in cartilage tissue engineering. *J Biomater Sci Polym Ed* 2005;16:861–73.
- [350] Sundaray B, Subramanian V, Natarajan T, Xiang R-Z, Chang C-C, Fann W-S. Electrospinning of continuous aligned polymer fibers. *Appl Phys Lett* 2004;84:1222–4.
- [351] Zussman E, Theron A, Yarin A. Formation of nanofiber crossbars in electrospinning. *Appl Phys Lett* 2003;82:973–5.
- [352] Kameoka J, Orth R, Yang Y, Czaplewski D, Mathers R, Coates GW, Craighead HG. A scanning tip electrospinning source for deposition of oriented nanofibres. *Nanotechnology* 2003;14:1124–9.
- [353] Kameoka J, Craighead H. Fabrication of oriented polymeric nanofibers on planar surfaces by electrospinning. *Appl Phys Lett* 2003;83:371–3.
- [354] Kim KW, Lee KH, Khil MS, Ho YS, Kim HY. The effect of molecular weight and the linear velocity of drum surface on the properties of electrospun poly(ethylene terephthalate) nonwovens. *Fibers Polym* 2004;5:122–7.
- [355] Kessick R, Fenn J, Tepper G. The use of AC potentials in electrospraying and electrospinning processes. *Polymer* 2004;45:2981–4.
- [356] Stitzel J, Liu J, Lee SJ, Komura M, Berry J, Soker S, Lim G, Van Dyke M, Czerw R, Yoo J. Controlled fabrication of a biological vascular substitute. *Biomaterials* 2006;27:1088–94.
- [357] Kidoaki S, Kwon IK, Matsuda T. Mesoscopic spatial designs of nano- and microfiber meshes for tissue-engineering matrix and scaffold based on newly devised multilayering and mixing electrospinning techniques. *Biomaterials* 2005;26:37–46.
- [358] Teo W, Kotaki M, Mo X, Ramakrishna S. Porous tubular structures with controlled fibre orientation using a modified electrospinning method. *Nanotechnology* 2005;16:918–24.
- [359] Theron A, Zussman E, Yarin A. Electrostatic field-assisted alignment of electrospun nanofibres. *Nanotechnology* 2001;12:384–90.
- [360] Buttafoco L, Kolkman N, Engbers-Buijtenhuijs P, Poot A, Dijkstra P, Vermes I, Feijen J. Electrospinning of collagen and elastin for tissue engineering applications. *Biomaterials* 2006;27:724–34.
- [361] Bhattacharai N, Edmondson D, Veiseh O, Matsen FA, Zhang M. Electrospun chitosan-based nanofibers and their cellular compatibility. *Biomaterials* 2005;26:6176–84.
- [362] Zhang D, Chang J. Patterning of electrospun fibers using electroconductive templates. *Adv Mater* 2007;19:3664–7.
- [363] Zhang D, Chang J. Electrospinning of three-dimensional nanofibrous tubes with controllable architectures. *Nano Lett* 2008;8:3283–7.
- [364] Vaquette C, Cooper-White JJ. Increasing electrospun scaffold pore size with tailored collectors for improved cell penetration. *Acta Biomater* 2011;7:2544–57.
- [365] Tzezana R, Zussman E, Levenberg S. A layered ultra-porous scaffold for tissue engineering, created via a hydrospinning method. *Tissue Eng, C* 2008;14:281–8.
- [366] Yokoyama Y, Hattori S, Yoshikawa C, Yasuda Y, Koyama H, Takato T, Kobayashi H. Novel wet electrospinning system for fabrication of spongiform nanofiber 3-dimensional fabric. *Mater Lett* 2009;63:754–6.
- [367] Ki CS, Park SY, Kim HJ, Jung H-M, Woo KM, Lee JW, Park YH. Development of 3-D nanofibrous fibroin scaffold with high porosity by electrospinning: implications for bone regeneration. *Biotechnol Lett* 2008;30:405–10.
- [368] Baker BM, Gee AO, Metter RB, Nathan AS, Marklein RA, Burdick JA, Mauck RL. The potential to improve cell infiltration in composite fiber-aligned electrospun scaffolds by the selective removal of sacrificial fibers. *Biomaterials* 2008;29:2348–58.
- [369] Kim G, Kim W. Highly porous 3D nanofiber scaffold using an electrospinning technique. *J Biomater Sci Mater Res, B* 2007;81:104–10.
- [370] Simonet M, Schneider OD, Neuenschwander P, Stark WJ. Ultra-porous 3D polymer meshes by low-temperature electrospinning: use of ice crystals as a removable void template. *Polym Eng Sci* 2007;47:2020–6.
- [371] Chang C, Limkrallassiri K, Lin L. Continuous near-field electrospinning for large area deposition of orderly nanofiber patterns. *Appl Phys Lett* 2008;93, 123111/1–123111/3.
- [372] Sun D, Chang C, Li S, Lin L. Near-field electrospinning. *Nano Lett* 2006;6:839–42.
- [373] Zheng G, Li W, Wang X, Wu D, Sun D, Lin L. Precision deposition of a nanofibre by near-field electrospinning. *J Phys D* 2010;43, 415501/1–415501/6.
- [374] Di JC, Zhao Y, Yu JH. Fabrication of molecular sieve fibers by electrospinning. *J Mater Chem* 2011;21:8511–20.